Fakultät für Medizin

Institut für Molekulare Immunologie – Experimentelle Onkologie

Modified messenger RNA and its application in bone tissue engineering

Dipl.-Ing. (FH) Mehrije Ferizi

Vollständiger Abdruck der von der Fakultät für Medizin der Technischen Universität München zur Erlangung des akademischen Grades eines

Doctor of Philosophy (Ph.D.)

genehmigten Dissertation.

Vorsitzender: Univ.-Prof. Dr. Dr. Stefan Engelhardt

Betreuer: apl. Prof. Dr. Christian Plank

Prüfer der Dissertation:

1. Univ.-Prof. Dr. Dr. Martijn van Griensven

2. Priv.-Doz. Dr. Carsten Rudolph,

   Ludwig-Maximilians-Universität München

Die Dissertation wurde am 19.11.2015 bei der Fakultät für Medizin der Technischen Universität München eingereicht und durch die Fakultät für Medizin am 01.02.2016 angenommen.

To my beloved parents and Isuf Zykolli

Table of contents

1. Summary

In the last few years messenger RNA (mRNA) has emerged as a new drug entity as an alternative to gene therapy. In contrast to DNA, which has to reach the cell nucleus to yield production of a therapeutic protein, mRNA has to be delivered only into the cytoplasm to be translated without any risks of insertional mutagenesis. In order to develop the so-called "transcript therapy", the mRNA molecule has to be optimized with respect to mRNA stability and translation. So far several approaches have been implemented such as the inclusion of chemically modified nucleotides, prolonging the poly(A) tail and the insertion of untranslated regions (UTRs). The latter has been shown to play a pivotal role both in protein translation and stability of the resulting mRNA.

The goal of this project was to improve the translational efficiency and stability of mRNAs comprising 5-methyl cytidine and 2-thio uridine, an extended poly(A) tail and human cellular UTRs putatively conveying long mRNA half-lives. UTRs from human CYBA, DECR1, GMFG, MAPBPIP and MYL6B were cloned upstream (5'-UTR) and/or downstream (3'-UTR) of reporter genes. For each cellular UTR five different combinations were investigated namely 5'UTR, 3'UTR, 5'+3'UTR, 5'+2x3'UTR and 2x3' UTR. All *in vitro* transcribed mRNA constructs were screened in NIH3T3 and A549 cells, respectively. The highest protein translation over specified time, presented as area under the curve (AUC) was observed for mRNA constructs furnished with 5'+3' CYBA UTR followed by 5' UTR and 2x3' CYBA UTR mRNA constructs. In further experiments, physical and functional half-life of mRNA were assessed. The physical half-life of the three best working mRNA combinations, 5' CYBA, 5'+3' CYBA and 2x3' CYBA was quantified via qRT-PCR in both cell lines. Whereas no increased stabilization effect could be observed for any of the CYBA UTR containing mRNAs, their functional half-lives were prolonged. The functional half-life was determined by using a micropattern-based single-cell transfection assay. Interestingly, the productivity of mRNAs, being defined as the amount of encoded protein produced normalized to the mRNA dose, increased with decreasing amounts of mRNA. Here the mRNA construct containing 2x3' UTR was identified as the best candidate compared to the other constructs and the control without UTRs. The mRNA construct with the combination of 2x3' CYBA UTR also resulted in the highest protein translation of the physiological protein hBMP2 in C2C12 cells. Moreover *in silico* analysis revealed that 5' CYBA UTR was not involved in any secondary structures independent of the downstream sequence. Last but not the least, the release of various cytokines and chemokines after mRNA transfection coding for hBMP2 was investigated. All mRNA constructs with and without CYBA UTRs caused a secretion of both cytokines and chemokines including IL-6 and IP-10. In spite of the inflammatory response, CYBA UTR was defined as a potential candidate for further studies to enhance translation.

Summary

Insertion of CYBA UTRs increases the mRNA productivity rather than the physical mRNA stability. The mechanisms underlying the observed increased productivity of mRNA constructs furnished with CYBA UTRs need to be investigated in further studies.

1. Zusammenfassung

In den letzten Jahren hat Boten-RNS, auch als messenger RNA (mRNA) bekannt, als Alternative zu Gentherapeutika an Bedeutung gewonnen. Im Gegensatz zu DNS, welche den Zellkern erreichen muss, um die Produktion eines therapeutischen Proteins zu erzielen, muss mRNA lediglich ins Zytoplasma einer Zelle transportiert werden und birgt damit nicht die Gefahr der insertionellen Mutagenese. Um die sogenannte "Transkript-Therapie" zu entwickeln, muss das mRNA-Molekül bezüglich seiner Stabilität und Translationseffizienz optimiert werden. Bisher sind mehrere Methoden wie der Einbau chemisch modifizierter Nukleotide, die Verlängerung des poly(A)-Schwanzes und das Einfügen untranslatierter Bereiche (UTRs) implementiert worden. Letzteres spielt eine entscheidende Rolle in der Regulation der Translation und der Stabilität eines mRNA-Moleküls.

Das Ziel dieses Projektes war es, die Translationseffizienz und Stabilität von mRNAs, welche die chemisch modifizierten Nukleotide 5-Methylcytidin und 2-Thiouridin und einen verlängerten Poly-A-Schwanz enthalten, durch Einfügen humaner zellulärer UTRs mit putativ langer Halbwertszeit zu verbessern. UTRs der humanen Gene CYBA, DECR1, GMFG, MAPBPIP und MYL6B mRNA wurden vor (5' UTR) und/oder nach (3' UTR) die kodierenden Sequenz eines Reportergens kloniert. Für jede zelluläre UTR wurden fünf verschiedene Kombinationen, nämlich 5' UTR, 3' UTR, 5' + 3' UTR, 5' + 2x3' UTR und 2x3' UTR untersucht. Alle mRNA-Konstrukte wurden mittels *in vitro* Transkription produziert und in den Zelllinien NIH3T3 und A549 getestet. Die höchste Proteinmenge im Laufe einer festgelegten Zeit, bezeichnet als „Area Under the Curve" (AUC), wiesen mRNA-Konstrukte auf, die mit 5' + 3' CYBA UTR ausgestattet worden waren, gefolgt von mRNAs mit 5' UTR und 2x3' CYBA UTR. In den folgenden Experimenten wurde die physikalische und funktionelle Halbwertzeit (HWZ) von mRNA Molekülen bewertet. Die physikalische Halbwertzeit der am besten translatierten mRNA-Kombinationen nämlich 5' CYBA, 5' + 3' CYBA und 2x3' CYBA wurde mittels qRT-PCR in beiden Zelllinien gemessen. Die funktionelle HWZ wurde verlängert, allerdings konnte keine physikalische Stabilisierung durch den Einbau von CYBA UTRs in mRNA erzielt werden. Die funktionelle Halbwertzeit wurde mit Hilfe der sogenannten „Micropattern-Based Single-Cell Array" – Methode ermittelt. Interessanterweise nahm die Produktivität von mRNAs, definiert als die Menge des produzierten Proteins pro mRNA Dosis, mit abnehmender mRNA Menge zu. Hier wurde das mRNA-Konstrukt mit 2x3' CYBA UTR als bester Kandidat im Vergleich zu den anderen Konstrukten und der Kontrolle ohne UTRs identifiziert. Neben der Testung von der Translation von Reportergenen wurde das humane Bone Morphogenetic Protein 2 (hBMP2) ausgewählt und mit CYBA UTR-Kombinationen kloniert. Das mRNA-Konstrukt mit der Kombination 2x3' CYBA UTR resultierte ebenfalls in höchster Translationseffizienz in

Zusammenfassung

C2C12 Zellen. Zudem wurden *in silico* Analysen durchgeführt mit dem Fazit, dass 5' CYBA UTR nicht in Sekundärstrukturen involviert ist, unabhängig von der nachfolgenden mRNA-Sequenz. Schließlich wurde die Sekretion von verschiedenen Zytokinen und Chemokinen nach Transfektion von humaner BMP2-mRNA in C2C12 Zellen untersucht. Alle mRNA-Konstrukte mit und ohne CYBA UTRs verursachten eine Freisetzung von Zytokinen bzw. Chemokinen wie IL-6 und IP-10. Trotz der inflammatorischen Antwort wurde CYBA UTR als ein potenzieller Kandidat für weitere Studien zur Steigerung der Translation definiert. Das Einfügen von CYBA UTRs erhöht die mRNA-Produktivität, aber nicht die physikalische mRNA-Stabilität. Die Mechanismen, die der beobachteten erhöhten Produktivität durch mRNA-Konstrukte mit CYBA UTRs zugrunde liegen, müssen in weiteren Studien untersucht werden.

Schlagwörter: zelluläre UTRs, chemisch modifizierte Nukleotide; mRNA Halbwertszeit; mRNA Produktivität, hBMP2

2. Introduction

2.1 Messenger RNA (mRNA)

2.1.1 Messenger RNA and its role in gene expression

With the discovery of messenger RNA (mRNA) by Sydney Brenner, Francis Crick, Francois Jacob and Jacques Monod in 1960, the missing mediator between DNA and protein was identified. Messenger RNA by definition is a single-stranded transcript containing the coding sequence of a given DNA gene. The life cycle of mRNA during gene expression includes several steps. Among these steps are the generation of mRNA by transcription of the double stranded DNA, translation and the mRNA decay. The first step is the transcription of DNA into the precursor mRNA by RNA polymerase II [1]. Secondly, the precursor mRNA is further processed by addition of a cap structure at the 5'-end as well as polyadenylation at the 3'-end. The precursor mRNA binds to a variety of proteins, forming a messenger ribonucleoprotein (mRNP), and to nuclear export factors which enable mRNA translocation from the cell nudeus into the cytoplasm. Next translation takes place which is the process of protein synthesis. During translation special RNAs such transfer RNA (tRNA) and ribosomal RNA (rRNA) are involved and take part in the conversion of the nucleotide sequence of a given mRNA molecule into the amino acid sequence of the protein. The role of tRNA and rRNA during protein synthesis has been described extensively in many studies [2-4]. Some parts of the mRNA are not directly translated into amino acids. Among these are the 5'- and the 3'-end of the mRNA body called untranslated regions (UTRs). Decades ago it was assumed that UTRs have no important function. Nowadays it is known that UTRs play an important role in mRNA stability, translation and mRNA localization in the cell. More details are described in section 2.1.3. The last step of the mRNA life cycle is the mRNA decay and has an impact on the mRNA stability. The mRNA degradation pathway is described in section 2.1.2.

2.1.2   mRNA decay, stability and mRNA half-life measurements

The regulation of the mRNA stability within a cell is crucial and is controlled by mRNA degradation. The mRNA degradation in the cytoplasm is a complex process and involves different enzymes. Firstly, in every eukaryotic cell mRNA decay begins mostly with a shortening of the poly(A) tail by 3' to 5' exonucleolytic deadenylation triggered by a variety of mRNA deadenlysases forming a complex. Three examples of deadenylases for instance are the Ccr4p, Pop2p and poly(A) ribonuclease nucleases (PARN) and are conserved in many eukaryota. After removing most of the poly(A) tail, the rest of the mRNA body is degraded by one of the two mRNA degradation pathways. The first pathway starts with the decapping of the mRNA from the 5'-end by decapping proteins Dcp1 and Dcp2, followed by 5'-3' exonucleolytic degradation which is catalyzed by Xrn1p. The second pathway specifies the exoribonucleolytic degradation and begins from the 3'-end to the 5'-end which is induced by a cytoplasmic exosome.

It is known that in eukaryotes nascent mRNAs have highly variable mRNA half-lives ranging from several minutes to hours [5-7]. For instance mRNA coding for β-globin is extraordinary stable and has a half-life ranging from 16 to 48 hours [8]. On the other hand, the transcript of hexokinase II is very short lived with a half-life of 1-3.6 hours [9]. A study could demonstrate that mRNA stability correlates with its structure rather than its function [10]. In case of β-globin, structural features have been identified within the 3'-UTR enabling mRNA stability. The mRNA structure and its impact on stability are described in section 2.1.3.

In order to measure mRNA half-lives, several approaches have been implemented. The first method which was used to quantify mRNA amount was Northern Blot [11]. However this kind of approach measures a certain transcript at a specific time and is time consuming. Furthermore, inhibition of transcription induces stress thereby changing the physiological state of the cell [12, 13]. Nowadays, mRNA quantification methods such as quantitative real time PCR (qRT-PCR) [14], expressed sequence tag (EST) [15], serial analysis of gene expression (SAGE) [16], DNA microarrays [17] and fluorescence labelling techniques for imaging mRNA inside cells are available. Depending on the choice of measurement the physical and the functional mRNA half-live can be distinguished. The physical half-life is a term for mRNA which measures the physical presence of mRNA molecules whereas the functional half-life is obtained by only translated mRNA [18]. A classical method of determining the physical half-life is qRT-PCR. In order to quantify the functional half-life, the protein amount of the corresponding mRNA molecule has to be measured. One example is shown by Leonhardt *et al.* describing a novel approach to determine the functional mRNA half-life by single-cell transfection study on micro-structured substrates. They postulate that mRNA delivery is predictable in terms of a two-step stochastic mathematical model. In order to prove their model, they

performed micro-structured single-cell mRNA transfection studies and measured GFP translation over time at single-cell level. Their model allows a statistical determination of onset times, protein and mRNA life times as well as degradation rates [19].

2.1.3   Messenger RNA structure and untranslated regions

mRNA stability is not solely determined by degradation pathway but also by specific response to regulatory factors which are located in the mRNA structure. The structure of an mRNA contains three major segments. These parts include the 5'-end, the coding region (cds) and the 3'-end. As mentioned before within both the 5'- and 3'-end UTRs are located and can vary in length. The median length of 5'-UTRs in vertebrates is 170 nucleotides (nt) whereas 3'-UTRs can be around 1000 nt. The 5'-end includes additionally a cap structure which is bound to the first nucleotide of the mRNA. The 3'-end also includes a poly(A) tail beside the untranslated region. UTRs are known not to affect the amino acid sequence in a protein, but rather influence the mRNA stability as well as the efficiency of translation. This is due to the regulation of mRNA stability by cis-acting factors, which are localized within the mRNA structure [20]. Examples of cis-acting elements are poly(A) tail, the AU-rich elements (AUE), iron-responsive elements (IRE) and other elements forming stem-loop structures.

The poly A-length is known to stabilize the mRNA. Some reasons why poly(A) tail seems to play an important role in mRNA stability are listed below: Many studies could reveal that mRNA degradation pathway starts firstly with the deadenylation, which implies the protective function of poly(A) tail for the mRNA [21-23]. Bernstein *et al.* could show that binding of the poly(A)-binding protein (PABP) to the poly(A) tail protects the 3'-end of the mRNA from degradation *in vitro*. Besides protecting the mRNA from degradation, the poly(A) tail is multifunctional and is also involved in nuclear processing of the precursor mRNA, nuclear export to the cytoplasm and facilitating translation [24-26]. For *in vitro* transcribed mRNA (IVT mRNA) the poly(A) tail can be added via enzymatic post-adenylation reaction or is genetically inserted in the DNA template. In case of post-adenylation the length of poly(A) is determined by the incubation time of the *Escherichia coli* poly(A) polymerase I (E-PAP) enzyme while the size is exactly determined by inserting the specific length of poly(A) tail into the DNA template.

The AU-rich elements are only located at the 3'-UTR and are known to cause instability of mRNA and their destabilizing effects were demonstrated by an experiment where AU-rich element of an unstable RNA coding for granulocyte/macrophage colony-stimulating factor (GM-CSF) was inserted into the 3'-UTR of β-

globin [27, 28]. The iron-responsive elements are located on the 5'-UTR as well as on the 3'-UTR and regulate the half-lives of mRNAs coding for ferritin and transferrin receptors. This element responds to a lack of iron which leads to binding of IRE with the iron-regulatory protein (IRP) resulting in mRNA stabilization [29-31]. Other elements such as stem-loop motives are also involved in mRNA stability. Such secondary structures are found for instance in all mRNAs encoding for histone proteins, which are involved in cell cycle regulation and chromatin formation. Histone mRNAs lack poly(A) tails and are therefore regulated mainly by motifs within the 3'-UTR [32, 33]. Further cis-acting elements which have an influence on mRNA stability are the cap-structure and motives located in the 5'-UTR. Using oocytes and cell-free reaction assays, it could be shown that capped mRNA has a longer half-life than uncapped mRNA [34-36]. Within the 5'-UTR, in particular cis-acting elements called internal ribosome entry sites (IRES) in viruses have been identified and are specified as cap-independent translational enhancers [37, 38].

Trans-acting elements in general are RNA binding proteins, which bind to the mRNA and protect from or support mRNA degradation. One example is the poly(A) binding protein (PABP). Another RNA binding protein is tristetraprolin (TTP) which regulates the mRNA stability of GM-CSF and tumor necrosis factor (TNF) [39]. Last not but the least, some observations revealed that the coding region of the mRNA itself has also impact on the mRNA half-life by the attachment of RNA-binding proteins to the mRNA sequence.

Furthermore regulation of mRNA stability is also depending on the localization and differentiation status of cells. For instance, it has been shown that histone mRNA stability is responsible that histone production is restricted only to the S-phase [40].

Introduction

Taken together all segments of the mRNA can either enhance or decrease mRNA stability or translation. UTRs play a pivotal role in mRNA stability and translational efficacy and are known to influence translational initiation, termination and mRNA stabilization as well as intracellular localization through their interaction with RNA binding proteins. So far genome wide analysis of mRNA half-lives have been explored in murine NIH3T3 cells, human B-lymphocytes, HepG2, the primary fibroblast cell line Bud8, C2C12 mouse muscle cells, pluripotent and differentiating mouse embryonic stem cells [10, 41-44].

Recently, data on mRNA half-lives and the corresponding UTR sequences have been published [10, 45]. Five cellular UTRs from human genes, which displayed long mRNA half-life in mouse embryonic stem cells are listed as follows: Firstly, the gene coding for 2-4-dienoyl-CoA reductase (DECR1), whose mRNA is found in mitochondria, has an mRNA half-life of 7.1 hours. Within the 5' and 3' DECR1 UTR, a single small nucleotide polymorphism (SNP) is localized. Additionally a polyadenylation signal (PAS) is also located in the 3' DECR1. The glia maturation factor, gamma (GMGF) has an mRNA half-life of 24 hours and contains an upstream open reading frame (uORF) in the 5'-UTR as well as a PAS region in the 3'-UTR. Upstream open reading frames are involved in regulating translation by inhibiting the translation of the downstream main open reading frame (ORF) [46, 47]. GMFG protein is predominantly expressed in lung, heart, and placenta. The other mRNA transcripts are the mitogen-activated protein-binding protein-interacting protein (MAPBPIP), located ubiquitously in late endosomes and lysosomes and the myosin, light chain 6B (MYL6B), located in smooth muscle and non-muscle. Both MAPBPIP and MYL6B transcripts include a PAS region in the 3'-UTR and have an mRNA half-life of 9.8 and 8.4 hours, respectively. Last but not the least, one of them with particular long mRNA half-life are the UTRs of the human cytochrome b-245 alpha polypeptide (CYBA) gene. According to the UTR-database, while no regulatory motives are known for the CYBA 5'-UTR unit, the CYBA 3'-UTR contains two of them. Firstly, the PAS element, which interacts with the cytoplasmic polyadenylation element binding protein (CPEB), as well as with the cleavage and polyadenylation signaling factor (CPSF). CPEB is responsible for the prolongation of the poly(A) tail in the cytoplasm, whereas CPSF primes the pre-mRNA through cleavage at a specific site for the upcoming addition of poly(A) [48, 49]. The second regulatory motif within the CYBA 3'-UTR is the insulin 3'-UTR stability element (INS_SCE). The INS_SCE sequence has been shown to bind to the polypyrimidine tract binding protein (PTB) under reducing conditions, increasing the mRNA half-life of insulin [50]. CYBA mRNA transcript is found in many cell lines tested, including phagocytes, hepatic cells, endothelial cells, B cells, and erythroleukemic cells, but the 22-kD protein was barely detectable in the non-phagocytic cells. The mRNA half-life of CYBA is about 24 hours. All UTRs of CYBA, DECR1, GMFG, MAPBPIP and MYL6B are shown in Table 4.

As mentioned before, mRNA stability is also depending on translation. It is known that the 5' cap interaction with the 3' poly(A) tail results in circularization of mRNA [51, 52]. Thus, the circular shape of the mRNA increases the initiation rate of ribosomes resulting in increased translation and also protects mRNA against degradation. Proteins involved in holding the 5'-end and poly(A) tail together are a cap-binding protein complex eIF4F consisting of eukaryotic initiation factor 4E (eIF4E), eIF4E, eIF4G as well as eIF4A. The eIF4G is the responsible molecule for the binding to the PABP located on the poly(A) tail [53-55]. Stable secondary structures close to the cap can inhibit translation without changing the physical mRNA-half life. This effect is described in the following section.

2.1.4 mRNA secondary structures in 5'-end affecting translation and stability

Two major structures have been identified within the 5'-end including the cap structure and the 5'-UTR. Both cap and 5'-UTR are crucial for translation and stability. On the one hand initiation of translation starts at the 5' –methyl-G cap, where it is bound by the initiation factor eIF4E followed by forming an eIF4E initiation complex. Subsequently, the binding site of the pre-initiation complex is exposed and the 40S complex scans along the mRNA until it reaches the initiation codon by unwinding secondary structures [56-58]. Therefore the interaction of the eIF4E complex with the 40S complex is crucial for ribosomal binding and determines the translation initiation [48, 59]. This interaction can be hindered by structural barriers such hairpin structures within the 5'-end blocking ribosomal binding [60, 61]. Kozak *et al.* showed that inserting different hairpin structures with defined thermal stability (ΔG) into the 5'-UTR as well as the distance of cap-hairpin structure have an eminent influence in the translational outcome in Cos7 cells. For instance hairpin structures with a thermal stability of -30 kcal/mol have no influence on translation whereas hairpin structures with ΔG of -50 kcal/mol reduced translation drastically [62]. Babendure *et al.* could further show that high GC content, which is highly structured, negatively influences the translational efficiency in live cells, independent of thermal stability and cap-hairpin distance [63]. In general, long 5'-UTRs imply a higher risk of GC richness thereby increasing the potential of higher amount of secondary structures which reduce translational efficiency [64, 65].

In order to be able to determine secondary structures and their functional impact, analysis of the mRNA sequence and its secondary structures, which is the folded molecule in terms of paired bases, is performed by *in silico* analysis specifying the Gibbs-minimum free energy (ΔG). The assumption is that secondary structures are influencing the mRNA stability and can be therefore picked as a value for mRNA stability. For the prediction of secondary structures of RNA molecules two platforms are available, which are statistical techniques or the calculation of the minimum free energy (MFE). The latter will be the main focus of this work. The final ΔG for a secondary structure is calculated from the sum of the free energies assigned to all of the formed loops and base pair stacks. mFOLD is a computer algorithm and is commonly used to predict the energetically most stable structure of a complete RNA sequence. Additionally the current computer algorithm assumes that all secondary structure configurations along the RNA sequence are possible. However, still prediction of ΔG and its impact on mRNA molecule in terms of translation is not completely solved. For instance since the translational machinery starts at the 5' cap and folding of secondary structures within the 5'-end can interfere with the translational progress, the complete RNA sequence analysis is an inappropriate method to predict the effects of the thermal stability on translation. Hughes and McElwaine postulated that the local-minimization of free energy of nucleotides and their ΔG is a better biological approach to investigate the influence of secondary structures on translation in the 5'-UTR [66]. In order to obtain these values, they started their analysis at the 5'-end of the RNA sequence and serially added ten nucleotides to the 3'-end up to 100 nucleotides into the coding region of the axin2 mRNA. For each extended RNA length the corresponding ΔG was determined by computer algorithm and plotted against the number of nucleotides. As a consequence they observed fluctuations in the ΔG, thus resulting in different secondary structures within the 5'-UTR. They claim that by investigating the RNA sequence in multiple steps, secondary structures with its true functional purpose can be determined.

2.2 messenger RNA as a therapeutic tool

In the last few years therapy approaches such as gene therapy and protein therapy, have been developed for a variety of medical indications ranging from hereditary or acquired metabolic diseases to regenerative medicine. Gene therapy has the potency to treat gene mal-function by inserting genetic material into the genome but at the same time carries the risk of insertional mutagenesis. In contrast protein therapy has less safety concerns regarding causing mutagenesis. However disadvantages of protein therapy are high immunogenic response, costs, storage, applicability and the low efficacy with delivering the protein into the target tissue. Since mRNA is known to play a central role in gene expression, it becomes more important as a new drug entity. As a consequence, scientists were eager to develop an alternative platform, so called transcript therapy. Here, mRNA is used as a therapeutic entity instead of its counterpart DNA or protein. The reasons for picking mRNA as a new drug are as follows: I) mRNA can be directly translated into a protein. II) mRNA has only to be delivered into the cytoplasm and is therefore advantageous in slowly dividing or non-mitotic cells. III) no risk of genomic integration. IV) no need of specific promoters for mRNA production which make the synthesis relatively easy and reproducible. These features make mRNA increasingly relevant as an alternative approach for gene and protein therapy. *In vitro* transcribed mRNA and its functionality were first shown by Krieg and Melton in 1984 [67]. Up to now *in vitro* transcribed (IVT) mRNA was commonly used for immunotherapeutic vaccination strategies and has been favoured to trigger an innate immune response by using naked mRNA injection, mRNA liposomes, replicative mRNA, mRNA gene gun and mRNA transfection *in vitro* and *in vivo* in antigen-presenting cells (APCs) [68-76]. An induction of immune response could be achieved by small amounts of exogenous mRNA with low amount of translation and were so successful that mRNA vaccination reached clinical trials [77-80]. All these vaccination methods are intended to induce an immune response whereas for non-immunotherapy-related applications the activation of the immune response is not desired.

In 1992 the group of Bloom could show for the first time that unmodified IVT mRNA is capable of gene replacement [81]. They injected mRNA coding for vasopressin into the hypothalamus of vasopressin-deficient rats. Another promising example for mRNA as a therapeutic agent was shown by Kormann and his colleagues. In a mouse model for surfactant protein B (SP-B) deficiency, they could successfully replace the protein by chemically modified mRNA coding for SP-B resulting in a higher life expectancy compared to untreated mice [82]. The study of Mays *et al.* used the same chemical modifications as Kormann *et al.*, including 5-methyl CTP and 2-thio UTP, for mRNA production to use their mRNA coding for treatment of asthma. In their study they could protect asthma by delivering naked FoxP3 mRNA intratracheally using high pressure spraying [83]. In the field of cancer research Okumura *et al.* could show that unmodified Bax mRNA delivered into malignant melanoma reduced the tumor size [84]. Moreover, mRNA is also used in the field of cellular reprogramming [85]. For instance, Yakubov and colleagues were able to reprogram human fibroblasts to pluripotent stem cells by using non-modified mRNA. They transfected the cells five times daily with mRNA coding for the Yamanaka factors Oct4, Lin28, Sox2 and Nanog using a lipid-based delivery system [86].

Nonetheless, two major obstacles have still to be overcome to successfully implement mRNA-mediated therapy. Firstly, the stability of mRNA has to be increased drastically to reduce repeated dosing and secondly the activation of immune system by externally delivered mRNA has to be reduced. The major aim in developing mRNA therapeutics is to achieve a therapeutic outcome without inducing an inflammatory response since it can hinder the translation of the desired protein. Therefore, scientists have developed several strategies over the past decades to overcome these obstacles and are described in the next chapter.

2.2.1   mRNA engineering

In the last few years several strategies have been implemented successfully to reduce the immune response and to increase the protein translation by externally administered mRNA into mammalian cells or living organisms. Among these are the optimization of the mRNA including modifications of the cap structure, prolonging the poly(A) tail, insertion of UTRs and inclusion of chemically modified nucleotides into the mRNA sequence during IVT and codon optimization.

The cap structure is involved in mRNA stability and enhancing translation [34, 87]. The cap consists of a 7-methylguanosine (m^7G) and is linked to the first transcribed nucleotide of the 5'-end of the mRNA via a 5' to 5' triphosphate bridge (ppp). Yet, during mRNA synthesis the cap structure can be incorporated in the reverse orientation resulting in $Gpppm^7GpN$ instead of $m^7GpppGpN$. As a consequence, the mRNA product consists of capped and reverse-capped mRNA molecules which result in low translational efficiency. To circumvent reverse orientation of the cap structure, anti-reverse cap analogs called ARCAs, such $m_2^{7,2'-O}GpppG$ and $m_2^{7,3'-O}GpppG$ are beneficial in increasing translation [88-90]. On the one hand modifications of cap-structures ensure correct mRNA capping. On the other hand other cap modifications such diastereomers capped with an ARCA phosphorothioate-substituted in the ß-position, called ß-S-ARCA, can influence the stability and translation of a given RNA molecule [91]. Furthermore, the work of Banchereau *et al.* could show that capped RNA is differently translated, depending on the cap-structure and the differentiation status of the cell [92]. They observed the highest translational efficiency and mRNA stability with RNA capped with D1 diastereomer of ß-S-ARCA in immature dendritic cells (DCs). In mature DCs instead the protein translation levels were not as pronounced as in immature DCs.

The poly(A) tail is also crucial for mRNA stability and translation. Several reports have shown the impact of the poly(A) length of IVT transcribed RNA on dendritic cells [89, 93, 94]. Holtkamp *et al.* could reveal that a poly(A) length of 120nt is beneficial to increase reporter protein translation in immature and mature DCs. In their study they generated IVT mRNA coding for enhanced green fluorescent protein (eGFP) furnished with different length of poly(A) tails ranging from 16 to 120 nucleotides. Afterwards they delivered the mRNA constructs via electroporation into immature and mature dendritic cells and measured RNA amount via qRT-PCR and protein translation. They could find enhanced RNA stability and protein amount by increasing the poly(A) length with mRNA constructs with poly(A) 120 being the most efficient construct [93]. The same group revealed that inclusion of two copies of 3'-UTRs, such as 3'-UTR of human β-globin between the coding region and the poly(A) tail of 120nt enhances translation and mRNA stability compared

to constructs with one copy of 3'-UTR or without UTR. Another example of enhancing translation by UTRs *in vivo* is shown by Kariko *et al.* In their study they used mRNA encoded for murine erythropoietin (mEpo) furnished with a 5'-UTR of the tobacco etch virus and the 3'-UTR of *Xenopus leavis* β-globin [95]. Thus, the insertion of certain UTRs can be beneficial in term of translation and mRNA stability. The use and selection of UTRs as translational enhancer are based on knowledge of the mRNA half-lives rather than being experimental-tested by *in vitro* or *in silico* measurements.

As mentioned before chemically modified nucleotides are another opportunity to optimize mRNA and have been shown to enhance translation and are capable of reducing the immune response. This was shown by Kormann *et al*. where the replacement of 25% of uridine and cytidine residues by 2-thiouridine and 5-methyl-cytidine enabled prolonged protein translation over time as well as the reduction of the immune response [82]. To prove the functionality of their mRNA, they injected mRNAs coding for murine mEpo, which were furnished with a poly(A) tail of 120nt and ARCA cap as well as containing the double chemical modification, intramuscularly and observed higher mEpo levels compared to unmodified mRNA. Additionally they observed that chemically modified mEpo mRNA was binding less to pattern recognition receptors (PRRs) resulting in reduced immune activation. Even better results were shown by Kariko *et al* in 2012 showing no detection of inflammatory cytokines *in vivo*. In their study they used IVT mRNA containing pseudouridine or uridine instead of 2-thiouridine and purified the IV-transcribed mRNA via high-performance liquid chromatography (HPLC) [95].

Finally, codon optimization of the coding region has itself a strong impact on translational efficiency [96, 97]. For instance Al-Saif and Khabar could show that reduction of UA and UU (*UW*) dinucleotides in the coding region resulted in increased protein translation and mRNA stability. Other studies were focusing on replacement of A/U rich regions, which are known to destabilize the mRNA, by G/C nucleotides [98].

2.2.2   mRNA immunogenicity

After transfection, the mRNA is recognized by so-called pattern recognition receptors (PRRs). Among this PRR family are the Toll-like receptors- (TLR), the cytoplasmic retinoic-acid-inducible gene I (RIG-I)-like receptors (RLRs) and the NOD-like receptors (NLRs).

The TLRs are predominantly expressed in immune cells and are transmembrane receptors consisting of extracellular leucine-rich repeats and a signal-transduction or Toll/interleukin (IL)-1 domain in the cytosolic region. The TLRs, which are involved in the recognition of single-stranded RNA (ssRNA) are TLR-7 and -8 and are located in the endosome [99, 100].

This activation of immune cells is followed by high cytokine secretion, but low expression of co-stimulation factors such as CD86 by APCs [101]. The interaction between the TLRs and ssRNA activates downstream signaling pathways via adaptor molecules such as the myeloid differentiation primary response gene 88 (MyD88) [102]. As a consequence, transcription factors including the nuclear factor-κB (NF-κB) and interferon regulatory factor (IRF)3 and IRF7 translocate from the cytoplasm to the nucleus and bind to type I interferon (IFN) gene promoter. This induces the expression of IFN-α and IFN-β and pro-inflammatory cytokines including Il-6, IL-12 and tumor necrosis factor α (TNF-α) triggered by NF-κB activation [102, 103]. Noteworthy, double-stranded RNA (dsRNA) or secondary structures formed by mRNA such hairpins bind to TLR-3 receptors and activate downstream signalling via TIR-domain-containing adaptor-inducing IFN-β (TRIF) resulting in interleukin (IL)-8 secretion [104-106]. The other family of PRRs is the RIG-I-like receptors (RLRs) including RIG-I, melanoma differentiation-associated protein 5 (MDA5) and laboratory of genetics and physiology 2 (LGP2). Both receptors, the RIG-I and MDA5, are described in detail elsewhere [107].

The ssRNA can be also detected by NOD2 receptors whereas dsRNA is recognized by NLRP3 in the cytoplasmic compartment. Both receptors belong to the family of NOD-like receptors (NLRs) [108, 109].

However, not only the mRNA itself but depending on the delivery cargo complexed with or without the IVT mRNA can trigger an immune response, which is also an important aspect in developing mRNA therapeutics. Details in mRNA delivery are described in the next chapter 2.2.3.

2.2.3   mRNA delivery

The successful delivery of a nucleic acid into the target tissue is another crucial aspect for any kind of disease treatment. Up to now many strategies have been developed to deliver nucleic acids into target cells. Among these are viral and non-viral delivery systems. The latter will be the main focus of this thesis. Delivery systems for DNA have been studied extensively. However, studies could reveal that not more than 10% of non-virally delivered pDNA reaches the nucleus [110, 111]. The delivery of mRNA would be a better alternative to enhance the efficacy of non-viral vectors, since mRNA has only to enter the cytoplasm. So far, few methods have been explored for mRNA delivery. These can be subdivided in two different categories namely the disruption of the cell membrane by physical forces or by using cationic carries. Among the physical delivery methods of mRNA are microinjection, electroporation, gene gun and hydrodynamic injection. The first report of a successful mRNA delivery into oocytes using microinjection was published in 1977 [112]. Electroporation is widely used for vaccination purposes. One of the most successful examples is the electroporation of DCs with mRNA coding for prostate specific antigen in tumor vaccination and has already been tested in clinical trials [113]. However, the electric field and duration of the applied voltage has to be chosen carefully to avoid severe irreparable damage to cells resulting in death as well as the accessibility of other organs for electroporation is limiting [114]. The gene gun or biolistic delivery system is successfully used for *in vitro* and *in vivo* applications of different cell types and indicates a huge potential in the application of wound healing, determining mRNA half-life and mRNA vaccination [115-117]. The use of hydrodynamic pressure enables nucleic acid transfer by rapidly injecting a large volume into a blood vessel. Thereby protein translation was mainly measured in the liver with low amounts of transgene expression in other organs such lung and spleen [118].

The other subgroup for mRNA delivery is the use of cationic carriers such polymers and liposomes. It has been shown that cationic carriers condense mRNA into small particles and protect the mRNA against degradation [119]. The complexation of the nucleic acid, both DNA and mRNA are negatively charged, with the cationic carriers occurs via simple electrostatic interaction [120]. Finally the complexes are slightly positively charged allowing an interaction with the negatively charged cell surface resulting in uptake of the particles via endocytosis into the cell [110, 121]. Up to now, many studies have been performed using liposomes and polymers *in vitro* and *in vivo*. It has been observed that cationic lipids resulted in much better transfection efficiency *in vitro* but with slightly higher toxicity compared to cationic polymers [122]. Commercially available transfection agents such Lipofectamine® are liposomal formulations and are also used for mRNA delivery resulting in 90% GFP translation for up to 8-9 days post-transfection. Nonetheless,

differences in peak expression and duration between plasmid DNA (pDNA) and mRNA delivery are still observed [89, 123].

In vitro transfection efficiency is also dependent on the amount of lipoplexes or polyplexes on the cell surface. The complexes are reaching the cells by diffusion. Diffusion itself is a slow and ineffective process for some transfection protocols resulting in inefficient cell-complex contact yielding low expression levels with no physiological outcome. The frequency of cell-complex attachment can be enhanced by increasing the dose, but that leads to higher cell toxicity [124, 125].

An alternative method called magnetofection is capable of circumventing the diffusion problem. Magnetofection describes the delivery of nucleic acid associated with magnetic nanoparticles under the influence of a magnetic field. In case of lipoplex or polyplex transfection protocols, small particles attach to the cell membrane by diffusion, which takes couple of hours, whereas magnetic complexes sediment by applying a magnetic field thereby accelerating and synchronizing transfection of cells within minutes. The concept and techniques of magnetofection have been described elaborately in many other studies [126-129]. This method has been proven to be effective *in vitro* and *in vivo* [124, 130, 131]. The complexation of magnetic nanopartides with the nucleic acid or viral delivery systems is achieved by electrostatic interaction, biotin–streptavidin or antigen–antibody interactions [124, 132-134]. Different magnetic particles are available commercially. Several studies have shown that magnetofection achieves a high reproducible transfection efficiency and improve dose-response kinetics in numerous cell types induding cells which are difficult to transfect [128]. Magnetofection is intensely explored with pDNA while its impact on mRNA delivery is not fully explored yet.

mRNA delivery through physical disruption of the cell membrane such as microinjection and electroporation are known not to activate endosomal RNA receptors, while the usage of cationic carrier systems results in the stimulation of the immune response [135]. Moreover, it has been revealed that carrier without mRNA complexation showed an immune response alone [136]. For instance Lipofectamine® has been shown to induce pro-apoptotic and pro-inflammatory molecules via activation of intracellular immune pathways [137].

2.3 Bone regeneration

2.3.1 Clinical relevance of bone injuries

The second part of my thesis deals with bone regeneration. In general, fractures in wrist (radius), hip and upper humerus in men and women are the most common bone injuries with the highest incidence rate caused by osteoporosis [138]. Osteoporosis by definition is the loss of bone mass resulting in a higher bone fracture risk. Current therapies for bone fractures are based on invasive or non-invasive treatment. Treatments such as internal and external fixation, bone grafting and amputation belong to the invasive treatment and mostly require a second surgical intervention to stabilize the fracture and stimulate bone regeneration. In contrast to invasive therapies, non-invasive treatments are hormone-based including parathyroid hormone (PTH), such teriparatide, and bisphosphonates and can be also administered preventitatively [139]. Both therapies are associated with high healthcare-costs and time-lasting healing process. Therefore, modern biotechnologies are aiming to develop treatments to accelerate bone healing.

2.3.2 Bone healing

Bone healing is a complex process and involves different cell types including fibroblasts, macrophages, osteoblasts, osteoclasts as well as the expression of different factors such as growth factors and transcription factors at the right time and place. In 1975, Cruess and Dumont postulated three phases during bone fracture healing [140]. These phases are the inflammatory phase, reparative phase and the remodelling phase. The processes are described in detail elsewhere [141-143]. As mentioned earlier, during bone healing growth factors, cytokines, prostaglandins, hormones and growth factor antagonists are involved. Growth factors are transforming growth factors (TGF), bone morphogenetic proteins (BMP), fibroblast growth factors (FGF), platelet-derived growth factors (PDGF) and insulin-like growth factors (IGF).

Introduction

The human body experiences everyday small bone microcracks and is capable to regenerate such bone defects on its own. However, the capability of the bone to repair large bone fractures is limited and needs support from outside. One way to cope with bone healing of larger defects is by using implants. However, surgeries are mostly technically challenging with a suboptimal outcome for the patients. Therefore new skeletal reconstructive strategies have been implemented such as stem cell-based therapy with and without scaffolds including growth factors enabling bone healing. In the last 30 years, clinical trials have been conducted with autologous mesenchymal stem cells (MSCs) injection into the long bones [144, 145]. These studies could show that local application of the MSCs into the bone defect was a safe approach. However, these studies could not show any improvement in bone healing compared to conventional methods. In contrast, Marcacci *et al.* could show that the combination of isolated MSCs from patients with scaffolds, in particular hydroxyapatite scaffolds lead to good integration of the implant into the large bone defect without secondary fractures [146]. The biological mechanism underlying the transplantation of MSCs embedded in a bioactive material is not completely understood.

Further concepts of treatment are the inclusion of growth factors to initiate proliferation and differentiation of the MSC-derived cells. Few recombinant growth factors have been already in clinical trials and are FDA-approved like the recombinant human BMP2 [147, 148]. Human BMP2 is an active molecule mediator for starting the regenerative process. It has been shown that human BMP2 is involved in the endochondral bone formation in segmental defects and is known to increase the proliferation of immigrating cells. Moreover, hBMP2 is also one of the most potent growth factors in osteoblastic differentiation and is the earliest gene to be induced [149]. The use of recombinant hBMP2 is restricted mainly due to the high costs [150, 151].

Other approaches for bone healing are gene therapies, in particular viral gene delivery using retroviral, adenoviral or lentiviral vectors and are more stable and efficient compared to non-viral gene therapy systems [152, 153]. However, it is known that viral gene therapies imply several safety concerns such as insertional mutagenesis and immune response to viral coat proteins. Thus, the delivery of mRNA as gene replacement would be a better choice, since it has to be delivered only into the cell cytoplasm and could also achieve an earlier onset of protein translation in slowly dividing cells or non-mitotic cells compared to pDNA. This novel approach, called transcript therapy, has been shown to be a promising alternative in a variety of diseases [82, 95, 154]. For instance Zangi and colleagues could show that using modified mRNA has the potential to induce vascular regeneration after myocardial infarction [155]. One future approach could be the transfection of mRNAs coding for hBMP2 in MSCs resulting in proliferation and osteogenic

differentiation without causing any insertional mutagenesis or excessive bone formation. One study already could show that mRNA can be successfully be delivered to induce osteogenic differentiation [156].

3. Aims and Objectives

Summarizing the previous chapters, the state of knowledge in the field has been that using chemically modified nucleotides for mRNA production can yield mRNAs that are less immunogenic but translationally more active than unmodified mRNAs. Furthermore it has been known that UTRs and elements within UTRs have a profound impact on mRNA stability and translation in cells and that the length of the poly(A) tail has a particular impact on the rate of mRNA decay.

The aim of this thesis was to generate mRNAs featuring high levels and persistence of translation inside cells combined with low immunogenicity.

A first hypothesis underlying this thesis was that the stability of known long-lived mRNAs is conferred by their UTRs and would be a feature that can be conveyed to foreign coding sequences of any gene. A second hypothesis of this thesis was that combining UTRs of long-lived mRNAs with chemical modification of mRNA and a substantially long poly(A) tail ought to yield mRNA species with significantly advantageous properties in terms of level and persistence of translation, in other words in terms of mRNA productivity compared with mRNA lacking such UTRs.

The aim of this thesis should be achieved according to the following objectives:

- Cloning of reporter mRNA constructs furnished with different cellular UTRs. Among these were CYBA, DECR1, GMFG, MYL6B and MYL6B which were to be cloned upstream and/or downstream of the coding region. Additionally, for each cellular UTR five different combinations were to be generated containing 5' or 3' UTR alone, 5'+3' UTR, 5' with two copies of 3' UTR and 2x3' UTR

- Identification of the best mRNA constructs by determining the highest peak translation over time, called area under the curve (AUC) after transfection of all mRNA combinations in NIH3T3 and A549 cells

- Investigation of the physical and functional mRNA half-lives as well as the mRNA productivity of the best working mRNA constructs

- Validation of the impact of secondary structure in the 5'-end on translational initiation via *in silico* analysis

- Investigation of chemically modified hBMP2 mRNA furnished with the best cellular UTR in C2C12 cells

- Validation of cytokine and chemokine release after transfection in cell culture supernatants triggered by mRNA encoding hBMP2

4. Materials & Methods

4.1 Materials

4.1.1 Cell lines and culture medium

Table 1: List of cell lines used and its media as well as their providers

Cell line	Source	Provider	Culture medium
A549	human alveolar adenocarcinoma cell line	ATCC, Wesel (Germany)	MEM supplemented with 10% fetal bovine serum (FBS) and 1% Penicillin/Streptomycin
C2C12	murine muscle myoblast cell line	Sigma Aldrich, Steinheim (Germany)	DMEM, 10% FBS and 1% Penicillin/Streptomycin
Huh7	human hepatoma epithelial cell line	Kindly provided by AG Wagner (LMU)	DMEM with 10% FBS and 1% Penicillin/Streptomycin
NIH3T3	murine fibroblast cell line	ATCC, Wesel (Germany)	DMEM, 10% FBS and 1% Penicillin/Streptomycin

4.1.2 Plasmid vectors and Primers

Table 2: List of all plasmids, which were used for mRNA production and their providers

Cloned plasmids are described in section 4.2 (Cloning). Plasmid vectors have a poly A-tail of 90nt unless stated otherwise.

Nr.	Name	Type	Provider
1	pVAX1-A-tail MetLuc	DNA-plasmid	GeneArt, Regensburg (Germany)
2	pVAX1-A-tail MetLuc 5' CYBA	DNA-plasmid	Eurofins MWG Operon, Ebersberg (Germany)
3	pVAX1-A-tail MetLuc 5' DECR1	DNA-plasmid	Eurofins MWG Operon, Ebersberg (Germany)
4	pVAX1-A-tail MetLuc 5' GMFG	DNA-plasmid	Eurofins MWG Operon, Ebersberg (Germany)
5	pVAX1-A-tail MetLuc 5' MAPBPIP	DNA-plasmid	Eurofins MWG Operon, Ebersberg (Germany)
6	pVAX1-A-tail MetLuc 5' MYL6B	DNA-plasmid	Eurofins MWG Operon, Ebersberg (Germany)
7	pVAX1-A-tail MetLuc 5'+3' CYBA	DNA-plasmid	Eurofins MWG Operon, Ebersberg (Germany)
8	pVAX1-A-tail MetLuc 5'+3' DECR1	DNA-plasmid	Eurofins MWG Operon, Ebersberg (Germany)
9	pVAX1-A-tail MetLuc 5'+3' GMFG	DNA-plasmid	Eurofins MWG Operon, Ebersberg (Germany)
10	pVAX1-A-tail MetLuc 5'+3' MAPBPIP	DNA-plasmid	Eurofins MWG Operon, Ebersberg (Germany)
11	pVAX1-A-tail MetLuc 5'+3' MYL6B	DNA-plasmid	Eurofins MWG Operon, Ebersberg (Germany)
12	pVAX1-A-tail MetLuc 3' CYBA	DNA-plasmid	cloned, Planegg (Germany)
13	pVAX1-A-tail MetLuc 3' DECR1	DNA-plasmid	cloned, Planegg (Germany)
14	pVAX1-A-tail MetLuc 3' GMFG	DNA-plasmid	cloned, Planegg (Germany)
15	pVAX1-A-tail MetLuc 3' MAPBPIP	DNA-plasmid	cloned, Planegg (Germany)
16	pVAX1-A-tail MetLuc 3' MYL6B	DNA-plasmid	cloned, Planegg (Germany)
17	pVAX1-A-tail MetLuc 5'+2x3' CYBA	DNA-plasmid	cloned, Planegg (Germany)
18	pVAX1-A-tail MetLuc 5'+2x3' DECR1	DNA-plasmid	cloned, Planegg (Germany)
19	pVAX1-A-tail MetLuc 5'+2x3' GMFG	DNA-plasmid	cloned, Planegg (Germany)
20	pVAX1-A-tail MetLuc 5'+2x3' MAPBPIP	DNA-plasmid	cloned, Planegg (Germany)
21	pVAX1-A-tail MetLuc 5'+2x3' MYL6B	DNA-plasmid	cloned, Planegg (Germany)
22	pVAX1-A-tail MetLuc 2x3' CYBA	DNA-plasmid	cloned, Planegg (Germany)
23	pVAX1-A-tail MetLuc 2x3' DECR1	DNA-plasmid	cloned, Planegg (Germany)
24	pVAX1-A-tail MetLuc 2x3' GMFG	DNA-plasmid	cloned, Planegg (Germany)
25	pVAX1-A-tail MetLuc 2x3' MAPBPIP	DNA-plasmid	cloned, Planegg (Germany)

26	pVAX1-A-tail MetLuc 2x3' MYL6B	DNA-plasmid	cloned, Planegg (Germany)
27	pVAX1-A120 d2EGFP	DNA-plasmid	cloned, Planegg (Germany)
28	pVAX1-A120 d2EGFP 5' CYBA	DNA-plasmid	cloned, Planegg (Germany)
29	pVAX1-A120 d2EGFP 3' CYBA	DNA-plasmid	cloned, Planegg (Germany)
30	pVAX1-A120 d2EGFP 5'+3' CYBA	DNA-plasmid	cloned, Planegg (Germany)
31	pVAX1-A120 d2EGFP 5'+2x3' CYBA	DNA-plasmid	cloned, Planegg (Germany)
32	pVAX1-A120 d2EGFP 2x3' CYBA	DNA-plasmid	cloned, Planegg (Germany)
33	pVAX1-A-tail hBMP2	DNA-plasmid	cloned, Planegg (Germany)
34	pVAX1-A-tail hBMP2 5' CYBA	DNA-plasmid	cloned, Planegg (Germany)
35	pVAX1-A-tail hBMP2 3' CYBA	DNA-plasmid	cloned, Planegg (Germany)
36	pVAX1-A-tail hBMP2 5'+3' CYBA	DNA-plasmid	cloned, Planegg (Germany)
37	pVAX1-A-tail hBMP2 5'+2x3' CYBA	DNA-plasmid	cloned, Planegg (Germany)
38	pVAX1-A-tail hBMP2 2x3' CYBA	DNA-plasmid	cloned, Planegg (Germany)

Table 3: Lists all primers and their melting temperature as well as their application

Two primer sets for full length MetLuc (FL-MetLuc) were designed. Primer set 1 (FL1-MetLuc) binds to mRNA constructs furnished 5' CYBA UTR and the control without UTRs. Primer pair FL2-MetLuc binds solely to mRNAs including 5'+3' CYBA UTRs and two copies of 2x3' UTR

Name	Forward Sequence (5'-3' end)	Reverse Sequence (5'-3' end)	Usage	Tm (°C)
hBMP2	ATCGCTAGCGGATCCGCCACCATGGTC GCCGGCACCAG	GCTGAATTCTCATCTACAGCCACAG CCTTCC	PCR- cloning	60
MetLuc	aatggaagccaacgccttca	ttggcggtgcacttgatctt	qRT-PCR	60
FL1- MetLuc	gagacccaagctggctagcgt	tgcagaattctcatctgtcgccg	qRT-PCR	60
FL2- MetLuc	gagacccaagctggctagcgt	tgcagaatcccggcttcgctg		
d2EGFP	caaccactacctgagcaccc	gtccatgccgagagtgatcc	qRT-PCR	60
hBMP2	agctcatttcaccaccggat	acgtcgaagctctcccatct	qRT-PCR	60

4.1.3   Untranslated regions (UTRs) sequences

UTRs were selected from the human genes CYBA, DECR1, GMFG, MAPBPIP and MYL6B, featuring long mRNA half-lives [10, 45]. The sequences of 5' and 3' untranslated regions of each cellular gene were obtained from the UTR database (http://utrdb.ba.itb.cnr.it/search). The sequences and special features of each UTR are listed in Table 4.

Table 4: Summary of selected human cellular UTRs

Sequences and features of selected UTRs. A polyadenylation signal (PAS, bold) is located in every 3' UTR region of each of the cellular genes. CYBA UTR has furthermore an insulin 3'UTR stability element (INS_SCE, underlined) and the 3' UTR of DECR1 contains a small nucleotide polymorphism (SNP, big letters). In the 5' UTR region, DECR1 indicates another SNP and the 5' UTR of GMFG includes an upstream open reading frame (uORF, cursive). In all the other UTRs no known 5' UTR regions could be identified.

UTRs	Human UTR Sequences [from 5' to 3']		Features	
	5' UTR	**3' UTR**	**5' UTR**	**3' UTR**
CYBA	cgcgcctagcagtgtcccagccgggttcgtgtcgcc (36bp)	cctcgccccggacctgccctcccgccaggtgcacccacctgcaataaatgcagcgaagccggga (64bp)	-	INS_SCE; PAS
DECR1	acGccgcctgggtcccagtccccgtcccatccccggcggcctaggcagcgtttccagccccgagaactttgttcttttttgtcccgcccccctgcgcccaAccgcctgcgccgccttccggcccgagttctggagactcaac (141bp)	Gaccactttggccttcatcttggttacagaaaagggaatagaaatgaaacaaattatctctcatcttttgactatttcaagtctaataaattcttaattaac (102bp)	SNP (rs67780505; rs72368577)	PAS; SNP (rs7162)
GMFG	gttgg*atgaaaccttcctcctactgcacagcccgcccccctacagccccggtccccacgcctagaagacagcggaactaa*gaaaagaagaggcctgtggacagaacaatc (110bp)	tctctgggctggggactgaattcctgatgtctgagtcctcaaggtgactggggacttggaaccccctaggacctgaacaaccaagactttaaataaattttaaaatgcaaaaactcgga (118bp)	uORF;	PAS
MAPBPIP (ROBLD3)	ggtggggcggggtttgagtcggaaccacaatagccaggcgaagaaactacaactcccagggcgtcccggagcaggccaacgggactacgggaagcagcggggcagcggccccgcgggaggcacctcggagatctgggtgcaaaagcccagggttaggaaccgtaggc (164bp)	cggcattggtggaagctgggggtcagaaaagagaaatgaccatttggagggcgggcctcctagaagaaccttcttagacaatggggggaggatgggactttgttttttccaagaataaacttcaactcctgtcatgtg (139bp)	-	PAS
MYL6B	ggccaccggaattaacccttcagggctgggggccgcgctatgccccgccccctccccagcccagacacggaccccgcaggagatgggtgccccccatccgcacactgtcctttggccaccggacatc (127bp)	gtgctgcagatccagtggggtccggacactgggccccgcaggcgaaagcacgttccagccaccaggaggccacctattgtttcaaaataaagactgggttcctctcttggtttca (115bp)	-	PAS

4.1.4 Chemicals and Reagents

Table 5: Chemicals and reagents

All chemicals and reagents are listed in alphabetic order.

Substance	Concentration/Purity	Provider
2x RNA loading dye	2x	Thermo Scientific, Waltham (USA)
6x loading dye	6x	Thermo Scientific, Waltham (USA)
Agarose Standard	Molecular Biology grade?	Carl Roth, Karlsruhe (Germany)
Coelenterazin native	10mg	Synchem, Felsberg (Germany)
Disodium-hydrogenphosphate	≥99 % pure	Carl Roth, Karlsruhe (Germany)
DMEM (1x) + GlutaMax™	1x	Gibco® Life Technologies, Darmstadt (Germany)
dNTP Mix	10x	Fermentas, Darmstadt (Germany)
DreamFect Gold™		OZ Bioscience, Marseille (FR)
Dulbecco's PBS without Ca^{++} and	1x	Gibco® Life Technologies, Darmstadt

Materials

Mg^{++}		(Germany)
DuoSet®ELISA hBMP2	-	R&D Systems, Minneapolis (USA)
Ethidiumbromide solution	0.0025%	Carl Roth, Karlsruhe (Germany)
ElectroMAX^{TM} DH10B^{TM} cells	-	Invitrogen^{TM}, Darmstadt (Germany)
Fetal bovine serum (FBS)	100%	Gibco® Life Technologies, Darmstadt (Germany)
First Strand cDNA Synthesis Kit		Thermo Scientific, Waltham (USA)
1 kb DNA Ladder	50µg	Plasmid Factory, Bielefeld (Germany)
100 bp DNA Ladder	50µg	Plasmid Factory, Bielefeld (Germany)
Glycerol for molecular biology	≥99% pure	Sigma Aldrich, Steinheim (Germany)
Kanamycinsulfat	5g	Carl Roth, Karlsruhe (Germany)
LB-Medium (Luria/Miller)	1kg	Carl Roth, Karlsruhe (Germany)
Lipofectamine^{TM} 2000 Reagent	-	Invitrogen^{TM}, Darmstadt (Germany)
MEM, GlutaMAX™ Supplement	1g/L	Gibco® Life Technologies, Darmstadt (Germany)
Methanol	≥ 99.5 % pure	Carl Roth, Karlsruhe (Germany)
Mouse IFN-alpha Simplex	-	Affymetrix-eBioscience, Wien (AT)
Mouse IFN-gamma Simplex	-	Affymetrix-eBioscience, Wien (AT)
Mouse IL-1 beta Simplex	-	Affymetrix-eBioscience, Wien (AT)
Mouse IL-2 Simplex	-	Affymetrix-eBioscience, Wien (AT)
Mouse IL-6 Simplex	-	Affymetrix-eBioscience, Wien (AT)
Mouse IL-10 Simplex	-	Affymetrix-eBioscience, Wien (AT)
Mouse IL-10/CXCL10 Simplex	-	Affymetrix-eBioscience, Wien (AT)
Mouse IL-12p70 Simplex	-	Affymetrix-eBioscience, Wien (AT)
Mouse MCP-1/CCL2 Simplex	-	Affymetrix-eBioscience, Wien (AT)
Mouse TNF-alpha Simplex	-	Affymetrix-eBioscience, Wien (AT)
NucleoBond® Xtra Midi / Maxi	-	Macherey Nagel, Düren (Germany)
NucleoSpin® Gel & PCR Clean up	-	Macherey Nagel, Düren (Germany)
NucleoSpin® RNA kit	-	Macherey Nagel, Düren (Germany)
NucleoSpin® Plasmid	-	Macherey Nagel, Düren (Germany)
Penicillin/Streptomycin	100x	Gibco® Life Technologies, Darmstadt (Germany)
ProcartaPlex mouse basic kit	-	Affymetrix-eBioscience, Wien (AT)
RiboMax Large Scale RNA production System-T7	-	Promega, Madison (USA)
RiboRuler High Range RNA Ladder	-	Thermo Scientific, Waltham (USA)
Rotiphorese 50x TAE Puffer	50x	Carl Roth, Karlsruhe (Germany)
Sodium-dihydrogenphosphate	≥98% pure	Carl Roth, Karlsruhe (Germany)
SoMag5	15,8 mg/ml	Kindly provided by O.Mykhaylyk
SoMag6-115	1 mg/ml	Kindly provided by O.Mykhaylyk
Sso Advanced^{TM} Universal SYBR®Green Supermix	-	BIO-RAD, Steinheim (Germany)
TACS® MTT cell proliferation assay	-	Trevigen®, Gaithersburg (USA)
Trichlormethan/Chloroform	≥ 99.9 %	Carl Roth, Karlsruhe (Germany)
Trypanblue solution	(0.4%)	Sigma Aldrich, Steinheim (Germany)
Trypsin-EDTA	1x	Gibco® Life Technologies, Darmstadt (Germany)
Water for injection	-	Braun, Melsungen (Germany)

4.1.5 Buffers and Media

Preparation of 0.05 M Sodiumphosphate buffer (pH 7.0)

Firstly a 0.1 M sodiumphosphate solution was generated by mixing 29.9 ml of 1 M Na_2HPO_4 and 21.1 ml of 1 M NaH_2PO_4, adjusted to a pH of 7.0 and filled up to 500 ml with water for injection. To generate a 0.05 M sodiumphosphate buffer, a 1:2 dilution by mixing 0.1 M sodiumphosphate buffer with water was prepared.

Preparation of 50 mM coelenterazin working solution

Coelenterazin with a working concentration of 50 mM was produced as follows: A stock solution of 10mg/ml Coelenterazin was prepared in methanol. To prepare the working solution, 10 μl of the stock was transferred to a 15 ml Falcon tube (protected from light) to which 4.723 ml of 0.05 M degased sodiumphophate buffer (pH 7.0) was added. Degasing of the buffer was conducted by using an ultrasound bath for 10 minutes. The 50 mM coelenterazin working solution was stored at -20°C and kept on ice during usage.

Preparation of DMEM or MEM complete media

In order to prepare 500 ml DMEM or MEM complete media, 50 ml of the media without supplements were removed out of the bottle and replaced by 50 ml FBS (10% FBS in total) and 5 ml Pen/Strep solution (1% in total), respectively. The complete media were stored at 4°C and pre-warmed in 37°C water bath before usage.

4.1.6 Enzymes

Table 6: Enzymes

Restriction enzymes and other enzymes are listed below.

Enzymes	Provider
FastDigest BamHI	Thermo Scientific
FastDigest EcoRI	Thermo Scientific
FastDigest HindIII	Thermo Scientific
FastDigest NheI	Thermo Scientific
FastDigest NotI	Thermo Scientific
FastDigest PstI	Thermo Scientific
T4 DNA ligase (5 U/µl)	Thermo Scientific
T4 DNA polymerase (5U/µl)	Thermo Scientific
XbaI (50 U/µl)	Thermo Scientific

4.1.7 Consumables

Table 7: Consumables and their providers

Consumables	Provider
6 Well Platte, Tissue Culture Treated	Corning Incorporated, NY (USA)
24 Well Platte, Tissue Culture Treated	Corning Incorporated, NY (USA)
96 Well Platte, Tissue Culture Treated	Corning Incorporated, NY (USA)
Centrifuge tubes (15 ml; 50 ml)	Corning Incorporated, NY (USA)
Combitips advanced® 25 mL	Eppendorf Biopur, Hamburg (Germany)
Costar assay plate 96-well white polystyrene, flat bottom	Corning Incorporated, NY (USA)
Costar Stripette (5 ml, 10 ml, 25 ml, 50 ml)	Corning Incorporated, NY (USA)
Diamond® Tipack™ D1200ST	Gilson, Middleton, WI (USA)
Diamond® Tower Pack™ (DL10ST, D200ST, D300ST)	Gilson, Middleton, WI (USA)
Eppendorf tubes (1.5 ml, 2ml)	Corning Incorporated, NY (USA)

4.1.8 Equipment

Table 8: List of utilized equipment and their providers

Equipment	Provider
Centrifuge 5415 D	Eppendorf, Hamburg (Germany)
Eagle Eye II Still Video System Darkroom Cabinet	Stratagene, Böblingen (Germany)
Electrophoresis Power Supply PS3002	Life Technologies, Darmstadt (Germany)
LightCycler®96	Roche, Mannheim (Germany)
MagPix[TM]	Luminex, Vienna (AT)
Mastercycler gradient	Eppendorf, Hamburg (Germany)
MaxQ. 4000 orbital shaker	Thermo Scientific, Waltham (USA)
Multifuge 3L	Heraeus, Hanau (Germany)
Nanotrop 2000c spectrophotometer	Thermo Scientific, Waltham (USA)
Thermomixer compact	Eppendorf, Hamburg (Germany)
Varifuge 3.OR	Heraeus Sepatech, Hanau (Germany)
Wallac Victor[2] **1420 Multilabel counter**	Perkin Elmer, Waltham (USA)

4.2   Methods

4.2.1   Cloning

4.2.1.1   Restriction enzyme digestion

The sequences of 5'- and 3' -UTRs of each of the listed human gene (see Table 4) were cloned in five different combinations, namely 5' UTR and 3' UTR alone as well as 5'+3' UTR, 5' UTR with 2 copies of 3'UTR in direct repeats (5'+2x3' UTR) and two copies of 3' UTR without 5'UTR (2x3' UTR). All of these constructs were compared to a control without UTRs.

In a first step, the UTRs were cloned into the backbone pVAX1-A120 which had been described previously by Kormann *et al.* [82]. An illustration of the plasmid vector pVAX1-A120 is shown in supplementary Figure 15. In addition, reporter gene coding for *Medtridia* luciferase (*Met*Luc) was cloned into this this backbone between *BamH*I-*EcoR*I sites by Geneart. The resulting plasmid "pVAXA120-*Met*Luc" displayed a poly(A) tail of only 90As. Nonetheless since the *Met*Luc mRNA from this vector was functional with a poly(A) tail of approximately 90As, the vector was chosen for further cloning of UTR sequences. For all UTR containing plasmids, restriction digestion was performed to confirm that all compared mRNAs had poly A-tails of similar length. 5' -UTRs were cloned into pVAX1-A-tail *Met*Luc between *HindIII*-*BamH*I sites. For 3'-UTRs, cloning into *EcoR*I-*Pst*I sites was performed. The plasmids containing 5' UTR alone and 5'+3' UTR were produced by Eurofins MWG Operon.

The other combinations, including 3' UTR alone, 5'+2x3' UTR and 2x3' UTR were generated as follows: Cloning of plasmids with a 3' UTR were performed by cutting out the 5' UTR of the pVAX1-A-tail 5'+3' UTR backbone via *HindIII* (blunt) and *BamH*I (blunt) digestion. In order to clone constructs with 2x3' UTR and a 5' UTR, *Met*Luc containing 3' UTR (*BamHI*/*Pst*I blunt) was ligated into the backbone of pVAX1-A-tail *Met*Luc including 5'+3' UTR, thereby a second 3' UTR in front of the respective 3' UTR was inserted. Finally the constructs containing only two copies of 3' UTR were generated via removing the 5' UTR (*HindIII* and *BamH*I, both blunt) from the plasmid containing a 5' UTR and 2x3' UTR. The control plasmid pVAX1-A-tail *Met*Luc without UTRs was provided by GeneArt.

For the cloning of the reporter gene d2EGFP including CYBA UTRs the following cloning procedure was performed: Firstly, the insert d2EGFP was obtained from the donor plasmid pd2EGFP-N1 and was digested with *Nhe*I and *Not*I (blunt). Afterwards d2EGFP was ligated into the backbone pVAX1-A120 *Met*Luc 3' CYBA and 2x3' CYBA UTR, which were digested with *Nhe*I and *EcoR*I (blunt). Secondly, d2EGFP was cut out from pd2EGFP-N1 via *BamH*I and *Not*I (blunt) digestion and was ligated into pVAX1-A120 *Met*Luc furnished with

5' CYBA, 5'+3' CYBA and 5'+2x3' CYBA UTR, which were cut with *BamHI* and *EcoRI* (blunt), each. After all cloning steps the reporter gene *Met*Luc was replaced by d2EGFP insertion.

4.2.1.2   PCR cloning

In order to clone pVAX1-A-tail hBMP2 furnished with CYBA UTRs, the insert hBMP2 with the restriction sites *NheI* and *BamHI* at the 5' end and *EcoRI* at the 3'end was generated by PCR reaction. The used primers are listed in Table 3. The complete reaction is listed below:

PCR reaction to generate hBMP2:

Reagent	Volume [µl]	Stock concentration
water	30	
Pfu 10x buffer (with Mg^{++})	5	10x
dNTP mix	5	2mM
FRW hBMP2	2	10pmole/µl
REV hBMP2	2	10pmole/µl
pVAX1-A120 hBMP2 (Geneart)	5	4ng/µl
DNA Pfu polymerase	1	2.5 U/µl
Total volume	30 µl	

Thermal cycling conditions:

Program	Step	Temperature [°C]	Time	Cycles
1	Denaturation	95	3 min	1 cycle
2	Denaturation	95	30 sec	30 cycles
	Annealing	60	30 sec	
	Extension	72	3 min	
3	Final extension	72	15min	1 cycle
4	HOLD	4	-	

Successful reaction was verified by agarose gel electrophoresis followed by gel extraction and PCR clean-up of the hBMP2 PCR product (NucleoSpin® Gel & PCR Clean up, Macherey-Nagel).

Cloning of pVAX1-A-tail hBMP2 furnished with cellular CYBA UTRs, was accomplished by inserting PCR product hBMP2 via *BamHI* and *EcoRI* digestion into plasmids pVAX1-A-tail *Met*Luc consisting of the different combinations of cellular CYBA UTRs, including 5', 3', 5'+3', 5'+2x3' and 2x3', respectively. Thereby the reporter gene *Met*Luc was replaced by hBMP2. All plasmid vector cards with their corresponding cloning sites are illustrated in supplementary Figure 15.

4.2.1.3   Ligation and purification

T4 DNA ligase (5U/µl, Fermentas) was used following manufacturer's instructions. After ligation the plasmid vectors were purified via chloroform and ethanol precipitation. Here same volume of chloroform was added to the ligation and was thoroughly mixed on a vortexer for 15 seconds. The aqueous phase was removed and transferred into a new reaction tube. Then two volumes of pre-cooled 100% EtOH and 3 M sodium acetate to a final concentration 0.3 M into the aqueous solution were added followed by mixing. After one hour incubation time at -20°C, samples were centrifuged for 30 minutes at 4°C with 14 000 rpm. The DNA pellet was washed once with 70% EtOH and centrifuged for further 10 minutes. Finally DNA pellet was dissolved in 10 µl water for injection. The purified plasmids were transformed into E.coli bacteria.

4.2.1.4   Transformation of E.coli bacteria by electroporation

Here electroporation was conducted to transform *E.coli* bacteria allowing an uptake and amplification of plasmid vector constructs. Therefore, 2 µl of electrocompetent *E.coli* cells (ElectroMAX™ DH10B™ cells, Invitrogen) were mixed with 2 µl-4 µl purified plasmid vector filled up to 50 µl with nuclease-free water in a pre-cooled electroporation cuvette (GenePulser® cuvettes, 0.1 cm gap, BioRad). Electroporation was performed by using a Gene Pulser II (BioRad) with the following conditions: 1.8 kV, 100 Ω, 25 µF. The transformed solution was pipetted into 2 ml of LB medium without antibiotics and cultivated for 1 hour (h) at 37°C. After one hour incubation time the transformed *E.coli* bacteria were centrifuged at 4000 rpm for 10 minutes (min). Supernatant was discarded and the pellet was re-suspended with the remaining liquid. Agar plates with kanamycin (50 µg/ml) were plated with 200 µl of resuspension and incubated at 37°C overnight. On the next day, formed colonies were picked and transferred to kanamycin-LB medium. Cultivation of transformed *E.coli* bacteria is describes in the next section 4.2.1.5.

4.2.1.5   Cultivation of E.coli bacteria and preparation of glycerol stocks

Transformed *E.coli* cells were cultured on agar plates (15 g Agar-Agar in 1 l LB medium) including kanamycin (50 µg/ml) for selection. Bacterial colonies were grown in shaking suspension of approximately 6 ml LB medium containing 50 µg/ml kanamycin. All culturing conditions were performed overnight (12-16 h) at 37°C in an orbital shaker with 220 rpm.

Preparation of glycerol stocks for storing transformed E.coli cells with the desired clones is described by Maniatis (Molecular Cloning). Isolation and purification of the amplified DNA plasmid is described in section 4.2.1.6

4.2.1.6   Plasmid purification

In order to isolate and purify the plasmid vector after amplification of the DNA vector in *E.coli* cells, the bacterial cultures were processed according to the manufacturer's instructions using the NucleoSpin® Plasmid or NucleoBond® Xtra Midi / Maxi (Macherey Nagel), depending upon the amount needed.

4.2.1.7   Agarose gel electrophoresis

To perform agarose gel electrophoresis, the gel was made up of 1 % to 2 % agarose along with 1x TAE buffer and ethidiumbromide solution to visualize the nucleic acid. DNA ladder 1 kp, 100 bp (Plasmid Factory) or RiboRuler High Range RNA Ladder (Thermo Scientific) were used as the standardized ladder to determine the length of the nucleic acid of interest.

4.2.2   Messenger RNA production

Chemically modified mRNA was produced via *in vitro* transcription. Firstly, the plasmid vectors were linearized with *XbaI* and subsequently purified via chloroform/ethanol precipitation. For *in vitro* transcription, RiboMax Large Scale RNA production System-T7 (Promega) was utilized. The transcription mix contained the unmodified nucleotides: adenosine-triphosphate (ATP), guanosine-triphosphate (GTP), uridine-triphosphate (UTP) and cytosine-triphosphate (CTP) as well as the chemically modified nucleotides methyl-CTP and thio-UTP (Jena Bioscience, GmbH, Jena, Germany) with a final concentration of ATP:GTP:UTP:CTP:methyl-CTP:thio-UTP of 7.13 mM:1.14 mM:5.36 mM:5.36 mM:0.536 mM:0.536 mM.

Additionally the anti-reverse cap analog (ARCA) was added to the mix to ensure the incorporation of the 5'-cap in the right direction resulting in capped RNA for further downstream application. Finally, the linearized DNA template was added into the reaction mix filled up to a final volume of 20 µl. The IVT mix was incubated at 37°C for 2 h. Afterwards the DNA template was digested by adding DNase I and was incubated for further 20 min at 37°C. RNA precipitation was performed by addition of pre-cooled ammonium-acetate to a final concentration of 2.5 M and was incubated for 30 min on ice. After centrifugation at 4°C with 14 000 rpm, the RNA pellet was washed twice with 70% ethanol followed by centrifugation for 10 minutes. At last, the RNA was re-suspended in 30 µl water for injection. The RNA concentration was determined with a spectrophotometric device and mRNA quality was tested on agarose gel.

4.2.3   Cell culture and cell counting

All cell lines used are described in Table 1 and were grown in humidified atmosphere at 5% CO_2 level in a cell incubator (37°C). When cells reached a confluency of 85%-90%, they were trypsinated for passaging or subsequent seeding. The cells were passaged twice per week with a splitting ratio of 1:20. The determination of the cell number was performed by using the Neubauer chamber. The starting cell number for each transfection study is described in section 4.2.4 *In vitro* transfection.

4.2.4   *In vitro* transfection

4.2.4.1   *Transfection of NIH3T3 and A549 for screening studies*

To perform screening experiments, NIH3T3 and A549 cells were transfected with different doses of mRNA/well to evaluate dose dependent effects. The experimental set-up was as follows: $5x10^3$ NIH3T3 cells or $7x10^3$ A549 cells in 150 µl complete medium were seeded per well in 96-well plates and transfected 24 hours post-seeding, respectively. Cells were transfected at a starting dose of 500 ng/well using the commercial transfection reagent Dreamfect Gold (DFG). Complexes were prepared at a ratio of 4 µl DFG per 1 µg mRNA. The mRNA (3.6 µg) was diluted separately in DMEM without supplements in a reaction tube with a total volume of 340 µl for each mRNA. For the formation of lipoplexes a fresh 96 cell culture well plate was used. In well A1 14.4 µl DFG was mixed with 5.6 µl water for each mRNA complex. Complex formation took place when the mRNA dilution was added to the DFG solution in well A1 and mixed by up

and down pipetting. The mixtures were incubated at room temperature (RT) for 20 min. In the meanwhile the dilution series were prepared. In the remaining seven wells subjacent of the complex mix (well A1), 180 µl DMEM without supplements per well were added. After incubation time, 180 µl of the complex solution was removed and added into the first well of dilution series (1:2 dilution). This procedure was conducted until the last dilution step. Finally, 50 µl of the complex solution were added onto the cells and incubated for 4 hour. For every mRNA construct, biological triplicates were prepared. After 4 hours, the complete supernatant was removed from the cell culture plate for further analysis and fresh 200 µl medium was added to each well. Bioluminescence was measured after 4 h, 24 h, 48 h, 72 h, 96 h, 120 h and 144 h using a multilabel plate reader. For this, 50 µl of cell culture supernatant was mixed with 20 µl coelenterazin (50mM) and the generated light was measured.

4.2.4.2   Transfection of NIH3T3 and A549 for RNA isolation

To obtain enough cells for RNA isolation, transfection studies were conducted on 6 well cell culture plate. NIH3T3 cell and A549 cells were seeded 2×10^5 cells/well in complete medium 24 hours prior to transfection. Cells were transfected at a dose of 15 pg of mRNA/cell using DFG at a ratio of 4 µl DFG per 1 µg mRNA. For complex formation DFG and mRNA were separately diluted in medium without supplements to add up to a total volume of 200 µl, each. The mRNA dilution was then mixed into the DFG solution, followed by 20 minutes incubation at RT. After incubation 200 µl of the complex solution was added onto the cells to a final volume of 2 ml. At every measured time point, 4 h, 24 h, 72 h, 96 h and 120 hours post-transfection, supernatant was collected and the cells were harvested in lysis buffer RA1 buffer, supplied by the Nucleo Spin RNA kit (Macherey Nagel), followed by freezing and storage at -80°C until usage.

4.2.4.3   Transfection of C2C12 cells via DFG and magnetofection

Firstly, C2C12 cells were transfected with mRNA coding for hBMP2 without UTRs using two different transfection protocols including DFG transfection and magnetofection, respectively. Before transfection 5×10^4 cells/well were seeded in 1 ml DMEM complete medium in 24 well cell culture plate. For both transfection protocols the cells were transfected at a dose of 20 pg/cell and 10 pg/cell each at a ratio of 4 µl DFG per 1 µg mRNA coding for hBMP2 without UTRs. In case of Dreamfect Gold transfection, complex formation was prepared by mixing DFG and mRNA to a final concentration of 100 µg/ml, followed by 20

minutes incubation at RT. After incubation 250 µl of the complex solution was added onto the cells with 250 µl DMEM complete medium, each. With respect to magnetofection two different magnetic nanoparticles were tested comprising SoMag5 and SoMag6-115. Both magnetic particles were used at a ratio of 1 µg mRNA/4 µl DFG/0.5 µg Fe. Complex formation was prepared by mixing DFG, magnetic nanoparticles and mRNA to a final concentration of 100 µg/ml followed by 20 minutes incubation time at RT. After incubation the complex was further diluted to its working solution with DMEM without supplements. 250 µl of the complex solution was transferred onto the cell to a final volume of 500 µl. A magnetic field by using a special made 24 well magnetic plate, was applied under the cell culture plate for 30 minutes at 37°C. Human BMP2 translation was measured after 24 hours and 48 hours post-transfection using ELISA.

Secondly, to obtain enough cells for RNA isolation, transfection of mRNAs furnished with CYBA UTRs was performed on 6 well plates with 2×10^5 cells at a dose of 20 pg mRNA/cell using magnetofection with SoMag5. Complex preparation is described above. Here a different magnet plate was used during applying the magnetic field for 30 minutes. The supernatant was collected as well as the cultured cells were lysed for further analysis after 6 h, 12 h, 24 h, 30 h, 48 hours post-transfection.

4.2.4.4   Cell viability assay using MTT assay

The MTT [3-(4,5-dimethylthiazol-2-yl)-2,5-diphenyltetrazolium bromide] assay, a colorimetric assay, was conducted to assess the cell metabolic activity of cells after transfection. Therefore, MTT reagent was added onto the cells following the manufacturer's instructions. During incubation time the MTT, a membrane-permeable dye, is metabolized by the mitochondrial dehydrogenase of viable cells and leads to formation and accumulation of dark blue non-permeable formazan-crystals. By adding a solubilization solution the crystals are dissolved and the dye can be measured with a multilabel plate reader at 570 nm.

4.2.5   RNA isolation

In order to determine the actual mRNA amount at different time point(s) post-transfection, the cultured cells were lysed and RNA was isolated according to the manufacturer's protocol using Nudeo Spin RNA kit (Macherey Nagel). The isolated RNA was eluted in 40 µl RNAse free water and was examined in RNA

concentration and quality by spectrophotometric measurements and gel analysis, respectively. The isolated RNA was used for further downstream applications, such as quantitative RT-PCR.

4.2.6 Reverse transcription

By reverse transcription cDNA was synthesized from isolated RNA (1 µg of transfected NIH3T3 and A549 and 0.5 µg of transfected C2C12 cells, respectively) using First Strand cDNA Synthesis Kit (Thermo Scientific) following the manufacturer's instruction. The synthesized cDNA was stored at -20°C.

4.2.7 Quantitative Real time Polymerase Chain Reaction (qRT-PCR)

A conventional method to quantify the physical presence of mRNA at specific time points after transfection is the qRT-PCR. Here, the reaction was set up as follows: equivalent amounts of 8 µl cDNA (diluted 1:1000 of transfected NIH3T3 and A549 cell and 1:50 of transfected C2C12 cells, each) were mixed together with 11 µl of Master Mix filled up with water to a total volume of 20 µl. The Master Mix included for one single reaction the following components: 10 µl of Sso Advanced^{TM} Universal SYBR®Green Supermix, 0.5 µl of FRW primer and REV primer each (stock solution 20 µM for *Met*Luc primers and 5 µM for hBMP2 primers, respectively). The primers are listed in Table 3. Primer amplification efficiency was around 2 and was found to be appropriate for qRT-PCR measurement. For absolute quantification a standard curve was prepared with the following dilutions:

Dilution series for *Met*Luc using cDNA:

Standard	Sample	Volume [µl]	Water [µl]	Dilution factor
1	cDNA	4	396	$1:10^2$
2	Std. 1	20	180	$1:10^3$
3	Std. 2	20	180	$1:10^4$
4	Std. 3	20	180	$1:10^5$
5	Std. 4	20	180	$1:10^6$

Dilution series for hBMP2 using cDNA:

Standard	Sample	Volume [µl]	Water [µl]	Dilution factor
1	cDNA	4	396	$1:10^2$
2	Std. 1	40	360	$1:10^3$
3	Std. 2	40	360	$1:10^4$
4	Std. 3	40	360	$1:10^5$
5	Std. 4	40	360	$1:10^6$
6	Std. 5	40	360	$1:10^7$

The templates for Standard-*Met*Luc and -hBMP2 cDNAs synthesis were chemically modified mRNA produced via IVT. As negative control water was used instead of cDNA. The run was performed by using LightCycler®96 (Roche) with the following settings listed below:

qRT-PCR thermal conditions:

Program	Step	Temperature [°C]	Time	Cycles
Preincubation	Denaturation	95	600 sec	1 cycle
3 Step Amplification	Denaturation	95	10 sec	45 cycles
	Annealing	60	10 sec	
	Extension	72	10 sec	
Melting		95	10 sec	1 cycle
		65	60 sec	
		97	1 sec	

4.2.8 *Metridia* luciferase (*Met*Luc) measurement

To determine the transfection efficiency of transfected cells with mRNA coding for the reporter *Met*Luc, protein translation was measured via bioluminescence. The reporter protein *Met*Luc is secreted into the supernatant and can therefore be detected without lysing the cells allowing kinetic measurements of the same transfected cells. The experimental set-up looks like as follows: 50 µl of supernatant was mixed with 20 µl of substrate solution coelenterzin (50 mM, Sigma Aldrich) in a white 96 well plate. The bioluminescence was measured using Wallac Victor^2 (Perkin Elmer Life Sciences).

4.2.9 Human Bmp-2 ELISA

Cell culture supernatant of transfected cells was used for hBMP2 measurement. Human BMP2 protein levels were analyzed by ELISA following instructions of the DuoSet®ELISA Development system (R&D Systems).

4.2.10 Multiplex Immunoassay

Cell culture supernatants of the transfected C2C12 cells after 6 and 12 hours post-transfection were used for cytokine measurement. The analyzed cytokines were murine IL-10, IL-1 beta, IL-2, IP-10, IL-6, IFN-alpha, IFN-gamma, IL-12p70, TNF-alpha and MCP-1. The cytokine proteins were analyzed by Multiplex Immunoassay following instructions of the ProcartaPlex Immunoassay Kit (Affymetrix eBioscience). The immunoassay uses the xMAP®technology (multi-analyte profiling beads) which allows the detection and the quantification of several proteins within a single sample. The detection is based on flow cytometer in which fluorescent-dyed beads are coupled with the protein of interest. The multiplex immunoassay was measured using MagPix (Luminex).

4.2.11 Data analysis

Plasmid vector cards were designed using the free software pDRAW32.

The analysis of total protein translation over time, so called area under the curve (AUC) as well as of other obtained data was accomplished by using GraphPad Prism® Version 5 (GraphPad Software Inc., La Jolla, CA, USA). For the analysis of the multiplex immunoassay, xPONENT® version 4.2 was used.

Furthermore, secondary structure analysis comprising the minimum free energy (ΔG) was performed using the mfold web server (http://mfold.rna.albany.edu/?q=mfold/rna-folding-form).

5. Results

5.1 Generation of plasmid vectors furnished with cellular UTRs

Five cellular UTRs including CYBA, DECR1, GMFG, MAPBPIP and MYL6B were cloned upstream and or downstream of the reporter gene *Met*Luc, respectively. For each cellular UTR five different combinations were designed comprising 5' and 3' UTR alone, 5'+3' UTR, 5'+2x3' UTR and two copies of 3'UTR (2x3' UTR). For d2EGFP and human BMP2, only CYBA UTR and its combinations were cloned and tested. The plasmid vectors are listed in the Material and Methods part. Vector maps were generated using pDRAW32 and are illustrated in Supplementary Figures 15.1-15.19.

5.2 Determination of mRNA quality and purity

Spectrophotometric measurement (260 nm) was used to measure the concentration of the produced mRNA whereas the ratios 260/280 and 260/230 served as indicators of mRNA quality. All the tested constructs were comparable for mRNA yield and quality. All mRNA constructs furnished with different UTR combinations are illustrated in Figure 1.
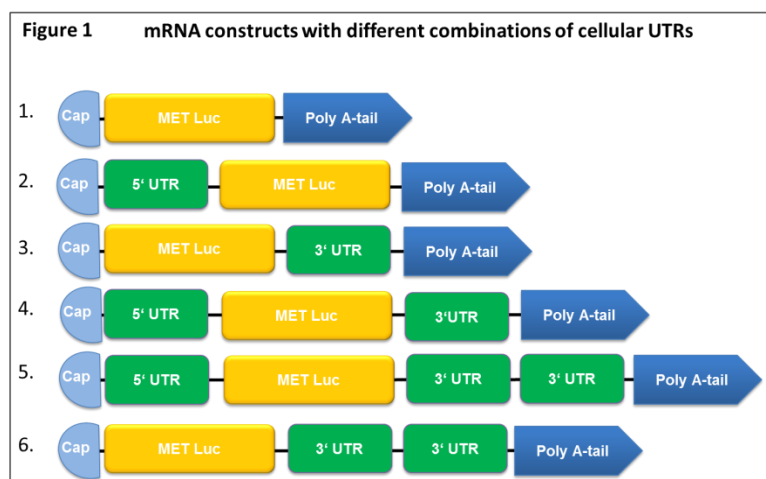
Figure 1: Messenger RNA constructs furnished with cellular UTRs.

Cellular UTRs (green) were inserted upstream and/or downstream of the reporter gene *Met*Luc. All produced mRNAs were containing chemically modified nucleotides into the mRNA as well as a cap structure (light blue). The poly A-tail was inserted downstream of the gene or the 3' UTR (blue). This figure represents all combinations for one cellular UTR.

Additionally, the integrity of the produced mRNA was checked on 1% agarose gel. All chemically modified mRNAs showed a single band of expected size on the gel (Figure 2). No smearing, an indicator of mRNA degradation could be observed. The length of *Met*Luc mRNA without UTRs is 840 bases. The mRNA constructs furnished with UTRs and their sizes are listed in Table 9.
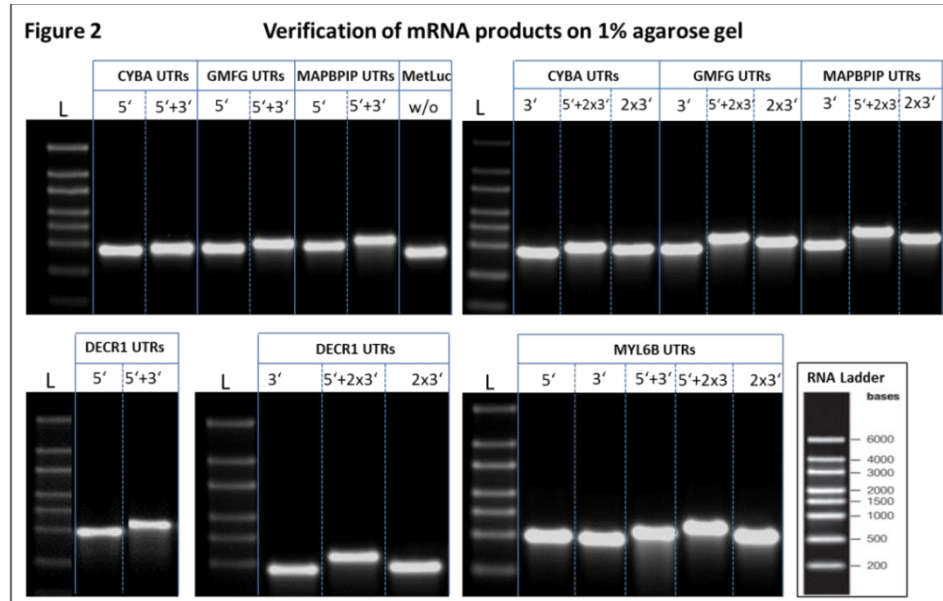

Figure 2: Agarose gel electrophoresis of chemically modified MetLuc mRNA

Different mRNA products were checked by loading 1 µg mRNA of each construct on 1% agarose gel. A RiboRuler High Range RNA ladder (L) was used to determine the correct length of the mRNA constructs (right picture below). As shown here all mRNAs showed only one single band as expected

Table 9: Size of mRNA coding for *Met*Luc

The size, length in bases (b), of each mRNA construct furnished with cellular UTRs is listed below.

UTRs	5' UTR	3' UTR	5+3' UTR	5+2x3' UTR	2x3' UTR
CYBA	789 b	800 b	858 b	932 b	874 b
DECR1	975 b	935 b	1082 b	1210 b	1051 b
GMFG	932 b	854 b	1055 b	1114 b	982 b
MAPBPIP	986 b	875 b	1130 b	1210 b	1024 b
MYL6B	977 b	948 b	1097 b	1222 b	1073 b

In conclusion all produced mRNA constructs showed a single band and were free of protein and organic contamination verified by agarose gel electrophoresis and spectrophotometric measurement, respectively. This mRNA starting material was used for the following transfection studies *in vitro*.

5.3 Screening different transfection reagents for mRNA delivery

In an initial experiment, different transfection reagents (TfR) were compared for mRNA delivery in NIH3T3 and A549 cell lines. Four different commercially available TfRs namely, Dreamfect Gold (DFG), Lipofectamine™2000, MetafectenePro and SM4-31 were investigated with respect to the resulting protein translation and cell viability post-transfection. In both tested cell lines, MetafectenePro resulted in significant higher protein translation over a broad range of transfected mRNA doses (Figure 3A and B). Nonetheless mRNA delivery with MetafectenePro resulted in extensive cell death with cell viabilities falling to below 50% at higher doses in both cell lines. DFG instead showed an overall survival rate of more than 75% in NIH3T3 (up to 500 ng/well) and A549 cells (up to 250 ng/well) compared to MetafectenePro (Figure 3C, D).
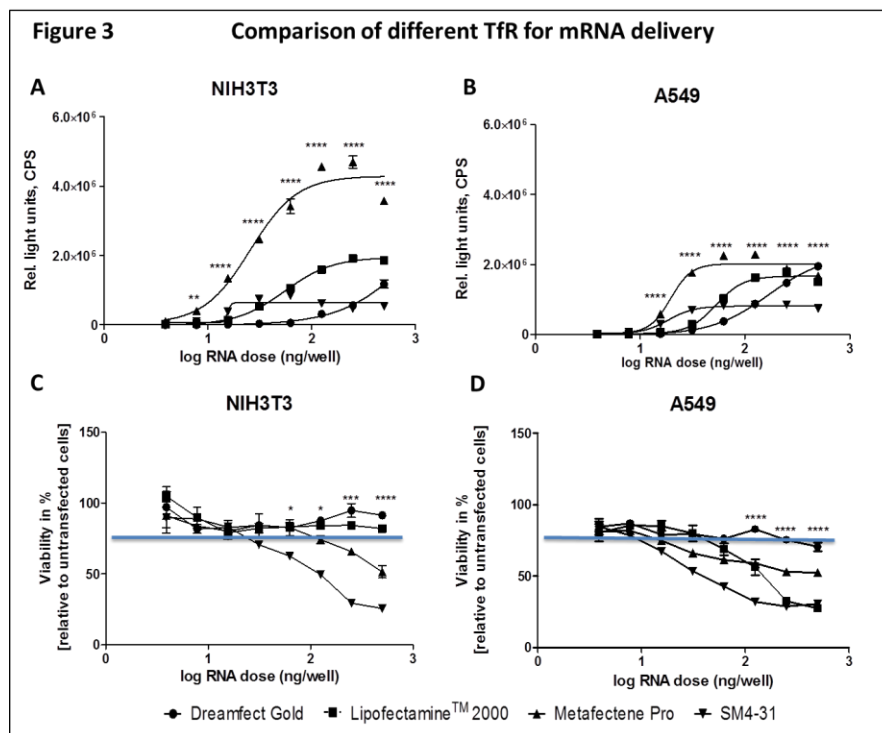
Figure 3: Testing of various TfRs for mRNA delivery with respect to dose-dependent protein translation and cell viability

Messenger RNA coding for *Met*Luc w/o UTRs was transfected with four different TfRs into NIH3T3 and A549. TfR screened were DFG, Lipofectamine™2000, Metafectene Pro and SM4-31. After 24 hours, *Metridia* luciferase activity (counts per second - CPS) in NIH3T3 (3A) and A549 (3B) as well as the cell viability of NIH3T3 (3C) and A549 (3D) were measured. Data represent means (n=3) ± standard error (SEM). Statistical significance was assessed by 2-way ANOVA test (Bonferroni multiple comparisons) with p values <0.05.

Despite the fact that DFG was the least effective reagent for all doses below 125 ng in both cell lines, DFG showed consistent cell viability among all doses. Comparable cell viabilities with a broad dose spectrum allow us to compare the different constructs without significant toxicity effects post-transfection. Therefore, DFG was used in further experiments for mRNA delivery.

5.4 Screening of different cellular UTRs *in vitro*

To assess the impact of various UTRs on translation, 25 mRNA constructs were furnished with various cellular UTRs (Figure 1) and were screened in NIH3T3 and A549 cell lines. All mRNA constructs coded for *Met*Luc, which is secreted into the medium. Dose-dependent translation kinetics were performed for up to 6 days post transfection and total protein translation, also defined as Area Under the Curve (AUC) was used to compare the different UTR constructs. In NIH3T3, cells mRNA dose ranging from 3.9 ng/well to 500 ng/well and in A549 cells mRNA dose of 3.9 ng/well up to 250 ng/well were transfected. The AUC values have been tabulated for NIH3T3 and A549 in Table 10 and 11, respectively. In murine NIH3T3 cells, UTRs from *CYBA* gene, with the exception of 3'UTR alone, in all tested combinations resulted in significantly higher translation compared to the control *Met*Luc mRNA without UTRs. This was observed over a broad range of transfected mRNA doses. Though the effects were not so strong in human A549 cells, significantly higher translation was observed with 5'+3'UTR combination of *CYBA* gene followed by 5' UTR and 2x3' CYBA UTR.

The mRNA productivity specifies the potential of a single mRNA to produce protein and was evaluated by normalizing the AUC of the different UTRs to the corresponding dose. The mRNA productivity in NIH3T3 and A549 are depicted in Figure 4 and 5, respectively. A plateau in mRNA productivity was reached between 62.5 ng – 250 ng mRNA/well and was similar for NIH3T3 and A549 cells. In general Figure 4 and 5 showed that single mRNA molecules furnished with 5', 5'+3' and 2x3' CYBA UTRs were the most productive constructs over time compared to the control in both NIH3T3 cells and A549 cells. These combinations of CYBA UTR were also most efficient in translation kinetics studies (Tables 3 and 4).

Table 10: Mean total protein translation over time (AUC) in NIH3T3 cells

Statistical significance was assessed by ANOVA One Way test (Newman Keuls comparison). Numbers in red indicate $p < 0.05$. Highest translation for each construct has been highlighted in yellow.

Area Under the Curve (AUC) in NIH3T3
(Relative light units, counts per second)

5' UTRs	Dose [ng/well]							
	500ng	250ng	125ng	62.5ng	31.3ng	15.6ng	7.8ng	3.9ng
CYBA	1,75E+08	1,81E+08	1,10E+08	5,39E+07	2,36E+07	5,70E+06	1,34E+06	3,35E+05
DECR1	8,75E+07	8,29E+07	3,46E+07	1,13E+07	3,67E+06	7,15E+05	1,70E+05	8,31E+04
GMFG	1,58E+08	1,47E+08	5,31E+07	2,14E+07	7,98E+06	1,17E+06	3,55E+05	1,39E+05
MAPBPIP	1,01E+08	7,40E+07	3,49E+07	1,22E+07	4,41E+06	6,47E+05	1,70E+05	8,51E+04
MYL6B	1,36E+06	8,69E+05	4,40E+05	1,74E+05	1,10E+05	7,47E+04	7,08E+04	9,34E+04
control	9,15E+07	3,39E+07	3,16E+07	5,48E+06	6,89E+05	2,19E+05	1,22E+05	8,63E+04

3' UTRs	Dose [ng/well]							
	500ng	250ng	125ng	62.5ng	31.3ng	15.6ng	7.8ng	3.9ng
CYBA	1,13E+08	7,86E+07	2,80E+07	7,25E+06	2,31E+06	4,21E+05	1,50E+05	9,76E+04
DECR1	9,01E+07	3,43E+07	1,49E+07	4,36E+06	1,22E+06	2,50E+05	1,06E+05	9,32E+04
GMFG	1,11E+08	8,85E+07	4,63E+07	1,35E+07	6,64E+06	1,32E+06	3,32E+05	1,67E+05
MAPBPIP	9,01E+07	3,48E+07	2,04E+07	4,99E+06	9,73E+05	2,27E+05	1,20E+05	7,11E+04
MYL6B	1,56E+08	1,33E+08	5,26E+07	1,74E+07	5,13E+06	1,29E+06	3,44E+05	1,79E+05
control	9,15E+07	3,25E+07	2,03E+07	3,80E+06	6,89E+05	2,19E+05	1,22E+05	7,23E+04

5'+3' UTRs	Dose [ng/well]							
	500ng	250ng	125ng	62.5ng	31.3ng	15.6ng	7.8ng	3.9ng
CYBA	2,26E+08	2,43E+08	1,44E+08	6,33E+07	2,72E+07	6,51E+06	1,46E+06	4,80E+05
DECR1	7,49E+07	6,71E+07	2,83E+07	1,13E+07	3,70E+06	6,97E+05	1,94E+05	9,76E+04
GMFG	2,05E+08	1,71E+08	8,59E+07	4,43E+07	9,74E+06	2,08E+06	7,48E+05	2,08E+05
MAPBPIP	2,05E+08	1,45E+08	6,08E+07	2,39E+07	7,52E+06	1,67E+06	5,04E+05	2,43E+05
MYL6B	5,81E+06	3,06E+06	1,88E+06	7,56E+05	2,24E+05	1,31E+05	1,58E+05	1,22E+05
control	9,15E+07	3,39E+07	3,16E+07	5,48E+06	6,89E+05	2,19E+05	1,22E+05	8,63E+04

5'+2x3' UTRs	Dose [ng/well]							
	500ng	250ng	125ng	62.5ng	31.3ng	15.6ng	7.8ng	3.9ng
CYBA	1,60E+08	1,17E+08	6,55E+07	2,83E+07	1,01E+07	1,36E+06	7,89E+05	3,51E+05
DECR1	4,98E+07	3,25E+07	1,18E+07	3,00E+06	6,04E+05	1,79E+05	8,27E+04	6,12E+04
GMFG	7,51E+07	6,78E+07	3,05E+07	8,96E+06	3,52E+06	7,47E+05	2,32E+05	1,18E+05
MAPBPIP	8,08E+07	6,74E+07	3,13E+07	1,03E+07	2,34E+06	7,77E+05	2,73E+05	1,30E+05
MYL6B	1,45E+06	1,03E+06	4,18E+05	1,98E+05	9,53E+04	6,62E+04	5,59E+04	5,76E+04
control	9,15E+07	3,39E+07	2,03E+07	5,48E+06	6,89E+05	1,68E+05	1,22E+05	8,63E+04

2x3' UTRs	Dose [ng/well]							
	500ng	250ng	125ng	62.5ng	31.3ng	15.6ng	7.8ng	3.9ng
CYBA	8,58E+07	9,18E+07	5,52E+07	2,25E+07	8,41E+06	2,04E+06	3,76E+05	2,19E+05
DECR1	9,71E+07	9,95E+07	5,25E+07	1,52E+07	4,71E+06	1,55E+06	2,87E+05	2,01E+05
GMFG	6,23E+07	4,87E+07	1,69E+07	4,47E+06	8,44E+05	3,67E+05	1,69E+05	1,28E+05
MAPBPIP	8,07E+07	7,15E+07	3,62E+07	9,49E+06	2,10E+06	8,26E+05	2,63E+05	1,42E+05
MYL6B	7,28E+07	7,51E+07	2,91E+07	5,52E+06	2,10E+06	8,02E+05	1,91E+05	1,55E+05
control	9,15E+07	3,39E+07	2,03E+07	5,48E+06	6,89E+05	2,19E+05	1,22E+05	8,63E+04

Table 11: Mean total protein translation over time (AUC) in A549 cells

Statistical significance was assessed by ANOVA One Way test (Newman Keuls comparison). Numbers in red indicate $p < 0.05$. Highest translation for each construct has been highlighted in yellow.

Area Under the Curve (AUC) in A549
(Relative light units, counts per second)

5' UTRs	Dose [ng/well]						
	250ng	125ng	62.5ng	31.3ng	15.6ng	7.8ng	3.9ng
CYBA	5,42E+07	4,30E+07	1,86E+07	5,88E+06	2,40E+06	4,52E+05	8,86E+04
DECR1	8,14E+06	1,01E+07	2,70E+06	5,30E+05	1,96E+05	7,55E+04	5,45E+04
GMFG	1,49E+07	1,68E+07	4,62E+06	8,96E+05	2,18E+05	8,60E+04	5,60E+04
MAPBPIP	8,33E+06	1,01E+07	3,28E+06	7,21E+05	1,82E+05	7,00E+04	5,34E+04
MYL6B	1,03E+05	1,43E+05	8,78E+04	6,57E+04	5,67E+04	6,16E+04	6,61E+04
control	6,95E+07	6,35E+07	1,46E+07	2,79E+06	5,65E+05	1,74E+05	9,63E+04

3' UTRs	Dose [ng/well]						
	250ng	125ng	62.5ng	31.3ng	15.6ng	7.8ng	3.9ng
CYBA	5,31E+06	1,23E+07	4,22E+06	5,42E+05	1,40E+05	7,07E+04	5,52E+04
DECR1	2,59E+06	3,07E+06	2,93E+06	4,72E+05	1,13E+05	6,29E+04	5,33E+04
GMFG	1,53E+07	1,70E+07	4,73E+06	1,09E+06	3,83E+05	8,53E+04	5,45E+04
MAPBPIP	1,73E+07	2,80E+07	1,54E+07	2,98E+06	3,78E+05	8,88E+04	5,74E+04
MYL6B	2,26E+07	2,62E+07	8,57E+06	1,88E+06	3,71E+05	1,01E+05	6,08E+04
control	6,95E+07	6,35E+07	1,46E+07	2,79E+06	5,65E+05	1,74E+05	9,63E+04

5'+3' UTRs	Dose [ng/well]						
	250ng	125ng	62.5ng	31.3ng	15.6ng	7.8ng	3.9ng
CYBA	1,26E+08	1,00E+08	4,55E+07	1,49E+07	3,86E+06	4,01E+05	8,36E+04
DECR1	1,96E+07	1,59E+07	5,44E+06	1,63E+06	3,98E+05	9,35E+04	5,86E+04
GMFG	8,08E+07	5,93E+07	3,63E+07	8,92E+06	1,53E+06	5,02E+05	7,33E+04
MAPBPIP	3,92E+07	3,62E+07	1,18E+07	2,93E+06	6,98E+05	1,36E+05	6,48E+04
MYL6B	9,31E+05	6,58E+05	3,32E+05	1,60E+05	8,12E+04	6,53E+04	8,05E+04
control	6,95E+07	6,35E+07	1,83E+07	2,79E+06	5,65E+05	1,74E+05	9,63E+04

5'+2x3' UTRs	Dose [ng/well]						
	250ng	125ng	62.5ng	31.3ng	15.6ng	7.8ng	3.9ng
CYBA	3,11E+07	2,95E+07	6,17E+06	1,70E+06	4,26E+05	1,37E+05	7,75E+04
DECR1	3,63E+06	1,16E+07	2,39E+06	5,68E+05	1,69E+05	7,36E+04	5,98E+04
GMFG	1,38E+07	1,99E+07	5,43E+06	9,87E+05	2,39E+05	8,84E+04	6,25E+04
MAPBPIP	1,45E+07	1,77E+07	3,26E+06	1,02E+06	3,53E+05	1,10E+05	6,47E+04
MYL6B	2,17E+05	2,40E+05	1,01E+05	6,88E+04	6,02E+04	5,68E+04	5,25E+04
control	6,95E+07	6,35E+07	1,83E+07	2,79E+06	5,65E+05	1,74E+05	9,63E+04

2x3' UTRs	Dose [ng/well]						
	250ng	125ng	62.5ng	31.3ng	15.6ng	7.8ng	3.9ng
CYBA	5,37E+07	4,30E+07	1,33E+07	5,80E+06	1,69E+06	2,82E+05	8,87E+04
DECR1	2,53E+07	4,35E+07	9,18E+06	2,05E+06	5,21E+05	1,23E+05	8,06E+04
GMFG	2,78E+07	3,67E+07	1,20E+07	1,90E+06	3,80E+05	1,16E+05	7,53E+04
MAPBPIP	3,85E+07	3,74E+07	1,10E+07	2,54E+06	5,22E+05	1,21E+05	7,04E+04
MYL6B	5,20E+07	4,51E+07	1,53E+07	4,07E+06	1,28E+06	2,12E+05	8,47E+04
control	6,95E+07	6,35E+07	1,46E+07	2,79E+06	5,65E+05	1,74E+05	9,63E+04
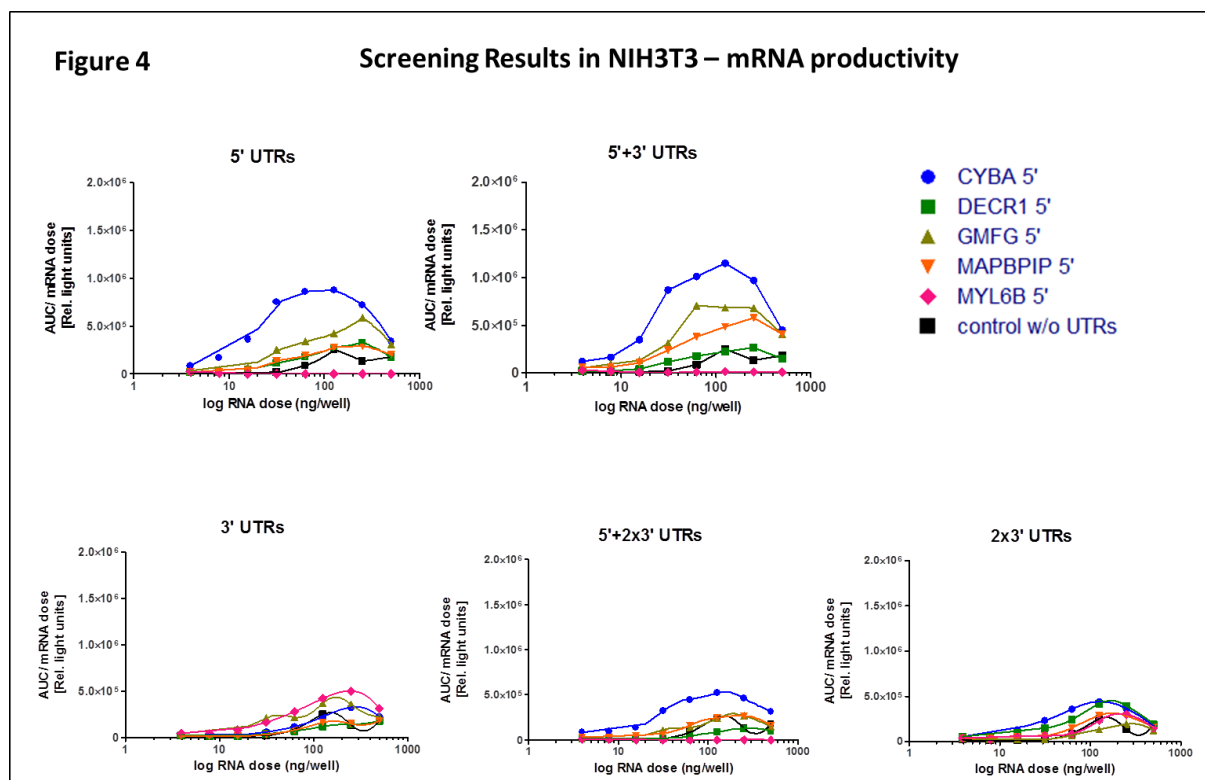
Figure 4: mRNA productivity of cellular UTRs in NIH3T3

The total peak protein translation over six days (AUC) was normalized to the corresponding dose specifying the mRNA productivity of a single mRNA molecule at each single dose. The tested cellular UTRs were CYBA, DECR1, GMFG, MAPBPIP and MYL6B for each mRNA combination including 5' UTR, 3' UTR, 5'+3' UTR, 5'+2x3' UTR and 2x3' UTR. The graph is depicted in a linear (relative light units)-log (RNA dose) scale plot.
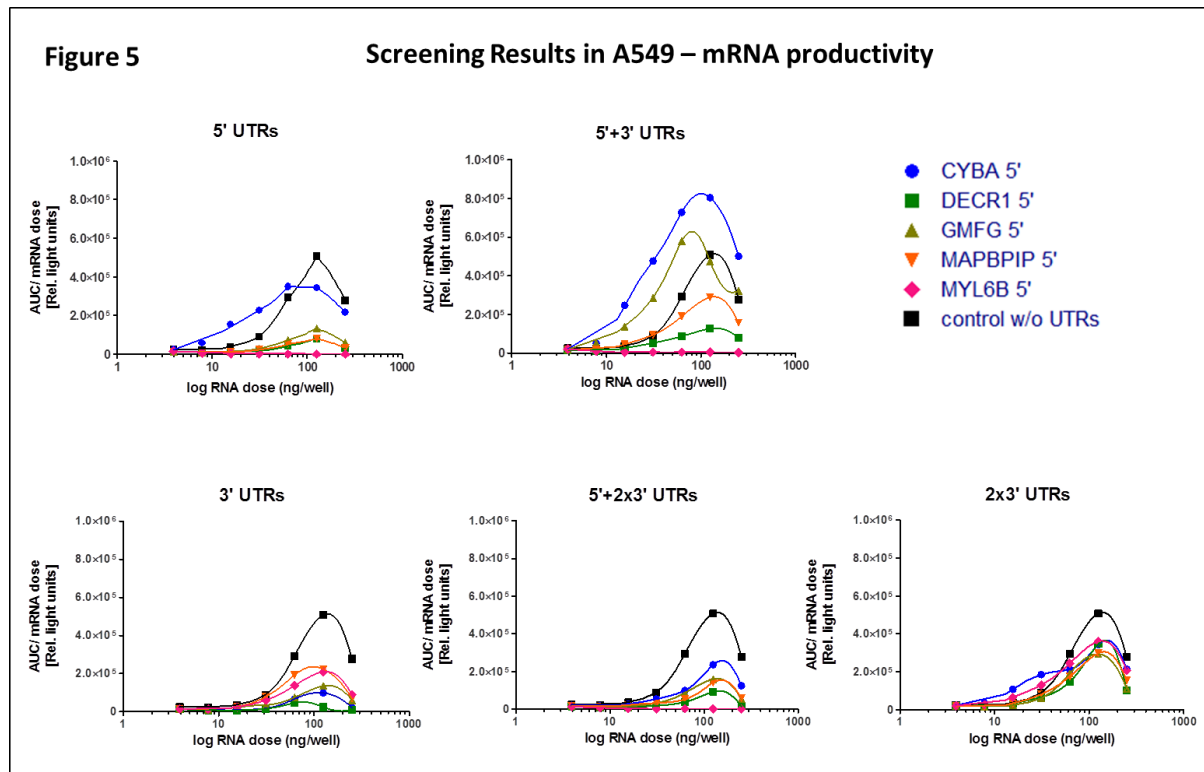
Figure 5: mRNA productivity of cellular UTRs in A549

The total peak translation over six days (AUC) was normalized to the corresponding dose specifying the mRNA productivity of a single mRNA molecule at each single dose. The tested cellular UTRs were CYBA, DECR1, GMFG, MAPBPIP and MYL6B for each mRNA combination including 5' UTR, 3' UTR, 5'+3' UTR, 5'+2x3' UTR and 2x3' UTR. The graph is depicted in a linear (relative light units)-log (RNA dose) scale plot.

In summary, it could be shown that incorporation of CYBA UTRs into an mRNA sequence significantly increased its productivity. To gain insights into the mechanisms underlying the observed increased mRNA productivity, with CYBA UTRs, experiments were performed to determine the half-lives of different CYBA UTR containing mRNA constructs. Furthermore, distinctions were made between the physical half-life and functional half-life for a given mRNA construct.

5.5   Determination of physical and functional mRNA half-life

So far, mRNA stability and turnover have been measured by a variety of approaches including direct and indirect analysis such as metabolic labelling, mass spectrometry, quantitative real time reverse transcription polymerase chain reaction (qRT-PCR), microarrays, blocking cellular transcription or fluorescence labelling techniques for imaging mRNA inside cells. These methods determine either the physical mRNA half-life or the functional half-life. For instance qRT-PCR is a conventional method to investigate the physical mRNA half-life, whereas fluorescence labelling techniques can determine the functional mRNA half-life. The major difference between the two is that physical half-life specifies the physical presence of mRNA molecules at time of measurement. However physical presence of mRNA does not necessarily lead to its translation into a functional protein, whereas functional mRNA is that fraction of mRNA which is translated into a functional protein. To develop mRNA for therapeutic purposes it is of importance to know the functional mRNA half-life. The functional half-life allows proper dosing in a patient. In the present study, both physical and functional half-lives of CYBA UTR containing mRNAs were assessed. In case of the physical mRNA half-life, qRT-PCR was performed. The functional half-life was determined by using µ-structured single cell mRNA transfection.

5.5.1   Determination of the physical mRNA half-life via quantitative RT-PCR and mRNA productivity

Based on UTR screening results (Table 10 & 11; Figure 4 and 5), CYBA UTR with the combinations of 5' alone, 5'+3' and 2x3' UTR revealed the best transgene translation compared to the other tested cellular UTRs in both NIH3T3 and A549 cells. Therefore, these mRNA constructs, coding for *Met*Luc, were selected for physical mRNA stability analysis and were investigated via quantitative RT-PCR. Two primer pairs were tested for mRNA quantification. As the primer pair binding downstream of the start codon gave better primer efficiency, quantification and specificity, this pair was used for quantification of *Met*Luc transcripts in further experiments. For comparison of the primer pairs with respect to their amplification efficiency, specificity and quantification see supplementary Figure 16 and 17. At 4 hours post-transfection only *Met*Luc with 5' CYBA UTR showed a significant increase in mRNA amount compared to the control without UTRs in NIH3T3 cells. For other CYBA UTR combinations, (5'+3' and 2x3' UTR), no significant difference in the physical stability of mRNA was observed compared to the control among all time points in NIH3T3 cells (Figure 6A). In contrast to the results in NIH3T3 cells, no significant increase in physical mRNA half-life could

be observed in A549 cells. Instead, a significant decrease in mRNA amount was observed with mRNA constructs containing combinations of 5'+3' and 2x3' CYBA UTR at 4 h and 24 h post-transfection (Figure 6B). For the same samples, *Met*Luc activity in NIH3T3 and A549 cells was measured and data is presented as Figure 6C and 6D, respectively. No significant differences in protein translation could be observed for the tested UTRs compared to the control at 4 h post-transfection in both cell lines. At later time points (24 hours onwards) enhanced transgene expression was observed in both cell lines with *Met*Luc mRNA containing 5'+3' CYBA UTR (Figure 6C and 6D).

Interestingly, although the mRNA itself was not stabilized over time, significantly higher transgene translation for some of the tested UTRs compared to the control at later time points could be measured. For instance in A549 reduced levels of *Met*Luc mRNA containing 5'+3' CYBA UTR, observed at later time points (24 hours onwards: Figure 6B), resulted in higher protein translation levels than control *Met*Luc mRNA for these time points (Figure 6D). Based on these data, "mRNA productivity", defined as protein produced per unit of mRNA quantified was calculated for each of the compared constructs. These values are presented as Figure 6E and 6F for NIH3T3 and A549 cells, respectively. Messenger RNA constructs furnished with 5'+3' CYBA UTR appeared to be species and tissue independent, whereas the construct with 5' UTR alone as well as two copies of 3' UTR enhanced mRNA productivity only in A549 and in NIH3T3, respectively. Combining the data from Figure 6 leads to the conclusion that incorporation of CYBA UTRs into mRNA significantly enhances their productivity without affecting their physical stability. Depending on the UTR combination these effects seem to be cell-type specific, with the exception of the 5'+3' CYBA UTR combination.
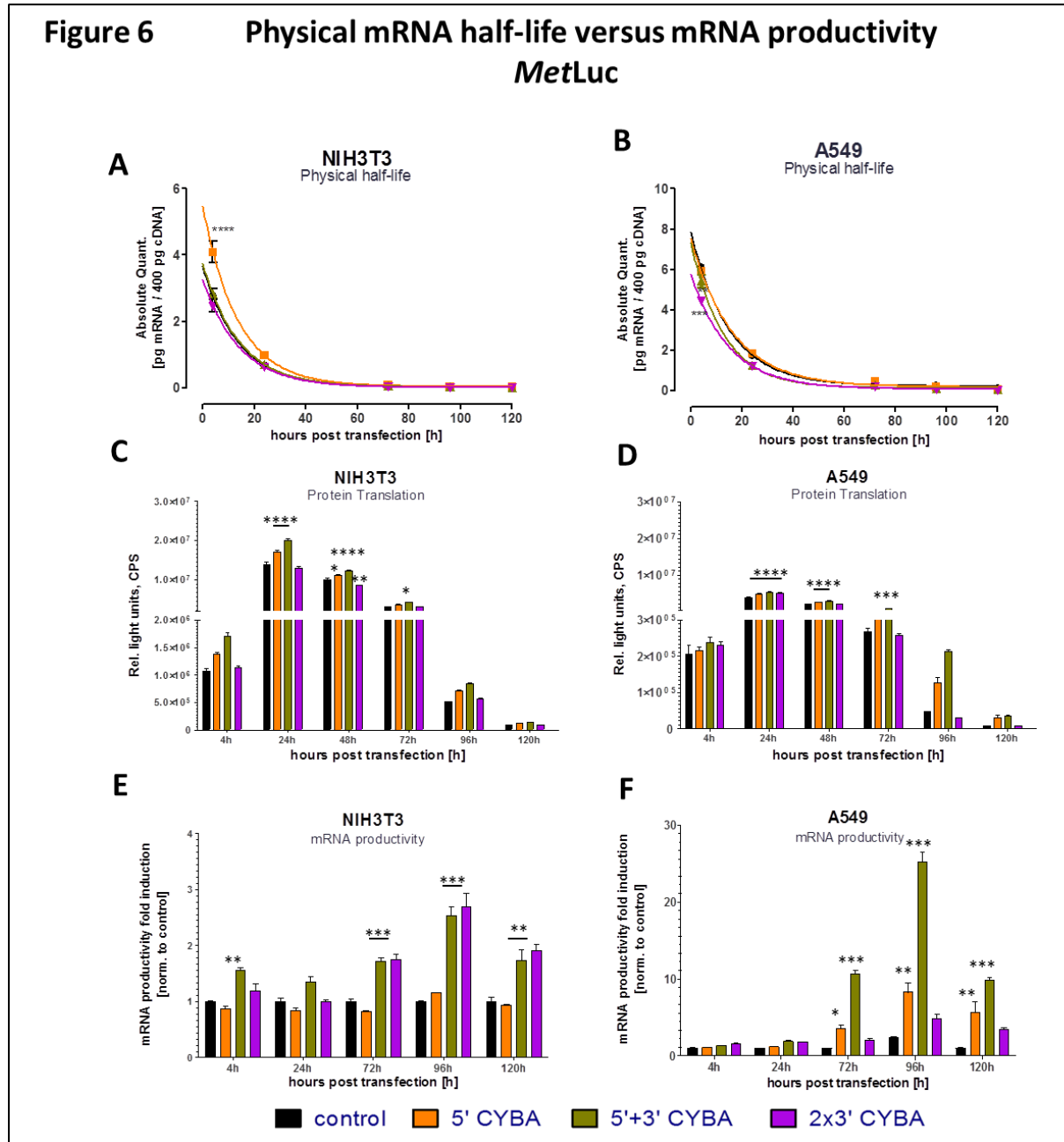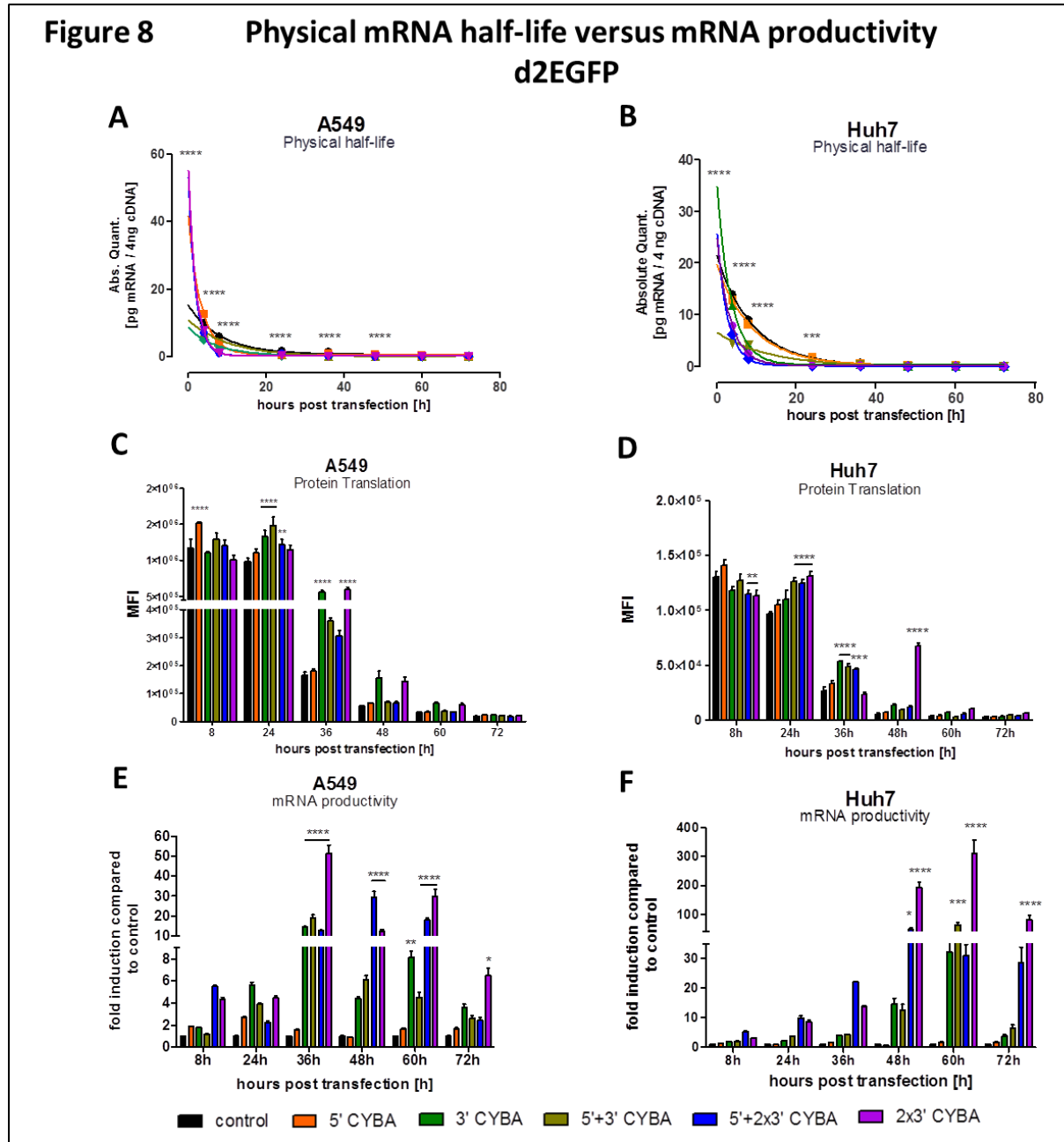
Figure 6: Determination of physical mRNA stability and the corresponding protein translation as wells as the resulting mRNA productivity (*Met*Luc)

Absolute mRNA amount reflecting the physical mRNA half-life kinetic in NIH3T3 (A) and A549 cells (B), which was quantified by RT-PCR. The corresponding *Met*Luc protein translation data at 4h, 24h, 48h, 72h, 96h and 120h post-transfection in NIH3T3 and in A549 cells are shown in Figure 6C and 6D, respectively. Figures 6E and 6F present the mean fold induction of the mRNA productivity of the different CYBA UTR combinations in NIH3T3 and A549 cells, respectively. Data represent means ± SEM. Statistical significance was assessed by 2-way ANOVA test (Bonferroni multiple comparisons) with p values <0.05.

As mentioned before, to develop mRNA therapeutics it is important to determine the protein amount produced by translatable mRNA within a cell. Since the physical mRNA half-life only indicates the presence of mRNA, but not the translational capacity of an mRNA unit, the functional mRNA half-life was investigated out of interest. The functional mRNA half-life of different mRNA constructs was quantified by using micro-structured multi-channel slides for parallel single-cell transfection studies (see section 6.5.2).

5.5.2 Determination of the functional mRNA half-life via µ-structured single cell transfection studies

This part of my thesis has been published in the journal Lab on a Chip [157]. For the sake of brevity, only the abstract has been cited here: "The measurement of mRNA turnover in living cells plays an important role in the search for stable mRNA constructs for RNA-based therapies. Here we show that automated time-lapse microscopy combined with micropatterned arrays allows for efficient high-throughput monitoring of fluorescent reporter protein translation at the single-cell level. The fluorescence time courses after mRNA transfection yield the distribution of individual mRNA translation and degradation rates within a population. We compare mRNA constructs with combinations of 5' and 3' UTR sequences and find a systematic broadening and shift towards longer functional half-lives for UTR stabilized mRNA. At the same time the life time distribution of the destabilized EGFP reporter protein was found to be constant and narrowly distributed. Using mathematical modeling, we show that mRNA functional life-time predicts the time-integrated protein level, i.e. the area under the curve (AUC) of mRNA translation. Our approach paves the way for quantitative assessment of hitherto unexplored mRNA functional life time heterogeneity, possibly predicated on multiple mRNA secondary structures and its dependence on UTR sequences." The complete article is enclosed as Appendix 11.1.

Beside these analyses, physical half-life of d2EGFP mRNAs furnished with CYBA UTRs and their productivity (EGFP translation) were also assessed in A549 and Huh7 cells (see Figure 8). Firstly, the integrity of the produced d2EGFP CYBA mRNA constructs was checked on 1% agarose gel. All chemically modified mRNAs showed a single band of expected size on the gel (Figure 7). No smearing could be observed. With respect to the physical mRNA half-life, with a single exception at one time point in A549 cells (5'UTR alone), all other CYBA UTR containing mRNA constructs had either comparable or significantly lower half-lives (Figure 8A and B) in both cell lines. In contrast to the physical half-life, the corresponding protein translation (mRNA productivity) was significantly increased by all CYBA UTR containing constructs with exception of 5' CYBA UTR up to 36 hours post transfection in both A549 and Huh7 cells, respectively. Increase in mRNA productivity was evident at later time points (36 hours onwards) with 5'+3' CYBA UTR as well as 2x3' CYBA and 5'+2x3' being the most productive mRNA constructs compared to the control.

Figure 7: Agarose gel electrophoresis of d2EGFP mRNA

The different mRNA constructs were tested on agarose gel. As shown here, all mRNAs have one single band. The sizes of the mRNA constructs (bases): 955 b (w/o UTRs), 991 b (5' CYBA UTR), 1059 b (3' CYBA UTR), 1060 b (5'+3' CYBA UTR), 1134 b (5'+2x3' CYBA UTR) and 1133 b (2x3' CYBA UTR).

Figure 8: Determination of physical mRNA stability and the corresponding protein translation as wells as the resulting mRNA productivity (d2EGFP)

Absolute mRNA amount reflecting the physical mRNA half-life kinetic in A549 (A) and in Huh7 cells (B), which was quantified by RT-PCR. The corresponding d2EGFP protein translation kinetics in A549 (C) and in Huh7 cells (D) is illustrated in time-dependent manner. In Figure 8E and 8F the mean fold increase of mRNA productivity is shown of the different CYBA UTR combinations over time in A549 and in Huh7 cells, respectively. Data represents means ± SEM. Statistical significance was assessed by 2-way ANOVA test (Bonferroni multiple comparisons) with p values <0.05.

In conclusion, insertion of CYBA UTRs into the mRNA sequence increased its productivity.

5.6   mRNA secondary structures and their influence on translation

In order to investigate the enhanced translation by CYBA UTR, the 5' UTR region was analyzed. It is known that mRNA folding starts from the 5'end and secondary structure in the 5' UTR of the mRNA either enhances translation or can have inhibitory effects on translation [167]. Stable structures are unlikely to unfold, whereas instable secondary structures can unfold and allow binding of translation factors. Therefore, the influence of secondary structures of a given RNA sequence was assessed by analyzing the first 200 nucleotides including the 5' UTR and part of the coding region. The analysis of 5' secondary structures and its Gibbs free minimum energy (ΔG) was performed using mathematical algorithm software called mfold. Analysis was performed according to the work of Hughes et al. where 10 nucleotides were serially added to the 5' end of the mRNA and each mRNA length was calculated for its free minimum energy. At the beginning the first ten nucleotides of the mRNA sequence after the cap structure were analyzed and then the RNA molecule was extended by adding 10 nucleotides of the corresponding mRNA sequence at a time and calculated the new ΔG. This procedure was continued up to 200 nucleotides into the coding region. This kind of analysis allowed us to investigate the impact of the folding pattern caused by 5' CYBA UTR on the free minimum energy. In Figure 9 the impact of 5'CYBA UTR on mRNAs coding for *MetLuc* and d2EGFP on the ΔG, was investigated. For comparison the mRNA construct furnished only with 5' CYBA UTR was selected. As comparison, mRNA construct without UTRs was used. The 5' CYBA UTR is located within the first 100 nucleotides of the mRNA RNA length. A decrease in free energy with an increase in mRNA length was observed independently of the sequence and UTR structure (Figure 9A and 9C).

In order to gain further insights about the potential of secondary structures within the 5'UTR to affect translation by inhibiting the binding of translation factors, it is recommended by Hughes et al. to investigate the free energy per nucleotide. For this purpose, ΔG value was divided by the number of nucleotides of the corresponding RNA length of *MetLuc* and d2EGFP, respectively. These data are presented as Figure 9B and 9D. As a result no significant differences in ΔG/nt were observed between the control and mRNA construct furnished with 5' CYBA UTR. Similar to ΔG, the ΔG/nt value decreased by increasing the corresponding RNA length, independently of mRNA sequence and structure containing UTRs or without UTRs.

Taken together, mRNAs coding for *MetLuc*, d2EGFP furnished with 5' CYBA UTR showed no significant differences in thermal stability energy ΔG or ΔG/nt compared to the control. In conclusion our data show that the 5' CYBA UTR does not have any additional secondary structure.

Figure 9   **Modelling of RNA length and its impact on minimum free energy ΔG *Met*Luc and d2EGFP**
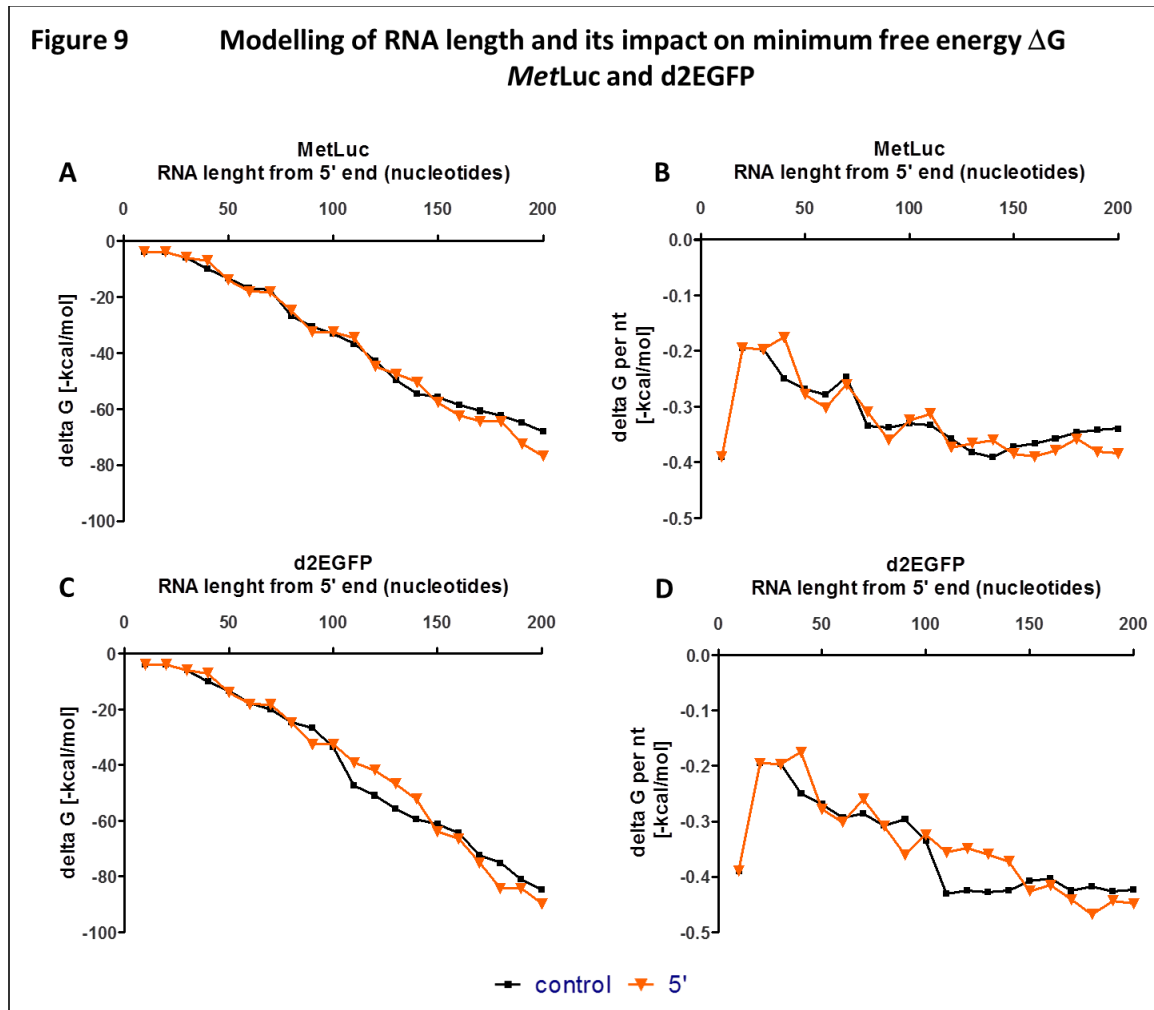
Figure 9: Investigation of the effects of RNA length of *Met*Luc and d2EGFP on the free minimum energy Δ G and Δ G per nucleotide

Both mRNA constructs coding for *Met*Luc, including control (black) and 5' CYBA UTR (orange), were investigated with respect to their free minimum energy ΔG (A) the ΔG per nucleotide of (B). Same was performed with mRNA coding for d2EGFP (C and D). By increasing the RNA length the free minimum energy as well as the ΔG/nt decreased. Statistical significance was assessed by 2-way ANOVA test.

5.7   Investigation of CYBA UTR in a physiological system

Previous experiments with *Met*Luc and d2EGFP demonstrated that some of the tested mRNA constructs furnished with CYBA UTR combinations resulted in enhanced transgene translation compared to the control without UTRs. Both *Met*Luc and EGFP are reporter proteins from non-mammalian organisms. In subsequent experiments, effects of CYBA UTR(s) on the functionality/half-life on a mammalian sequence were investigated. Human BMP2, which plays an important role in bone and cartilage development, was chosen for these experiments. Therefore, all different combinations of CYBA UTR were cloned upstream/downstream of hBMP2 coding sequence. Agarose gel electrophoresis was used to check the integrity and quality of *in-vitro* transcribed mRNA (see Figure 10).

Figure 10 hBmp2 mRNA products on 1% agarose gel
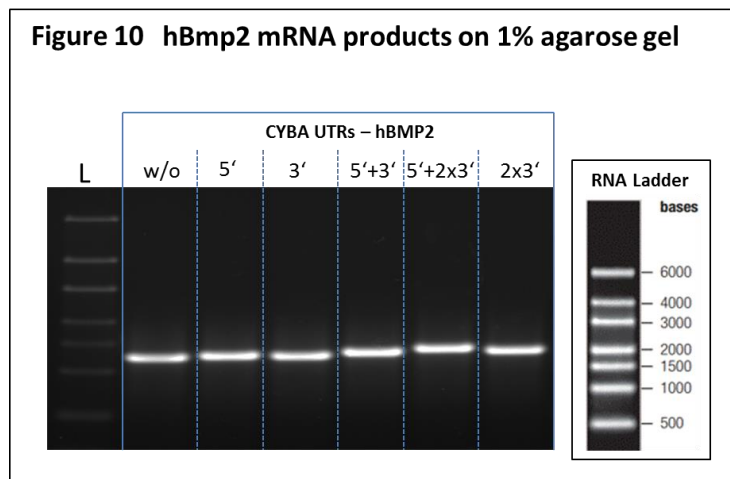
Figure 10: Agarose gel electrophoresis of mRNA coding for hBMP2

The different mRNA constructs were checked on 1% agarose gel. As shown here, all mRNAs indicated only one single band. The sizes of the mRNA constructs (bases): 1381 b (hBMP2 w/o UTRs), 1417 b (5' CYBA UTR), 1416 b (3' CYBA UTR), 1486 b (5'+3' CYBA UTR), 1560 b (5'+2x3' CYBA UTR) and 1490 b (2x3' CYBA UTR).

After production, the mRNAs were transfected into C2C12 cells. The murine C2C12 cells are derived from thigh muscle of C3H mice after a crush injury and are frequently used for differentiation into myoblast and osteoblast. Hence this cell line was selected to study the osteogenic potential of different mRNA constructs coding for hBMP2.

5.7.1   Comparison of different mRNA transfection protocols in C2C12 cells

Initial experiments were conducted to establish a protocol for efficient transfection in C2C12 cells with mRNA. For this, the conventional transfection protocol using DFG was combined with magnetofection using two different magnetic nanopartides, and experiments were performed using only the control mRNA construct i.e hBMP2 without any UTR(s). Magnetofection enables a synchronized, highly efficient and reproducible transfection of many cell lines and primary cells. Two different magnetic nanopartides, SoMag-5 and SoMag6-115, were tested for their efficacy to transfect chemically modified hBMP2 mRNA at two different doses, 20pg/cell and 10pg/cell. Both cell viability and hBMP2 translation post transfection were measured (Figure 11). Cell viability of 80% was considered reasonable for all tested transfection protocols at both doses (Figure 11A). With respect to protein translation, SoMag5 was significantly more effective than SoMag6-115 and DFG after 24 h post-transfection at a dose of 20pg/cell (Figure 11B). Transfection with 10 pg mRNA/cell revealed no significant differences between the two nanoparticles in hBMP2 translation, whereas DFG did not show any translation (Figure 11C). To summarize, the data of Figure 11 showed highest transfection efficiency in C2C12 after 24 hours post-transfection using SoMag5 magnetic nanoparticles for magnetofection with 20 pg mRNA/cell.
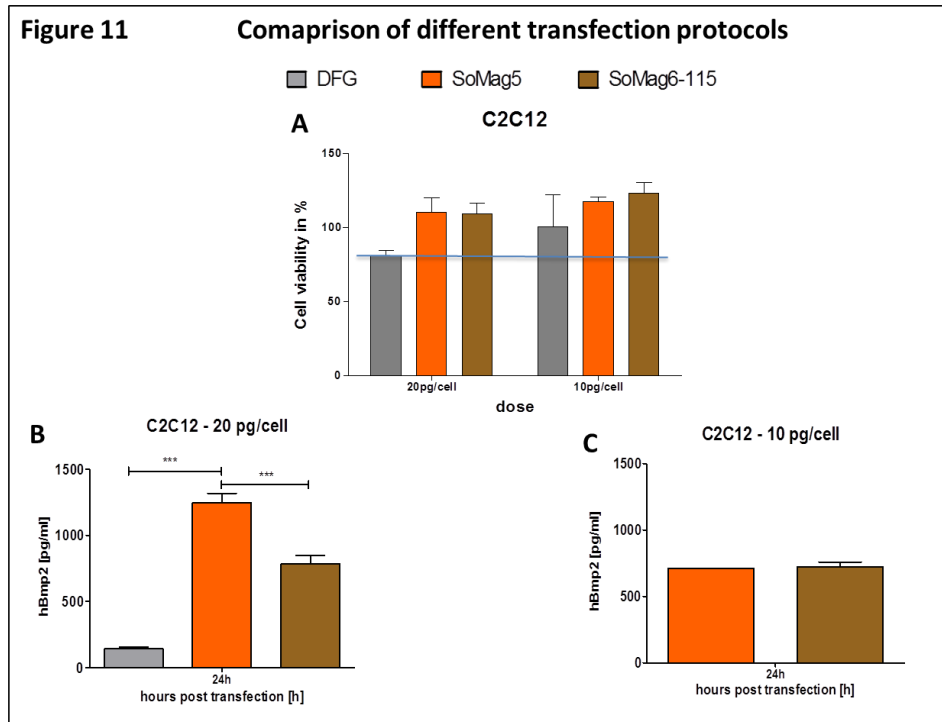
Figure 11: Cell viability and the corresponding hBMP2 translation after transfection with DFG or magnetofection

Percentage of cell viability is shown for various transfection conditions, such as DFG (grey), magnetofection using either SoMag5 (orange) and SoMag6-115 (brown) nanoparticles at two mRNA doses 20 pg/cell and 10 pg/cell (11A). The corresponding hBMP2 protein translation is shown for the same transfection conditions as mentioned previously comparing both doses 20 pg/cell (B) and 10 pg/cell (C). Data represent means ± SEM. Statistical significance was assessed by One-way ANOVA test (Newman Keuls comparison) with p values <0.05.

5.7.2 Screening of various CYBA UTR mRNA constructs coding for hBMP2

In order to exclude cell-specific effects by the various CYBA UTR combinations, all mRNA constructs containing CYBA UTR(s) coding for the physiological gene hBMP2 were investigated in C2C12 cells.

Based on the results in Figure 11, screening of the various CYBA UTR mRNA constructs were conducted by using magnetofection at a dose of 20 pg mRNA/cell. At 24 and 48 hours post-transfection hBMP2 was quantified using ELISA. The mRNA construct with 2x3' CYBA UTR showed the highest and significant increase in protein translation at both time points (Figure 12) compared to the control. Messenger RNA constructs with 3' and 5'+2x3' CYBA UTR showed also a significant improvement in hBMP2 translation after 48h post-transfection compared to the control. The mRNA construct 5'+3' CYBA UTR instead showed a significant decrease in hBMP2 translation after 24 hours post-transfection.
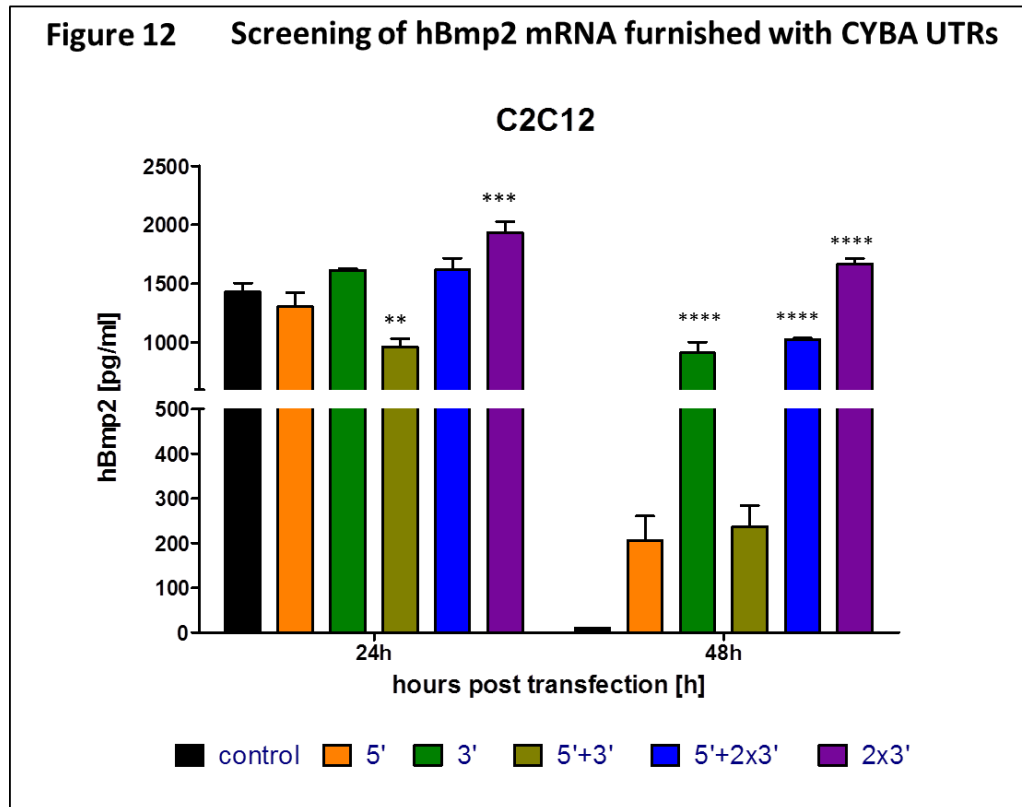
Figure 12: Comparing the hBMP2 translation after transfecting different mRNA constructs furnished with cellular UTRs

mRNA coding for hBMP2 with CYBA UTR combinations, including 5' (orange), 3' (green), 5'+3'(light green), 5'+2x3' (blue) and 2x3' (purple) UTR, were transfected into C2C12 cells. Human BMP2 translation was measured after 24 hours and 48 hours post-transfection. Means are followed by standard error deviation. Statistical significance was assessed by 2-way ANOVA test (Bonferroni multiple comparisons) with p values <0.05.

Taken together insertion of CYBA UTRs increased the productivity of hBMP2 mRNA in C2C12 cells. Two copies of 3' CYBA UTRs resulted in the highest protein translation compared to all other UTR combinations.

5.7.3 Determination of physical mRNA half-life and translation of hBMP2 mRNA furnished with CYBA UTRs in C2C12 cells

In a next step the physical half-life and mRNA productivity of hBMP2 mRNA constructs with the best working UTR combination, 2x3' CYBA, and the worst working one which was 5'+3' CYBA UTR were assessed. As a result, no beneficial effects could be observed in increasing the physical mRNA of mRNA constructs furnished with CYBA UTRs compared with the control without UTRs (Figure 13A). Instead a significant decrease in mRNA amount of mRNAs with CYBA UTRs at early time points was detected. However, the mRNA construct 2x3' CYBA UTR significantly resulted in the highest protein translation compared to the control after 24 hours post transfection, when lower level of mRNA amount was detected (see Figure 13B). mRNA productivity data revealed that addition of 2 copies of 3'CYBA UTR significantly increased the mRNA productivity (6-8 fold) over the control and 5'+3'UTR mRNA groups 24 hours post transfection (see Figure 13C). To conclude, insertion of 2 copies of 3'UTR from CYBA downstream of the coding region enhanced protein translation compared to the control without affecting the physical mRNA half-life.
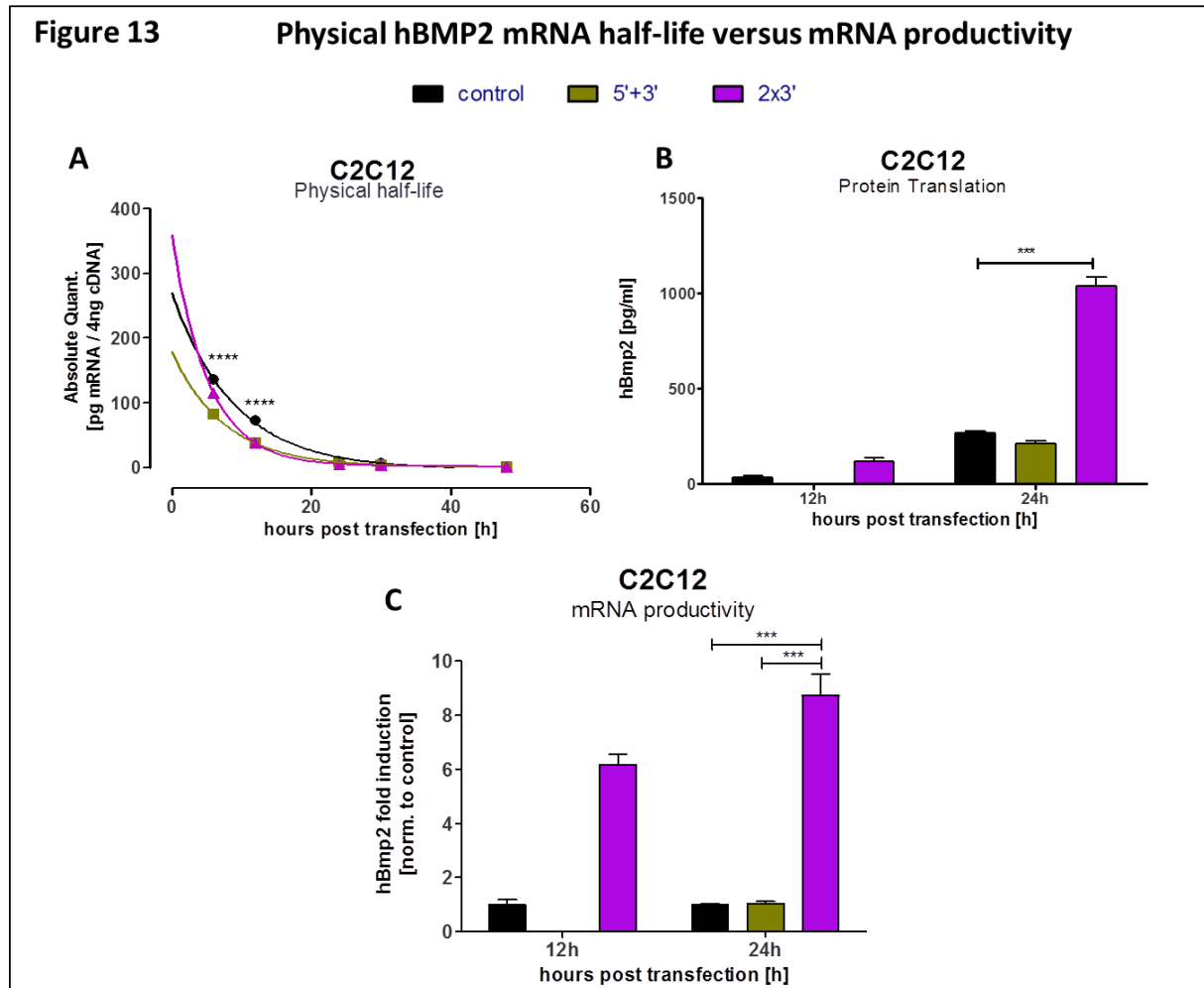
Figure 13: Determination of the hBMP2 mRNA stability via qRT-PCR and quantification of protein translation

C2C12 cells were transfected with hBMP2 mRNA furnished with 2x3' CYBA UTR (purple) and 5'+3' CYBA UTR (green) and were compared to the control without UTRs (black). Absolute mRNA quantification (A) as well as the corresponding protein translation (B) were determined by qRT-PCR and ELISA, respectively. In Figure 13C the mean fold induction of the mRNA productivity of the different CYBA UTR combinations after 12h and 24h post transfection is shown. Data represent means ± SEM. Statistical significance was assessed by One-way ANOVA test (Newman Keuls comparison) with p values <0.05.

To summarize, hBMP2 mRNA containing 2 copies of 3'UTR from CYBA gene significantly increased the translational capacity of the mRNA molecule without affecting its stability. In order to investigate the different translational efficiencies of the mRNA constructs coding for *Met*Luc, d2EGFP and hBMP2 with the CYBA combinations 5'+3' UTRs and 2x3' UTRs, secondary structure analyses were performed via mfold (see Results 5.7.4).

5.7.4 Secondary structure analysis of different mRNA sequences furnished with 5'+3' CYBA and 2x3' CYBA UTRs

Table 12: Secondary structure analysis of complete mRNA sequences via mfold

Table 12 shows the following features: the free minimum energy (ΔG) of each mRNA construct, folding patterns in the 5'- and 3'-end as well as secondary structures found within the UTRs. Therefore the mfold web server was used to predict mRNA secondary structures. Here the thermal stability was predicted for mRNA sequences coding for *Met*Luc, d2EGFP and hBMP2 with the CYBA UTR combinations 5'+3' and 2x3', respectively. As a consequence, mfold displays several structures, ranking the most stable structures with the lowest thermal stability ΔG at the top. For each mRNA construct the first eight structures with the lowest ΔG were compared. In case of mRNA sequences furnished with 5'+3', except of the hBMP2 sequence, a binding between 5' –UTR to the 3' –UTR was observed. The mRNA constructs with the CYBA combination of 2x3' UTR showed no interaction between the 5' UTR with the 3' UTR. Instead, the 5' –end was binding with the coding region (cds) and formed a stem loop structure. This was true for all mRNA constructs with the exception of mRNA coding for d2EGFP, which was binding with its 5'-end and formed a stem loop too. Within the 3' –end all, multi-branched loops as well as interior loops were formed by all mRNA sequences containing 2x3' CYBA UTRs. Additionally, the position of each formed stem loop after the cap structure is shown in Table 12. As a result, the stem loop of mRNA encoding d2EGFP and hBMP2 containing 2x3' CYBA UTR was placed 1 base after the cap structure (+1). The *Met*Luc mRNA construct with 2x3' CYBA UTR displayed a stem loop at position +20.

mRNA sequences flanked by 5'+3'CYBA UTRs:

Sequence	Δ G [kcal/mol]	5'end	3' end	5' UTR	3'UTR
*Met*Luc	-336.80	(5/8) binds to 3'end	(5/8) binds to 5' end	(5/8) binds to 3' UTR	(5/8) binds to 5' UTR
d2EGFP	-405.70	(3/8) binds to 3' UTR	(4/8) binds to 5' end	(4/8) binds to 3' UTR	(7/8) forms stem loop
hBMP2	-574.80	(5/8) binds to cds and forms stem loop (position+15; 4 out of 8)	(6/8) binds to cds	(5/8) binds to cds	(7/8) binds with itself (forms interior loop)

mRNA sequences flanked by 2x3'CYBA UTRs:

Sequence	Δ G [kcal/mol]	5'end	3' end	5' UTR	3'UTR
*Met*Luc	-340	(4/8) binds to cds and forms stem loop (position+20; 3 out of 8)	(4/8) binds to cds	none	(6/8) 1st 3' UTR: multi-branched loop; 2nd 3' UTR: interior loop
d2EGFP	-444.10	(8/8) binds to itself and forms stem loop (position +1; 8 out of 8)	(8/8) loose	none	(3/8) 1st 3' UTR: stem loop; 2nd 3' UTR: two stem loops
hBMP2	-575.40	(8/8) forms stem loop with cds (position +1; 5 out of 8)	(8/8) binds to cds	none	(3/8) 1st 3' UTR: multi-branched loop; 2nd 3' UTR: interior loop

5.8 Cytokine and chemokine screening

In order to investigate if incorporation of CYBA UTRs could activate the immune response, cytokines and chemokine release were measured in cell culture supernatants from C2C12 cells of Figure 13 at 6 and 12 hours post transfection. The cytokines and chemokines analyzed were IL-10, IL-1-β, IL-2, IP-10, IL-6, IFN-α, IFN-γ, IL-12p70, TNF-alpha and MCP-1. Measurements were performed using a magnetic bead-based immunoassay. As shown in Figure 14, mRNA transfection significantly induced IP-10 and IL-6 irrespective of the UTR combination. IFN-α was induced only by control hBMP2 mRNA (without UTRs) and MCP-1 expression was not affected by transfection. IL-10, IL-1-β, IL-2, IFN-γ, IL-12p70 and TNF-α were not detectable.
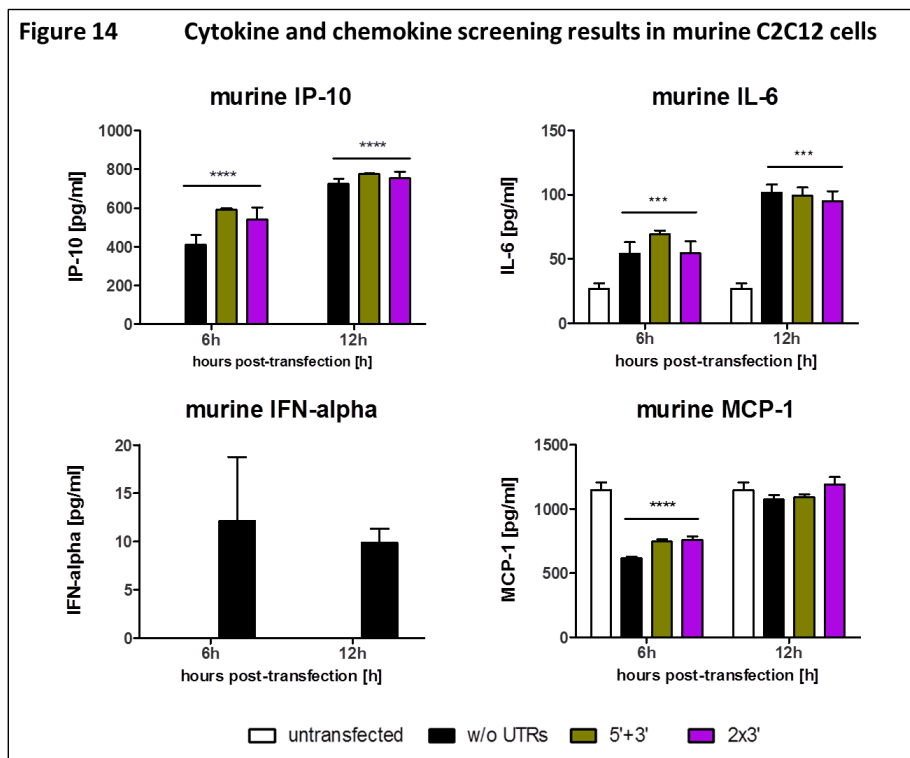
Figure 14: Screening of different cytokines with magnetic bead-based immunoassay

C2C12 cells were transfected with chemically modified hBMP2 mRNA furnished with 2x3' CYBA UTR (purple) and 5'+3' CYBA UTR (green), without UTRs (black) and were compared to untransfected cells (white). Supernatants were collected and measured for cytokines 6 and 12 hours post transfection. The cytokine release of murine IP-10, IL-6, IFN-alpha and MCP-1 was detected. Data represent means ± SEM. Statistical significance was assessed by Two-way ANOVA test (Bonferroni multiple comparisons) with p values <0.05.

6. Discussion

The development of new therapies, such as transcript therapy, faces many challenges. One of the most important factors determining the success of mRNA therapy is the efficacy of mRNA translation and stability. In order to enhance protein translation and mRNA half-life, the mRNA molecule can be optimized by including structural modifications using different approaches. So far, several strategies have been implemented such the elongation of the poly(A) tail, inclusion of chemically modified nucleotides, enhancing the capping efficiency and insertion of UTRs. In this study different cellular UTRs based on mRNA stability data were selected and were investigated with respect to translation and mRNA stability. Therefore mRNA molecules consisting of chemically modified mRNAs, a long poly(A) tail and with various cellular UTR combinations were designed. The UTRs of interest were obtained from the genes encoding CYBA, DECR1, GMFG, MAPBPIP and MYL6B.

In fact, some of the tested cellular UTRs, which were artificially flanking a foreign mRNA sequence, showed an increase in protein translation compared to the control without UTRs. One of the best working UTR was obtained from the CYBA gene. It could be shown that insertion of CYBA UTRs enhanced the mRNA productivity rather than increasing the mRNA stability However, the impact of CYBA UTR combinations on translation is gene - and cell-specific. In order to enable high-throughput screenings in future, an improved understanding in the influence of secondary structures on translation may lead to a better algorithm to identify optimal UTRs for a given coding region and target cell-type.

6.1 UTRs and protein translation

Untranslated regions are known to play a pivotal role in mRNA translation and stability and are located upstream and/or downstream of the coding region referred to as 5' -UTR and 3' -UTR, respectively. Up to now some UTR regions have been identified which play an eminent role in the regulation of protein translation [27, 158].

For instance one study showed that the insertion of 5' the UTR of rabbit β-globin resulted in increased protein translation in *in vitro* translation assays [159]. Another study reported an improvement in protein translation in dendritic cells by introducing mRNA molecules furnished with 3' -UTR of the *Xenopus leavis* β-globin [93]. In 2012 Kariko *et al.* furnished mRNA molecules coding for mEpo with a 5' -UTR derived from the tobacco etch virus 5' leader RNA and a 3' -UTR of the Xenopus β-globin mRNA resulting in enhanced translation *in vivo* [95]. These successful studies were consistent with many other previous studies, where UTRs obtained from *Xenopus leavis* or human β-globin were used [69, 160, 161]

In the current study, it could be shown that some of our tested human UTRs could also increase protein translation over time, called AUC, compared to the control without UTRs. The AUC was specified to determine the best working UTRs. Here, five different human cellular UTRs from mRNAs with relatively long half-lives (CYBA, DECR1, GMFG, MAPBPIP and MYL6B) were selected and were cloned upstream (5' -UTR) and/or downstream (3' -UTR) of the reporter gene coding for *Met*Luc. Subsequently, all UTRs were screened in two different cell lines. Goal of this study was to figure out whether long half-lives of our selected cellular UTRs are portable for any other gene of interest thereby enhancing transgene expression. Furthermore, five different UTR combinations such 5' and 3' alone, 5'+3', 5'+2x3' and two copies of 3' -UTR for every cellular UTR flanking the reporter gene were tested. As a result mRNA containing CYBA UTRs yielded the highest *Met*Luc reporter protein translation among all the tested UTRs in NIH3T3 and A549, respectively. In both cell types, the mRNA construct consisting of 5'+3' CYBA resulted in the highest relative AUC. Similar results were obtained for mRNA molecules encoding d2EGFP in A549 and Huh7.

In a next step, all combinations of CYBA UTR were cloned into the human hBMP2 mRNA sequence and screened in C2C12 cells. In contrast to the results with *Met*Luc and d2EGFP, mRNA combination 5'+3' CYBA UTR flanking hBMP2 did not result in the highest protein translation in C2C12 cells. Instead, the highest hBMP2 translation was detected for the mRNA construct furnished with 2x3' CYBA UTR followed by mRNA constructs containing 3' and 5'+2x3' CYBA UTRs (see Figure 12). This change in translation efficiency could be due to the different used cell types and/or different genes of interest [162-164]. The beneficial effect of

two copies of the same UTR has been reported previously by Holtkamp *et al.* They could show that the insertion of one 3' -UTR also enhanced transgene expression, but even higher translation was achieved by inserting two copies of human 3' β-globin UTR in dendritic cells.

Taken together, these observations lead to the assumption that the impact of CYBA UTRs on protein translation seems to be gene- and species-specific. Baudouin-Legros and colleagues observed similar effects. They could show that the mRNA stability of CFTR (cystic fibrosis transmembrane conductance regulator) is cell-specific. The CFTR mRNA is regulated by cytokines such TNFα by binding to the 3' -UTR end of the mRNA. In the presence of TNFα, CFTR mRNA level in human HT-29 colon cells was decreasing but not in pulmonary Calu-3 cells [164].

6.2   mRNA stability and productivity

Another important parameter in transcript development is the mRNA stability itself. The impact of mRNA stability on the control of translation is described elsewhere [39, 165, 166]. High mRNA stability is desired for prolonged protein turnover. One study could show that the insertion of two copies of 3'UTR from human β-globin gene leads to mRNA stabilization, which was quantified by qRT-PCR, thereby resulting in improved translational efficiency [93].

In the current study, mRNA constructs furnished with CYBA UTR yielded the highest protein translation. This enhanced protein translation could be due to stabilization of mRNAs. In order to proof the mRNA stability, two values for mRNA stability, which are the physical and the functional mRNA half-life, were determined. The physical mRNA half-life and the functional half-life were compared via qRT-PCR and μ-structured single-cell arrays, respectively. The physical half-life was investigated for the best working cellular CYBA UTR combinations, which were 5'+3' –UTR followed by 5' -UTR and 2x3' -UTR according to the screening results in NIH3T3 and A549. In all measured samples no mRNA stabilization of the tested constructs was observed compared to the control.

Noteworthy, the measurement of the physical half-life via qRT-PCR includes the entire population of translatable and non-translatable mRNA whereas the functional half-life determines solely mRNA which is finally translated into a protein. By using micro-pattern-based single-cell arrays the verification of the functional half-life in a high-throughput manner is possible. The functional mRNA half-life is considered as a better value to determine the functional stabilized population of modified mRNA molecules. Therefore the functional half-life of all mRNA constructs with CYBA combinations coding for d2EGFP was investigated in A549 and Huh7 cells. As a result, any insertion of 5' and 3' CYBA UTR resulted in increased functional half-life in both cell lines.

Although the physical mRNA half-life was not increased, mRNA constructs with UTRs resulted in enhanced protein translation at later time points compared to the control without UTRs. One explanation is the increased mRNA productivity, which is defined as the protein amount normalized to the mRNA amount and describes the translational capacity of a single mRNA molecule. As a consequence, the highest mRNA productivity of *Met*Luc translation was achieved with mRNA constructs furnished with 5'+3' CYBA UTR in NIH3T3 and A549, respectively. Other constructs which delivered high amounts of protein per mRNA molecule were the 2x3' CYBA UTR mRNA construct and the 5' CYBA UTR in both cell lines, NIH3T3 and A549. In case of d2EGFP productivity, mRNA constructs containing 2x3' CYBA UTR showed highest mRNA

productivity compared to the control without UTRs in A549 and Huh7, respectively. However, to determine the "functional mRNA productivity", the true population of functional and physical mRNA within an mRNA pool has to be identified. Therefore, the functional mRNA productivity over time would be a better value to determine the therapeutic relevance of a functional modified mRNA molecule instead of the AUC.

Having a closer look at the correlation between mRNA stability and translation caused by the insertion of CYBA UTRs, the following was observed: Data with high amounts of mRNA molecules at 4 hours post-transfection quantified via qRT-PCR, indicated low protein level. This phenomenon is due to the lag-phase between transcription and translation. For cellular genes, it is known that dysregulation of mRNA is evident followed by measureable changes in protein amounts [167]. Moreover, it is assumed that at the earliest time points after transfection (4 hours), the different mRNA constructs are released similarly from the lipoplexes resulting in equal protein and mRNA quantity levels (see Figure 6 & 8). At later time points, when the mRNA amount has drastically decreased, the impact of the different cellular UTR come into play and increased protein translation was monitored.

Furthermore, the choice of cell-type and differentiation status are also crucial to ensure accurate estimation of mRNA half-life and mRNA productivity of a given mRNA molecule in an appropriate disease-related model. In a first trial the physical mRNA-half life and the productivity of mRNA constructs coding hBMP2 containing CYBA UTRs, including the worst (5'+3') and best working combination (2x3'), were investigated in C2C12 cells, which are frequently used for differentiation into osteoblasts. The physical half-life of all mRNA constructs was not increased compared to the control without UTRs. In contrast the mRNA productivity of hBMP2 mRNA containing 2x3' CYBA UTR was 9-fold higher than the control without UTRs. In future experiments, mRNA containing 2x3' CYBA UTR are going to be investigated with respect to mRNA stability and productivity in mesenchymal stem cells. Subsequently, the functional potential of the chemically modified mRNA constructs to induce bone differentiation has to be evaluated.

6.3   CYBA 5' -UTR secondary structure

As described before CYBA UTR was identified as one of the best working cellular UTR with respect to enhance transgene expression including *Met*Luc, d2EGFP and the physiological protein hBMP2. Two hypotheses are laid to explain the effectiveness of CYBA UTR compared to the other tested UTRs. One is based on the structural feature of CYBA UTR. It is postulated that messenger RNA stability correlates with its structure rather than with its function [10]. CYBA UTR has no known cis-acting elements in the 5' -UTR and has no secondary structures influencing translational initiation compared to the control, which was verified by the thermal stability ΔG (Figure 9) analysis and the translational onset shown for *Met*Luc after 4 h post-transfection (see Figure 6C and D). In contrast, the INS_SCE element forming a stem loop in the 3' -UTR could be advantageous compared to other cellular UTRs with no known 3' -UTR motives by protecting against degradation. Surprisingly, no improvement in protein translation of *Met*Luc mRNA containing only 3' CYBA UTR compared to the control without UTRs could be found. In contrast, although 5' CYBA UTR has no known structural features, enhanced protein translation for mRNA constructs coding for *Met*Luc and d2EGFP in different cell lines was measured. These results are in contradiction to those reported by Sharova *et al.* and lead to the assumption that stability effects are rather structure-independent.

The second explanation takes the GC content into account of the various 5' cellular UTRs, which results in different translational efficiencies. A high GC content can drastically reduce protein translation in cells. It is known that GC-rich regions in the 5' end can hinder translational efficiency independently from hairpin structures formed within the 5' -UTR. The longer a UTR is, the higher is the probability to have GC-rich regions. Surprisingly, although 5' CYBA UTR is relatively short it has the highest GC content compared to all other human cellular UTRs (see supplementary Table 13). For instance, mRNA flanked with cellular 5' MYL6B UTR, containing a low GC content, did not improve protein translation in NIH3T3 and A549 compared to the control whereas mRNA constructs furnished with 5' CYBA UTR resulted in the highest protein translation. These results are contradicting the findings of Hughes and colleagues [66]. However, these observed effects evolved by GC-rich regions in the 5' end do not necessarily mean to appear *in vivo* [65, 168, 169].

Furthermore, hBMP2 translation data revealed that the insertion of 5' CYBA UTR is not necessary to enhance protein translation. In this case the hBMP2 mRNA constructs containing either 5'+3' -UTR or 2x3' CYBA UTR were compared and significant higher protein level for constructs lacking 5' CYBA UTR were detected (see Figure 12). In order to find an explanation for this different outcome in translation, both mRNA constructs were analyzed using mfold. As a consequence, both mRNAs consisting of 5'+3' CYBA UTR

or either 2x3' CYBA UTR displayed similar secondary structures within the 3' UTRs. However, differences with respect to the position of formed stem loop close to the cap structure were found. The mRNAs with 2x3' CYBA and 5+3' CYBA UTR displayed stem loops at position +1 and +15, respectively (see Table 14). It is known that structures close to the cap structures (position +1) can drastically inhibit protein translation [63]. Thus, is not convertible in this case. Previous data could show that within the 5' CYBA UTR no stable secondary structures were formed without having any negative effect on translation. Finally the GC content within the 5'-end of mRNA sequences coding for hBMP2 with the CYBA UTR combinations, 2x3' and 5'+3' UTR, was assessed and is shown also in Table 14. Here, the first bases of the mRNA sequence after the cap structure until the start codon AUG were used for calculation resulting in 67.7% and 62.9% for 2x3' and 5'+3' CYBA UTR, respectively. Again, these data are not in compliance with the findings of Hughes *et al.* [66].

Nonetheless, the *Met*Luc mRNA construct furnished with 5'+3' CYBA UTR revealed the highest AUC value in both cell lines, NIH3T3 and A549. Similar results were found for mRNA sequences coding for d2EGFP flanked with 5'+3' CYBA UTRs in A549 and in Huh7 cells. Structural configurations which are assumed to enable this increase in translation are for instance the binding of 3'-UTR with the 5'-UTR of the mRNA molecule. This structural conformation minimizes the distance of the 5' to 3' end which could enable a faster initiation of translation (see Table 12) [51, 52]. In case of mRNA CYBA UTR combinations such 5'+2x3' or 2x3'constructs encoding d2EGFP, secondary structures such stem loops in the 3'-UTR were formed (see Appendix 1, Table S1). These loops in the 3'–end might ensure protection against degradation leading to increased functional mRNA life time.

In summary, the 5'-UTR of CYBA is capable of enhancing translation but is not necessary depending on the tested cell line and gene of interest. The reasons behind this are still unclear.

6.4   mRNA immunology

Kormann and colleagues could show that the combination of chemically modified mRNA including a poly(A) tail of 120nt and ARCA cap did not lead to a significant induction of IFN-γ, Il-12 and IFN-α *in vitro* and *in vivo* [82]. Whereas, the tested combination in this study consisting of the same chemically modified nucleotides and cap structure, furnished with a long poly(A) tail and additional cellular UTRs resulted in a significant IP-10 and IL-6 release in *vitro*. The release of IP-10 is due to the delivery vehicle. However, the main difference between the two studies is in the mRNA complex formation. In the current study, mRNA complexes were formed with the cationic lipid Dreamfect Gold combined with magnetic nanoparticles while mRNA complexes by Kormann *et al.* were prepared with Lipofectamine™2000. Therefore a direct comparison is not possible. Nonetheless, to evaluate the true impact of the used complexes, transfections studies in an immunologically relevant cell model such as peripheral blood mononuclear cells PBMCs or direct *in vivo* applications have to be performed.

7. Conclusion and Outlook

Messenger RNA engineering remains as a major objective in the development of mRNA therapeutics. Here different modifications within a single mRNA molecule were combined, which were: the combination of chemically modified nucleotides including 5-methyl cytidine and 2-thio uridine, a long poly(A) tail and the insertion of different cellular UTRs. As a consequence, mRNA combinations containing CYBA UTR resulted in enhanced protein translation. For the first time it has been shown that the insertion of the 2x 3' CYBA UTR combination into a mRNA sequence is capable of increasing translation of a physiological protein, in particular hBMP2. More importantly, the mRNA productivity of a single molecule rather the physical stability is enhanced by inserting CYBA UTRs into the tested genes such *Met*Luc, d2EGFP and hBMP2. However, the biological functionality of chemically modified BMP2 mRNAs furnished with CYBA UTR has to be proved via differentiation assays.

The various combinations of UTRs have to be investigated for any kind of gene and cell-type of interest to ensure the right choice of combination, enabling the highest protein translation over time. The mechanism behind the improved translation triggered by the insertion of CYBA UTR has to be further investigated. Therefore, the translational turnover per mRNA molecule and the physical/functional half-life have to be identified of each mRNA construct. In order to examine protein-RNA interaction, which are influencing the binding of different factors and are involved in degradation or translational, assays such RNA immunoprecipitation have to be performed. The focus of future projects will be on mRNA engineering. Further structural optimization of mRNA molecules can be achieved by insertion of other cellular or viral UTRs, new chemically modified nucleotides, codon optimization and a poly(A) length of 150 nucleotides. On the one hand structural modifications can enable enhanced translation on the other hand other structural features can induce the opposite. Elements which are known to decrease mRNA stability and reduce protein translation are A/U-rich elements within the 3' -UTR or miRNA sequences in the mRNA sequence. The insertion of small RNA aptamer motifs into the 5' -UTR of mRNAs enables the reduction of protein production upon ligand addition. These methods together, allow a controlled degradation of the administered mRNA. Finally, another important aspect is the toxicity and immune response triggered by the externally administered mRNA. Not only the mRNA itself but also the delivery vehicle can activate an immunological reaction. Therefore, the optimization of mRNA delivery of single or repeated administration of chemically modified mRNAs plays an important role in future application.

8. Supplementary Information

8.1   Plasmid cards

Circular plasmid vectors and their restriction sites as well as their sizes are shown below. All plasmids are depicted linear and are double stranded. These DNA vectors were used as templates for *in vitro* transcribes messenger RNA. Restriction enzymes with one cutting side are indicated in blue, enzymes with two cutting sides are labeled in red.

Figure 15: Plasmid cards

Figure 15.1: pVAX-A120
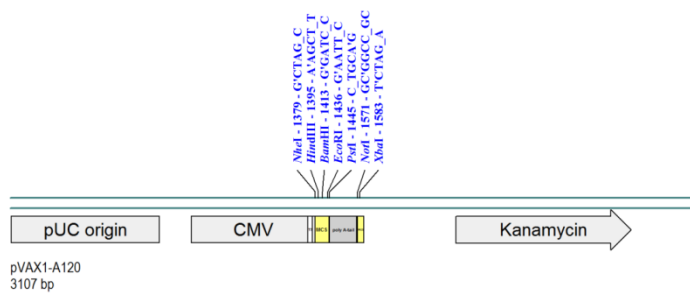
pVAX1-A120
3107 bp

Supplementary Figure 15.1: DNA vector pVAX1-A120 was described previously by Kormann *et al*. [82]. The plasmid contains a T7 promoter (white) beside the CMV promoter and a kanamycin resistance. To enable plasmid amplification in E.coli bacteria, a pUC origin sequence is also included in the DNA sequence. For cloning the multiple cloning sites (MCS) are highlighted in yellow. The poly A-tail (dark grey) is located in between the two MCS.

Figure 15.2: pVAX1-A-tail *Met*Luc

pVAX1-A-tail MetLuc
3753 bp
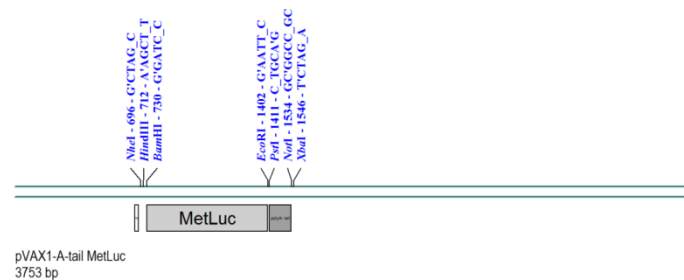
Supplementary Figure 15.2: Figure 15.2 shows the DNA vector pVAX1-A120 including the reporter gene *Met*Luc (grey) without UTRs. The reporter gene was inserted between the T7 promoter (white) and the poly A-tail (dark grey). Restriction sites are highlighted in blue.

Figure 15.3: pVAX1-A-tail *Met*Luc 5'

Vector card of pVAX1-A-tail *Met*Luc 5' CYBA is an example representing all other plasmids containing 5' cellular UTRs such DECR1, GMFG, MAPBPIP and MYL6B and all plasmids differ in size.
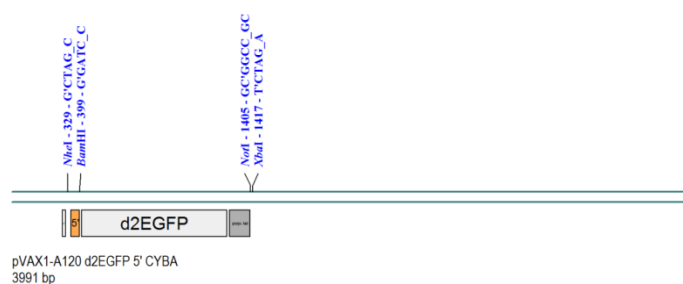

pVAX1-A-tail MetLuc 5' CYBA
3789 bp
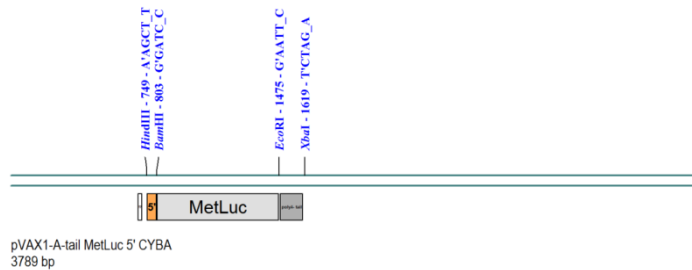
Supplementary Figure 15.3: DNA vector pVAX1-A-tail *Met*Luc comprises the 5' CYBA UTR (orange) and was inserted between the T7 promoter (white) and the reporter gene *Met*Luc (grey). Restriction sites are highlighted in blue. This DNA vector is a schematic representation for all other plasmids including a different cellular 5' UTR, for instance DECR1, GMFG, MAPBPIP and MYL6B.

Figure 15.4: pVAX1-A-tail *Met*Luc 5'+3'

Vector card of pVAX1-A-tail *Met*Luc 5'+3' CYBA is an example representing all other plasmids containing 5'+3' cellular UTRs such DECR1, GMFG, MAPBPIP and MYL6B and all plasmids differ in size.

pVAX1-A-tail MetLuc 5'+3' CYBA
3858 bp
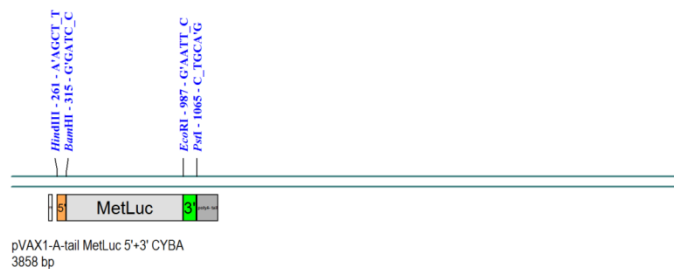
Supplementary Figure 15.4: DNA vector pVAX1-A-tail *Met*Luc comprises the 5' CYBA UTR (orange) and 3' CYBA UTR (green) and were inserted between the T7 promoter (white) and the reporter gene *Met*Luc (grey) and between the reporter gene and the poly A-tail (dark grey), respectively. Restriction sites are highlighted in blue. This DNA vector is a schematic representation for all other plasmids including a cellular combination of 5'+3' UTR, for instance DECR1, GMFG, MAPBPIP and MYL6B.

Figure 15.5: pVAX1-A-tail *Met*Luc 3'

Vector card of pVAX1-A-tail *Met*Luc 3' CYBA is an example representing all other plasmids containing 3' cellular UTRs such DECR1, GMFG, MAPBPIP and MYL6B and all plasmids differ in size.
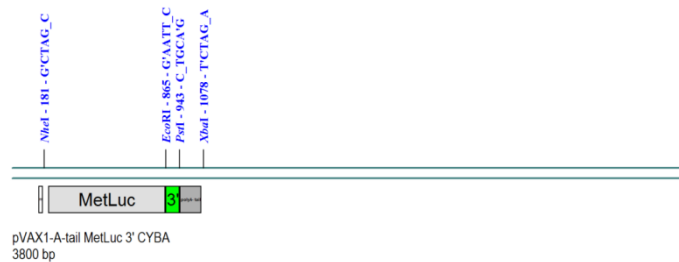
Supplementary Figure 15.5: DNA vector pVAX1-A-tail *Met*Luc comprises the 3' CYBA UTR (green) and was inserted between the reporter gene *Met*Luc (grey) and the poly A-tail (dark grey). Restriction sites are highlighted in blue. This DNA vector is a schematic representation for all other plasmids including a cellular 3' UTR, for instance DECR1, GMFG, MAPBPIP and MYL6B.

Figure 15.6: pVAX1-A-tail *Met*Luc 5'+2x3'

Vector card of pVAX1-A-tail *Met*Luc 5'+2x3' CYBA is an example representing all other plasmids containing 5'+2x3' cellular UTRs such DECR1, GMFG, MAPBPIP and MYL6B and all plasmids differ in size.
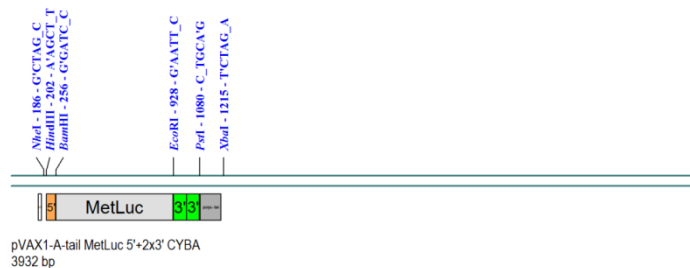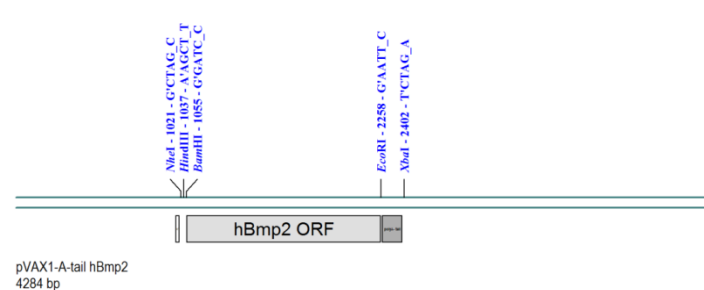

Supplementary Figure 15.6: DNA vector pVAX1-A-tail *Met*Luc comprises a 5' CYBA UTR (orange) and two copies of 3' CYBA UTR (green) and were inserted between the T7 promoter (white) and the reporter gene *Met*Luc (grey) and between the reporter gene and the poly A-tail (dark grey), respectively. Restriction sites are highlighted in blue. This DNA vector is a schematic representation for all other plasmids including a cellular combination of 5'+2x3' UTR, for instance DECR1, GMFG, MAPBPIP and MYL6B.

Figure 15.7: pVAX1-A-tail *Met*Luc 2x3'

Vector card of pVAX1-A-tail *Met*Luc 2x3' CYBA is an example representing all other plasmids containing 2x3' cellular UTRs such DECR1, GMFG, MAPBPIP and MYL6B and all plasmids differ in size.

pVAX1-A-tail MetLuc 2x3' CYBA
3874 bp
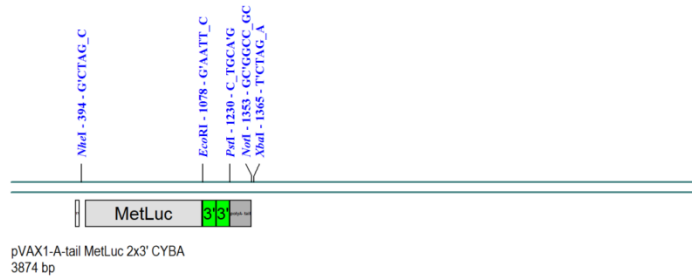
Supplementary 15.7: DNA vector pVAX1-A-tail *Met*Luc comprises two copies of 3' CYBA UTRs (green) which were inserted between the reporter gene *Met*Luc (grey) and the poly A-tail (dark grey). Restriction sites are highlighted in blue. This DNA vector is a schematic representation for all other plasmids including a cellular combination of 2x3' UTR, for instance DECR1, GMFG, MAPBPIP and MYL6B.

Figure 15.8: pVAX1-A120 d2EGFP

pVAX1-A120 d2EGFP
3955 bp

Supplementary Figure 15.8: Figure 15.8 shows the DNA vector pVAX1-A120 including the reporter gene d2EGFP (grey) without UTRs and was inserted between the T7 promoter (white) and the poly A-tail (dark grey). Restriction sites are highlighted in blue. Restriction sites with two cutting sites were marked in red.

Figure 15.9: pVAX1-A120 d2EGFP 5' CYBA

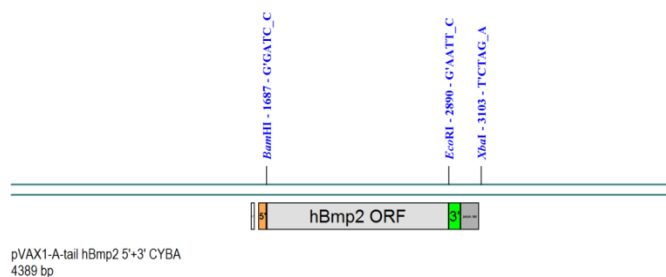pVAX1-A120 d2EGFP 5' CYBA
3991 bp

Supplementary Figure 15.9: DNA vector pVAX1-A120 d2EGFP comprises the 5' CYBA UTR (orange) and was inserted between the T7 promoter (white) and the reporter gene d2EGFP (grey). Restriction sites are highlighted in blue.

Figure 15.10: pVAX1-A120 d2EGFP 3' CYBA

pVAX1-A120 d2EGFP 3' CYBA
4059 bp
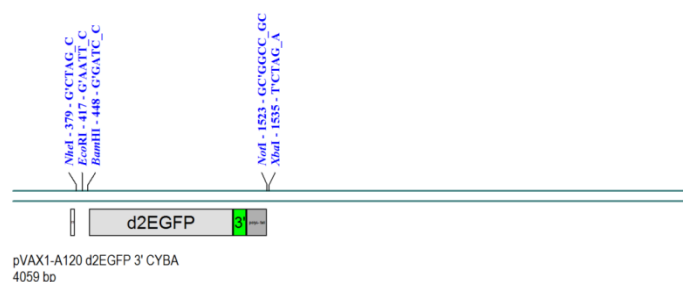
Supplementary Figure 15.10: DNA vector pVAX1-A120 d2EGFP comprises the 3' CYBA UTR (orange) and was inserted between the reporter gene d2EGFP (grey) and the poly A-tail (dark grey). Restriction sites are highlighted in blue.

Figure 15.11: pVAX1-A120 d2EGFP 5'+3' CYBA


pVAX1-A120 d2EGFP 5'+3' CYBA
4060 bp
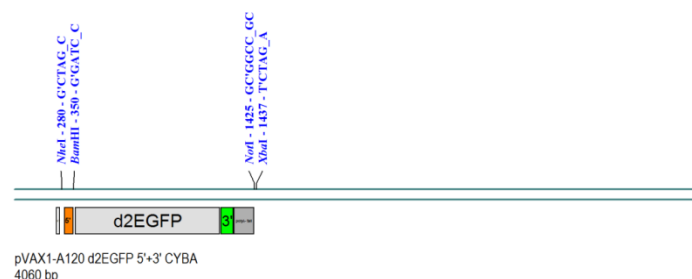
Supplementary Figure 15.11: DNA vector pVAX1-A120 d2EGFP comprises the 5' CYBA UTR (orange) and 3' CYBA UTR (green) and were inserted between the T7 promoter (white) and the reporter gene *Met*Luc (grey) and between the reporter gene and the poly A-tail (dark grey), respectively. Restriction sites are highlighted in blue.

Figure 15.12: pVAX1-A120 d2EGFP 5'+2x3' CYBA

pVAX1-A120 d2EGFP 5'+2x3' CYBA
4134 bp
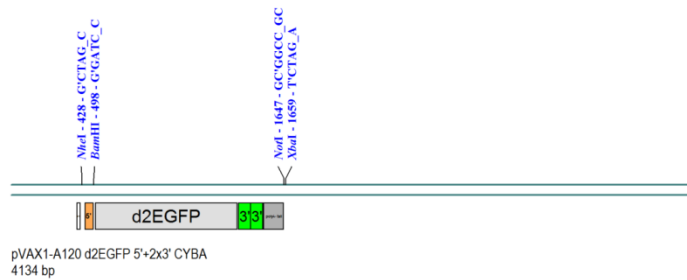
Supplementary Figure 15.12: DNA vector pVAX1-A120 d2EGFP comprises a 5' CYBA UTR (orange) and two copies of 3' CYBA UTR (green) and were inserted between the T7 promoter (white) and the reporter gene *Met*Luc (grey) and between the reporter gene and the poly A-tail (dark grey), respectively. Restriction sites are highlighted in blue.

Figure 15.13: pVAX1-A120 d2EGFP 2x3' CYBA

pVAX1-A120 d2EGFP 2x3' CYBA
4133 bp
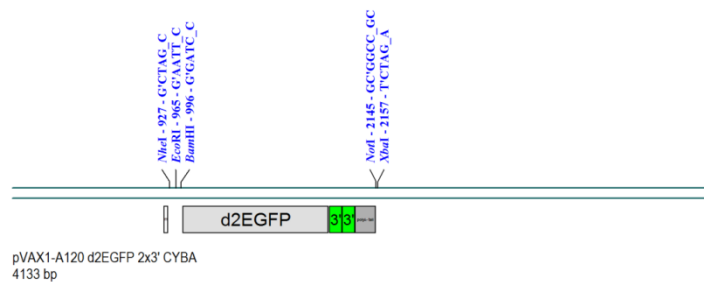
Supplementary Figure 15.13: DNA vector pVAX1-A120 d2EGFP comprises two copies of 3' CYBA UTRs (green) and were inserted between the reporter gene d2EGFP (grey) and the poly A-tail (dark grey). Restriction sites are highlighted in blue.

Figure 15.14: pVAX1-A-tail hBMP2 ORF

pVAX1-A-tail hBmp2
4284 bp

Supplementary Figure 15.14: Figure 15.14 shows the DNA vector pVAX1-poly A-tail including the physiological gene human BMP2 (grey) without UTRs and was inserted between the T7 promoter (white) and the poly A-tail (dark grey). Restriction sites are highlighted in blue.

Figure 15.15: pVAX1-A-tail hBMP2 5' CYBA

pVAX1-A-tail hBmp2 5' CYBA
4320 bp
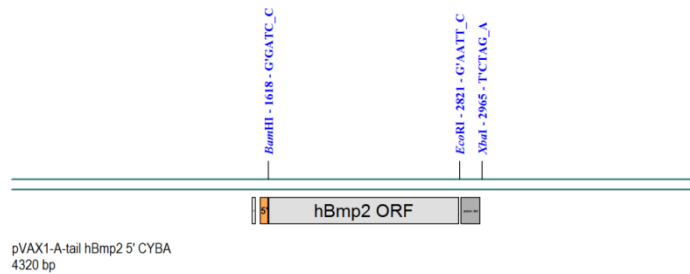
Supplementary Figure 15.15: DNA vector pVAX1-A-tail hBMP2 comprises the 5' CYBA UTR (orange) and was inserted between the T7 promoter (white) and the physiological gene hBMP2 (grey). Restriction sites are highlighted in blue.

Figure 15.16: pVAX1-A-tail hBMP2 3' CYBA

pVAX1-A-tail hBmp2 3' CYBA
4323 bp
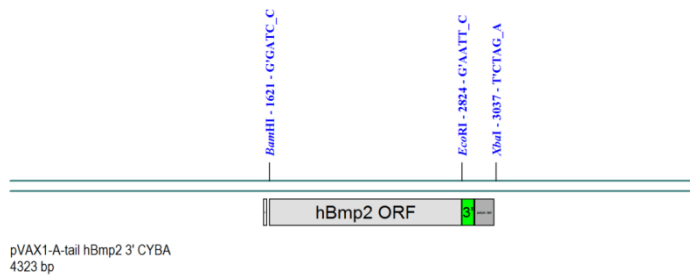
Supplementary Figure 15.16: DNA vector pVAX1-A-tail hBMP2 comprises the 3' CYBA UTR (orange) and was inserted between the hBMP2 (grey) and the poly A-tail (dark grey). Restriction sites are highlighted in blue.

Figure 15.17: pVAX1-A-tail hBMP2 5'+3' CYBA

pVAX1-A-tail hBmp2 5'+3' CYBA
4389 bp

Supplementary Figure 15.17: DNA vector pVAX1-A-tail hBMP2 comprises the 5' CYBA UTR (orange) and 3' CYBA UTR (green) and were inserted between the T7 promoter (white) and the physiological gene hBMP2 (grey) and between hBMP2 and the poly A-tail (dark grey), respectively. Restriction sites are highlighted in blue.

Figure 15.18: pVAX1-A-tail hBMP2 5'+2x3' CYBA

pVAX1-A-tail hBmp2 5'+2x3' CYBA
4463 bp
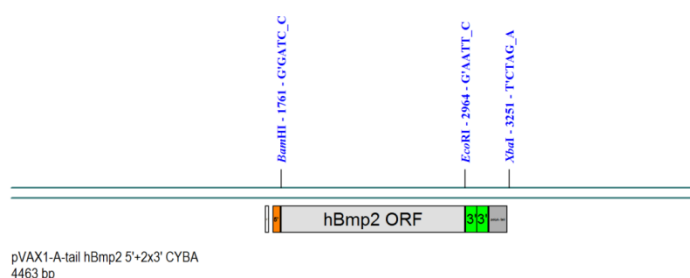
Supplementary Figure 15.18: DNA vector pVAX1-A-tail hBMP2 comprises a 5' CYBA UTR (orange) and two copies of 3' CYBA UTR (green) and were inserted between the T7 promoter (white) and the physiological gene hBMP2 (grey) and between hBMP2 and the poly A-tail (dark grey), respectively. Restriction sites are highlighted in blue.

Figure 15.19: pVAX1-A-tail hBMP2 2x3' CYBA

pVAX1-A-tail hBmp2 2x3' CYBA
4397 bp
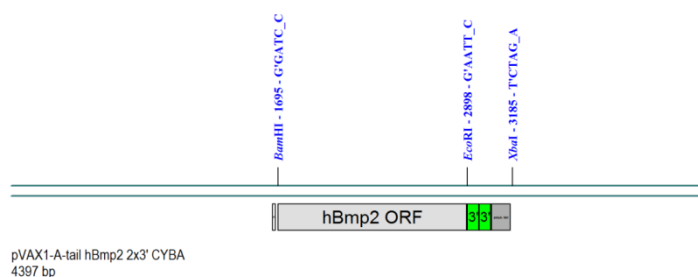
Supplementary Figure 15.19: DNA vector pVAX1-A-tail hBMP2 comprises the two copies of 3' CYBA UTR (green) and were inserted between the physiological gene hBMP2 (grey) and the poly A-tail (dark grey). Restriction sites are highlighted in blue.

8.2 Primer performance

In order to investigate the physical mRNA half-life via qRT-PCR two different primer pairs were tested with respect to their PCR performance. One primer pair was designed to detect the full length of *Met*Luc including the 5' CYBA UTR, the coding sequence and the 3' CYBA UTR. The second primer pair detects only a part of *Met*Luc and was binding 276nt downstream of the start codon. According to primer analysis by using an online software program (Primer-BLAST) no unspecific binding was predicted. Dilutions series were prepared according to the Material and Methods protocol with the cDNA samples 5'+3' *Met*Luc for primer pair 1 and *Met*Luc without UTRs for primer pair 2. The cDNAs were synthesized from *in vitro* transcribed mRNA. After qRT-PCR reaction the melting curves showed only one peak indicating one amplified product during PCR reaction. The primer efficiency for both primer pairs was approximately 2. Additionally the PCR products were loaded on agarose gel to verify the product length which was 729 base pairs (bp) and 78 bp for primer pair 1 and primer pair 2, respectively. In Figure 16 (A) primer pair 2 was showing full length *Met*Luc and some unspecific bands. In contrast primer pair 1 showed only one band as expected and is shown in Figure 16 (B). The lower cDNA dilutions (1:10 – 1:100) also showed a smear which is due to the high amount of impurities in the cDNA (Figure 16 B).
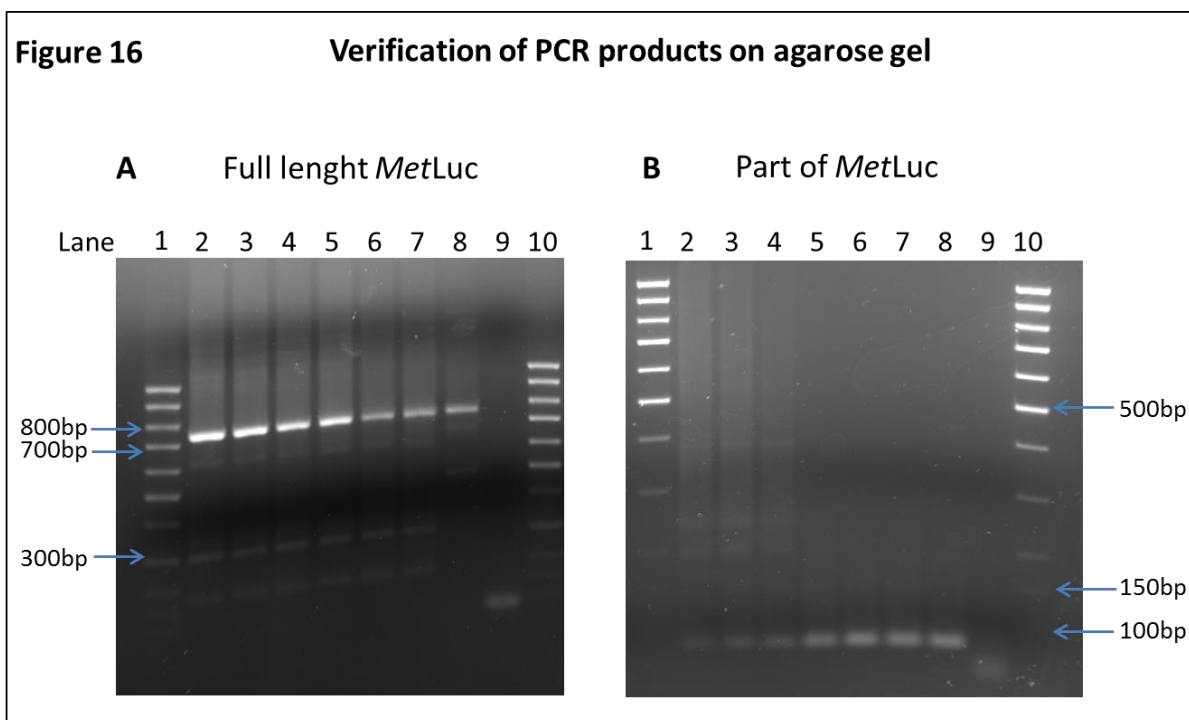
Figure 16: Agarose gel electrophoresis of PCR products FL-*Met*Luc and a part of *Met*Luc

Two different PCR products including full length *Met*Luc with a length of 729 bp (A) and partial length *Met*Luc showing a length of 78 bp (B) were investigated after qRT-PCR on 1% and 3% agarose gel, respectively. The following samples were loaded on the first gel (A): 100 bp DNA ladder (A1 and A10), cDNA dilution 1:100 (A2), 1:1000 (A3), 1: 10 000 (A4), 1:100 000 (A5) and 1:1 000 000 (A6), 1: 10 000 000 (A7), 1:100 000 000 (A8) and water (A9). The second gel (B) was loaded as follows: 100 bp DNA ladder (B1 and B10), cDNA dilution 1:18 (B2), 1:10 (B3), 1:100 (B4), 1:1000 (B5), 1: 10 000 (B6), 1:100 000 (B7) and 1:1 000 000 (B8), water (B9).

8.3 Investigation of full length and partial length MetLuc by qRT-PCR

As mentioned before the physical mRNA half-life of *Met*Luc was investigated in NIH3T3 by qRT-PCR. Two different primer pairs were designed for mRNA quantification including the full length *Met*Luc and partial length *Met*Luc, respectively. As shown in Figure 17 (A) and (B) both primer pairs showed a significant increase in mRNA amount triggered by insertion of 5' CYBA UTR compared to the control after 4 hours post-transfection. Afterwards any significant changes in mRNA stability could be observed. However, the measured mRNA quantity varies between the two primer pairs due to the different specificity of the primers (see Figure 16). Primer pair 2 which binds a part of *Met*Luc was more sensitive and specific compared to primer pair 1 specific for full length *Met*Luc. Therefore, all future analyses of physical mRNA half-life were assessed by using primers which bind a part of the gene of interest and are downstream of the start codon.
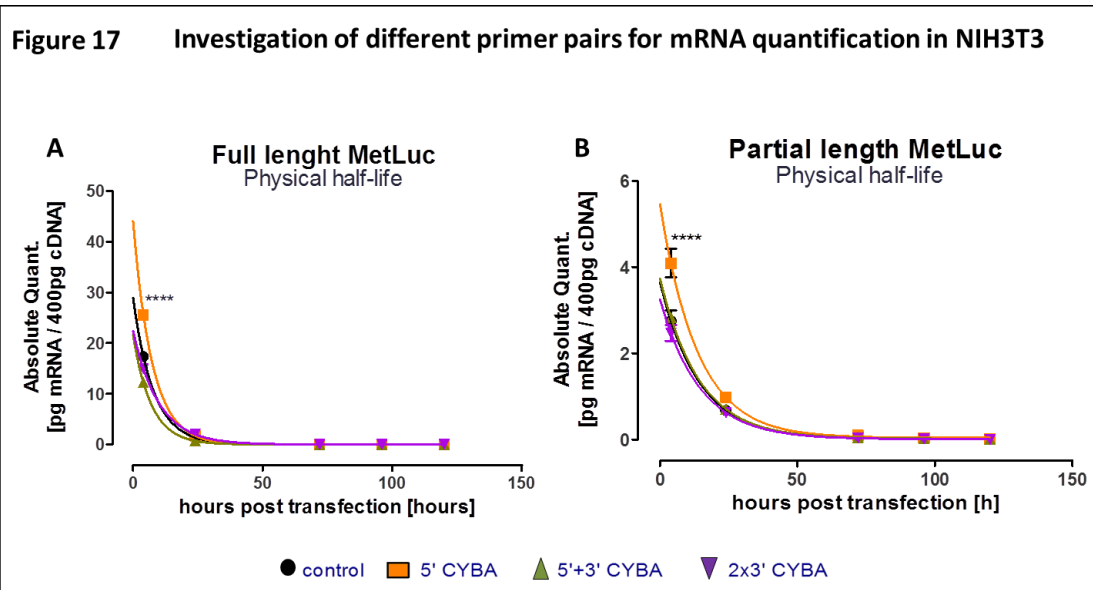
Figure 17: Comparison of two different primer pairs for MetLuc mRNA quantification in NIH3T3 via qRT-PCR

Messenger RNA amount of full length MetLuc (A) was compared to partial length MetLuc (B) in NIH3T3 via qRT-PCR with two different primer pairs. Absolute mRNA amount of the different mRNA constructs (5' CYBA UTR-orange, 5'+3' CYBA UTR-green, 2x3' CYBA UTR-purple and control without UTRs-black) was plotted against the logarithmic time. Statistical significance was assessed by 2-way ANOVA test (Bonferroni multiple comparisons) with p values <0.05.

8.4 Determination of GC content in 5' UTR

Table 13: GC content of different cellular 5' UTRs

5' UTR	GC content (%)	Length (bases)
CYBA	72.2	36
DECR1	68.8	141
GMFG	57.3	110
MAPBPIP	65.9	164
MYL6B	70.1	127

Table 14: GC content of hBmp2 mRNA furnished with CYBA UTRs

In table 14 the GC content in percentage and length of hBmp2 with the CYBA combinations, 2x3' and 5'+3', are listed. The length comprises the first nucleotide after the cap structure until the start codon.

CYBA UTR	GC content (%)	Length (first base-AUG)
2x3'	67.7	31
5'+3'	62.9	97

9. References

1. Clancy, S., *RNA splicing: introns, exons and spliceosome.* Nature Education, 2008. **1**(1): p. 31.

2. Chapeville, F., et al., *On the role of soluble ribonucleic acid in coding for amino acids.* Proceedings of the National Academy of Sciences of the United States of America, 1962. **48**(6): p. 1086.

3. Dahlberg, A.E., *The functional role of ribosomal RNA in protein synthesis.* Cell, 1989. **57**(4): p. 525-529.

4. Rodnina, M.V., R. Fricke, and W. Wintermeyer, *Transient conformational states of aminoacyl-tRNA during ribosome binding catalyzed by elongation factor Tu.* Biochemistry, 1994. **33**(40): p. 12267-12275.

5. Ross, J., *Messenger RNA turnover in eukaryotic cells.* Molecular biology & medicine, 1988. **5**(1): p. 1-14.

6. Hargrove, J.L. and F.H. Schmidt, *The role of mRNA and protein stability in gene expression.* The FASEB Journal, 1989. **3**(12): p. 2360-2370.

7. Hollams, E.M., et al., *MRNA stability and the control of gene expression: implications for human disease.* Neurochemical research, 2002. **27**(10): p. 957-980.

8. Russell, J. and S.A. Liebhaber, *The stability of human beta-globin mRNA is dependent on structural determinants positioned within its 3'untranslated region.* Blood, 1996. **87**(12): p. 5314-5323.

9. Printz, R.L., et al., *Hexokinase II mRNA and gene structure, regulation by insulin, and evolution.* Journal of Biological Chemistry, 1993. **268**(7): p. 5209-5219.

10. Sharova, L.V., et al., *Database for mRNA half-life of 19 977 genes obtained by DNA microarray analysis of pluripotent and differentiating mouse embryonic stem cells.* DNA research, 2009. **16**(1): p. 45-58.

11. Alwine, J.C., D.J. Kemp, and G.R. Stark, *Method for detection of specific RNAs in agarose gels by transfer to diazobenzyloxymethyl-paper and hybridization with DNA probes.* Proceedings of the National Academy of Sciences, 1977. **74**(12): p. 5350-5354.

12. Bhattacharyya, S.N., et al., *Relief of microRNA-mediated translational repression in human cells subjected to stress.* Cell, 2006. **125**(6): p. 1111-1124.

13. Blattner, C., et al., *UV-induced stabilization of c-fos and other short-lived mRNAs.* Molecular and cellular biology, 2000. **20**(10): p. 3616-3625.

14. Saiki, R.K., et al., *Enzymatic amplification of beta-globin genomic sequences and restriction site analysis for diagnosis of sickle cell anemia.* Science, 1985. **230**(4732): p. 1350-1354.

15. Adams, M.D., et al., *Complementary DNA sequencing: expressed sequence tags and human genome project.* Science, 1991. **252**(5013): p. 1651-1656.

16. Velculescu, V.E., et al., *Serial analysis of gene expression.* Science, 1995. **270**(5235): p. 484-487.

17. Schena, M., et al., *Quantitative monitoring of gene expression patterns with a complementary DNA microarray.* Science, 1995. **270**(5235): p. 467-470.

18. Gallie, D.R., *The cap and poly (A) tail function synergistically to regulate mRNA translational efficiency.* Genes & development, 1991. **5**(11): p. 2108-2116.

19. Leonhardt, C., et al., *Single-cell mRNA transfection studies: delivery, kinetics and statistics by numbers.* Nanomedicine, 2014. **10**(4): p. 679-88.

20. Cheneval, D., et al., *A review of methods to monitor the modulation of mRNA stability: a novel approach to drug discovery and therapeutic intervention.* J Biomol Screen, 2010. **15**(6): p. 609-22.

21. Brewer, G. and J. Ross, *Poly (A) shortening and degradation of the 3'A+ U-rich sequences of human c-myc mRNA in a cell-free system.* Molecular and cellular biology, 1988. **8**(4): p. 1697-1708.

22. Bernstein, P., S. Peltz, and J. Ross, *The poly (A)-poly (A)-binding protein complex is a major determinant of mRNA stability in vitro.* Molecular and cellular biology, 1989. **9**(2): p. 659-670.

23. Stoeckle, M.Y. and L. Guan, *High-resolution analysis of groα mRNA poly (A) shortening: regulation by interleukin-1β.* Nucleic acids research, 1993. **21**(7): p. 1613-1617.

24. Bernstein, P. and J. Ross, *Poly (A), poly (A) binding protein and the regulation of mRNA stability.* Trends in biochemical sciences, 1989. **14**(9): p. 373-377.

25. Peltz, S.W. and A. Jacobson, *mRNA stability: in trans-it.* Current opinion in cell biology, 1992. **4**(6): p. 979-983.

26. Sachs, A.B., *Messenger RNA degradation in eukaryotes.* Cell, 1993. **74**(3): p. 413-421.

27. Shaw, G. and R. Kamen, *A conserved AU sequence from the 3′ untranslated region of GM-CSF mRNA mediates selective mRNA degradation.* Cell, 1986. **46**(5): p. 659-667.

28. Caput, D., et al., *Identification of a common nucleotide sequence in the 3'-untranslated region of mRNA molecules specifying inflammatory mediators.* Proceedings of the National Academy of Sciences, 1986. **83**(6): p. 1670-1674.

29. Casey, J., et al., *Iron regulation of transferrin receptor mRNA levels requires iron-responsive elements and a rapid turnover determinant in the 3'untranslated region of the mRNA.* The EMBO Journal, 1989. **8**(12): p. 3693.

30. Koeller, D.M., et al., *Translation and the stability of mRNAs encoding the transferrin receptor and c-fos.* Proceedings of the National Academy of Sciences, 1991. **88**(17): p. 7778-7782.

31. Müllner, E.W. and L.C. Kühn, *A stem-loop in the 3′ untranslated region mediates iron-dependent regulation of transferrin receptor mRNA stability in the cytoplasm.* Cell, 1988. **53**(5): p. 815-825.

32. Marzluff, W.F. and N.B. Pandey, *Multiple regulatory steps control histone mRNA concentrations.* Trends in biochemical sciences, 1988. **13**(2): p. 49-52.

33. Schümperli, D., *Multilevel regulation of replication-dependent histone genes.* Trends in Genetics, 1988. **4**(7): p. 187-191.

34. Furuichi, Y., A. LaFiandra, and A.J. Shatkin, *5'-Terminal structure and mRNA stability.* Nature, 1977. **266**(5599): p. 235-239.

35. McCrae, M.A. and H.R. Woodland, *Stability of Non‐polyadenylated Viral mRNAs Injected into Frog Qucytes.* European Journal of Biochemistry, 1981. **116**(3): p. 467-470.

36. Peltz, S., et al., *Substrate specificity of the exonuclease activity that degrades H4 histone mRNA.* Journal of Biological Chemistry, 1987. **262**(19): p. 9382-9388.

37. Pogue, G.P., et al., *5'sequences of rubella virus RNA stimulate translation of chimeric RNAs and specifically interact with two host-encoded proteins.* Journal of virology, 1993. **67**(12): p. 7106-7117.

38. Frolov, I., E. Frolova, and S. Schlesinger, *Sindbis virus replicons and Sindbis virus: assembly of chimeras and of particles deficient in virus RNA.* Journal of virology, 1997. **71**(4): p. 2819-2829.

39. Carballo, E. and P.J. Blackshear, *Roles of tumor necrosis factor-α receptor subtypes in the pathogenesis of the tristetraprolin-deficiency syndrome.* Blood, 2001. **98**(8): p. 2389-2395.

40. Breindl, M. and D. Gallwitz, *On the translational control of histone synthesis.* European Journal of Biochemistry, 1974. **45**(1): p. 91-97.

41. Friedel, C.C., et al., *Conserved principles of mammalian transcriptional regulation revealed by RNA half-life.* Nucleic Acids Res, 2009. **37**(17): p. e115.

42. Yang, E., et al., *Decay rates of human mRNAs: correlation with functional characteristics and sequence attributes.* Genome research, 2003. **13**(8): p. 1863-1872.

43. Lee, J.E., et al., *Systematic analysis of cis-elements in unstable mRNAs demonstrates that CUGBP1 is a key regulator of mRNA decay in muscle cells.* PloS one, 2010. **5**(6): p. e11201.

44. Dölken, L., et al., *High-resolution gene expression profiling for simultaneous kinetic parameter analysis of RNA synthesis and decay.* Rna, 2008. **14**(9): p. 1959-1972.

45. t Hoen, P.A., et al., *mRNA degradation controls differentiation state-dependent differences in transcript and splice variant abundance.* Nucleic Acids Res, 2011. **39**(2): p. 556-66.

46. Vilela, C. and J.E. McCarthy, *Regulation of fungal gene expression via short open reading frames in the mRNA 5′ untranslated region.* Molecular microbiology, 2003. **49**(4): p. 859-867.

47. Son, G.H., et al., *Excision of the first intron from the gonadotropin-releasing hormone (GnRH) transcript serves as a key regulatory step for GnRH biosynthesis.* Journal of Biological Chemistry, 2003. **278**(20): p. 18037-18044.

48. Gebauer, F. and M.W. Hentze, *Molecular mechanisms of translational control.* Nature reviews Molecular cell biology, 2004. **5**(10): p. 827-835.

49. Pichon, X., et al., *RNA binding protein/RNA element interactions and the control of translation.* Current protein & peptide science, 2012. **13**(4): p. 294.

50. Tillmar, L., C. Carlsson, and N. Welsh, *Control of insulin mRNA stability in rat pancreatic islets Regulatory role of a 3′-untranslated region pyrimidine-rich sequence.* Journal of Biological Chemistry, 2002. **277**(2): p. 1099-1106.

51. Wells, S.E., et al., *Circularization of mRNA by eukaryotic translation initiation factors.* Molecular cell, 1998. **2**(1): p. 135-140.

52. Gallie, D.R., *A tale of two termini:: A functional interaction between the termini of an mRNA is a prerequisite for efficient translation initiation.* Gene, 1998. **216**(1): p. 1-11.

53. Hentze, M.W., *eIF4G--A Multipurpose Ribosome Adapter?* Science, 1997. **275**(5299): p. 500-501.

54. Mitchell, P. and D. Tollervey, *mRNA stability in eukaryotes.* Current opinion in genetics & development, 2000. **10**(2): p. 193-198.

55. Sachs, A.B. and R.W. Davis, *The poly (A) binding protein is required for poly (A) shortening and 60S ribosomal subunit-dependent translation initiation.* Cell, 1989. **58**(5): p. 857-867.

56. Pestova, T.V., et al., *Molecular mechanisms of translation initiation in eukaryotes.* Proceedings of the National Academy of Sciences, 2001. **98**(13): p. 7029-7036.

57. Takyar, S., R.P. Hickerson, and H.F. Noller, *mRNA helicase activity of the ribosome.* Cell, 2005. **120**(1): p. 49-58.

58. Kozak, M., et al., *Structural features in eukaryotic mRNAs that mod.* Biol Chem, 1991. **266**: p. 19867-19870.

59. Sonenberg, N. and T.E. Dever, *Eukaryotic translation initiation factors and regulators.* Current opinion in structural biology, 2003. **13**(1): p. 56-63.

60. Wang, L. and S.R. Wessler, *Role of mRNA Secondary Structure in Translational Repression of the Maize Transcriptional ActivatorLc.* Plant Physiology, 2001. **125**(3): p. 1380-1387.

61. Goossen, B. and M.W. Hentze, *Position is the critical determinant for function of iron-responsive elements as translational regulators.* Molecular and cellular biology, 1992. **12**(5): p. 1959-1966.

62. Kozak, M., *Regulation of translation in eukaryotic systems.* Annual review of cell biology, 1992. **8**(1): p. 197-225.

63. Babendure, J.R., et al., *Control of mammalian translation by mRNA structure near caps.* RNA, 2006. **12**(5): p. 851-61.

64. Short, J.D. and C.M. Pfarr, *Translational regulation of the JunD messenger RNA.* Journal of Biological Chemistry, 2002. **277**(36): p. 32697-32705.

65. van der Velden, A.W., et al., *Ribosomal scanning on the highly structured insulin-like growth factor II-leader 1.* The international journal of biochemistry & cell biology, 2002. **34**(3): p. 286-297.

66. Hughes, T.A. and J.N. McElwaine, *Mathematical and biological modelling of RNA secondary structure and its effects on gene expression.* Comput Math Methods Med, 2006. **7**(1): p. 37-43.

67. Krieg, P. and D. Melton, *Functional messenger RNAs are produced by SP6 in vitro transcription of cloned cDNAs.* Nucleic Acids Research, 1984. **12**(18): p. 7057-7070.

68. Wolff, J.A., et al., *Direct gene transfer into mouse muscle in vivo.* Science, 1990. **247**(4949): p. 1465-1468.

69. Conry, R.M., et al., *Characterization of a messenger RNA polynucleotide vaccine vector.* Cancer research, 1995. **55**(7): p. 1397-1400.

70. Hoerr, I., et al., *In vivo application of RNA leads to induction of specific cytotoxic T lymphocytes and antibodies.* European journal of immunology, 2000. **30**(1): p. 1-7.

71. Granstein, R.D., W. Ding, and H. Ozawa, *Induction of anti-tumor immunity with epidermal cells pulsed with tumor-derived RNA or intradermal administration of RNA.* Journal of investigative dermatology, 2000. **114**(4): p. 632-636.

72. Martinon, F., et al., *Induction of virus‐specific cytotoxic T lymphocytes in vivo by liposome‐entrapped mRNA.* European journal of immunology, 1993. **23**(7): p. 1719-1722.

73. Zhou, W.-Z., et al., *RNA melanoma vaccine: induction of antitumor immunity by human glycoprotein 100 mRNA immunization.* Human gene therapy, 1999. **10**(16): p. 2719-2724.

74. Nair, S., et al., *Synergy between tumor immunotherapy and antiangiogenic therapy.* Blood, 2003. **102**(3): p. 964-971.

75. Coughlin, C.M., et al., *RNA-transfected CD40-activated B cells induce functional T-cell responses against viral and tumor antigen targets: implications for pediatric immunotherapy.* Blood, 2004. **103**(6): p. 2046-2054.

76. Ponsaerts, P., et al., *Messenger RNA electroporation of human monocytes, followed by rapid in vitro differentiation, leads to highly stimulatory antigen-loaded mature dendritic cells.* The Journal of Immunology, 2002. **169**(4): p. 1669-1675.

77. Weide, B., et al., *Results of the first phase I/II clinical vaccination trial with direct injection of mRNA.* Journal of immunotherapy, 2008. **31**(2): p. 180-188.

78. Weide, B., et al., *Direct injection of protamine-protected mRNA: results of a phase 1/2 vaccination trial in metastatic melanoma patients.* Journal of Immunotherapy, 2009. **32**(5): p. 498-507.

79. Rittig, S.M., et al., *Intradermal Vaccinations With RNA Coding for TAA Generate CD8+ and CD4+ Immune Responses and Induce Clinical Benefit in Vaccinated Patients.* Molecular Therapy, 2011. **19**(5): p. 990-999.

80. Kreiter, S., et al., *Tumor vaccination using messenger RNA: prospects of a future therapy.* Current opinion in immunology, 2011. **23**(3): p. 399-406.

81. Jirikowski, G.F., et al., *Reversal of diabetes insipidus in Brattleboro rats: intrahypothalamic injection of vasopressin mRNA.* Science, 1992. **255**(5047): p. 996-998.

82. Kormann, M.S., et al., *Expression of therapeutic proteins after delivery of chemically modified mRNA in mice.* Nat Biotechnol, 2011. **29**(2): p. 154-7.

83. Mays, L.E., et al., *Modified Foxp3 mRNA protects against asthma through an IL-10– dependent mechanism.* The Journal of clinical investigation, 2013. **123**(3): p. 1216.

84. Okumura, K., et al., *Bax mRNA therapy using cationic liposomes for human malignant melanoma.* The journal of gene medicine, 2008. **10**(8): p. 910-917.

85. Warren, L., et al., *Highly efficient reprogramming to pluripotency and directed differentiation of human cells with synthetic modified mRNA.* Cell stem cell, 2010. **7**(5): p. 618-630.

86. Yakubov, E., et al., *Reprogramming of human fibroblasts to pluripotent stem cells using mRNA of four transcription factors.* Biochem Biophys Res Commun, 2010. **394**(1): p. 189-93.

87. Sonenberg, N., et al., *A polypeptide in eukaryotic initiation factors that crosslinks specifically to the 5'-terminal cap in mRNA.* Proceedings of the National Academy of Sciences, 1978. **75**(10): p. 4843-4847.

88. Stepinski, J., et al., *Synthesis and properties of mRNAs containing the novel "anti-reverse" cap analogs 7-methyl (3′-O-methyl) GpppG and 7-methyl (3′-deoxy) GpppG.* Rna, 2001. **7**(10): p. 1486-1495.

89. Mockey, M., et al., *mRNA transfection of dendritic cells: synergistic effect of ARCA mRNA capping with Poly (A) chains in cis and in trans for a high protein expression level.* Biochemical and biophysical research communications, 2006. **340**(4): p. 1062-1068.

90. Kuhn, A., et al., *Phosphorothioate cap analogs increase stability and translational efficiency of RNA vaccines in immature dendritic cells and induce superior immune responses in vivo.* Gene therapy, 2010. **17**(8): p. 961-971.

91. Grudzien-Nogalska, E., et al., *Phosphorothioate cap analogs stabilize mRNA and increase translational efficiency in mammalian cells.* RNA, 2007. **13**(10): p. 1745-1755.

92. Banchereau, J., et al., *Immunobiology of dendritic cells.* Annual review of immunology, 2000. **18**(1): p. 767-811.

93. Holtkamp, S., et al., *Modification of antigen-encoding RNA increases stability, translational efficacy, and T-cell stimulatory capacity of dendritic cells.* Blood, 2006. **108**(13): p. 4009-17.

94. Tcherepanova, I.Y., et al., *Ectopic expression of a truncated CD40L protein from synthetic post-transcriptionally capped RNA in dendritic cells induces high levels of IL-12 secretion.* BMC molecular biology, 2008. **9**(1): p. 90.

95. Kariko, K., et al., *Increased erythropoiesis in mice injected with submicrogram quantities of pseudouridine-containing mRNA encoding erythropoietin.* Mol Ther, 2012. **20**(5): p. 948-53.

96. Ikemura, T., *Codon usage and tRNA content in unicellular and multicellular organisms.* Molecular biology and evolution, 1985. **2**(1): p. 13-34.

97. Irwin, B., J.D. Heck, and G.W. Hatfield, *Codon pair utilization biases influence translational elongation step times.* Journal of Biological Chemistry, 1995. **270**(39): p. 22801-22806.

98. Al-Saif, M. and K.S. Khabar, *UU/UA dinucleotide frequency reduction in coding regions results in increased mRNA stability and protein expression.* Molecular Therapy, 2012. **20**(5): p. 954-959.

99. Diebold, S.S., et al., *Innate antiviral responses by means of TLR7-mediated recognition of single-stranded RNA.* Science, 2004. **303**(5663): p. 1529-1531.

100. Heil, F., et al., *Species-specific recognition of single-stranded RNA via toll-like receptor 7 and 8.* Science, 2004. **303**(5663): p. 1526-1529.

101. Scheel, B., et al., *Immunostimulating capacities of stabilized RNA molecules.* European journal of immunology, 2004. **34**(2): p. 537-547.

102. Yoneyama, M. and T. Fujita, *Structural mechanism of RNA recognition by the RIG-I-like receptors.* Immunity, 2008. **29**(2): p. 178-181.

103. Sahin, U., K. Karikó, and Ö. Türeci, *mRNA-based therapeutics [mdash] developing a new class of drugs.* Nature Reviews Drug Discovery, 2014.

104. Akira, S. and K. Takeda, *Toll-like receptor signalling.* Nature Reviews Immunology, 2004. **4**(7): p. 499-511.

105. Alexopoulou, L., et al., *Recognition of double-stranded RNA and activation of NF-κB by Toll-like receptor 3.* Nature, 2001. **413**(6857): p. 732-738.

106. Karikó, K., et al., *mRNA is an endogenous ligand for Toll-like receptor 3.* Journal of Biological Chemistry, 2004. **279**(13): p. 12542-12550.

107. Pichlmair, A., et al., *Activation of MDA5 requires higher-order RNA structures generated during virus infection.* Journal of virology, 2009. **83**(20): p. 10761-10769.

108. Kanneganti, T.-D., et al., *Bacterial RNA and small antiviral compounds activate caspase-1 through cryopyrin/Nalp3.* Nature, 2006. **440**(7081): p. 233-236.

109. Sabbah, A., et al., *Activation of innate immune antiviral responses by Nod2.* Nature immunology, 2009. **10**(10): p. 1073-1080.

110. Labat-Moleur, F., et al., *An electron microscopy study into the mechanism of gene transfer with lipopolyamines.* Gene therapy, 1996. **3**(11): p. 1010-1017.

111. Tachibana, K. and S. Tachibana, *The use of ultrasound for drug delivery.* Echocardiography, 2001. **18**(4): p. 323-328.

112. Zehavi-Willner, T. and C. Lane, *Subcellular compartmentation of albumin and globin made in oocytes under the direction of injected messenger RNA.* Cell, 1977. **11**(3): p. 683-693.

113. Heiser, A., et al., *Autologous dendritic cells transfected with prostate-specific antigen RNA stimulate CTL responses against metastatic prostate tumors.* Journal of Clinical Investigation, 2002. **109**(3): p. 409-409.

114. Isaka, Y. and E. Imai, *Electroporation-mediated gene therapy.* Expert Opin. Drug Deliv., 2007.

115. Sohn, R.L., et al., *In‐vivo particle mediated delivery of mRNA to mammalian tissues: ballistic and biologic effects.* Wound Repair and Regeneration, 2001. **9**(4): p. 287-296.

116. Rakhmilevich, A.L., et al., *Gene gun-mediated skin transfection with interleukin 12 gene results in regression of established primary and metastatic murine tumors.* Proceedings of the National Academy of Sciences, 1996. **93**(13): p. 6291-6296.

117. Qiu, P., et al., *Gene gun delivery of mRNA in situ results in efficient transgene expression and genetic immunization.* Gene therapy, 1996. **3**(3): p. 262-268.

118. Hattori, Y., et al., *The distribution of mRNA expression and protein after hydrodynamic injection of transgene in mice.* Biological and Pharmaceutical Bulletin, 2009. **32**(4): p. 755-759.

119. El Ouahabi, A., et al., *The role of endosome destabilizing activity in the gene transfer process mediated by cationic lipids.* FEBS letters, 1997. **414**(2): p. 187-192.

120. de Ilarduya, C.T., Y. Sun, and N. Düzgüneş, *Gene delivery by lipoplexes and polyplexes.* European journal of pharmaceutical sciences, 2010. **40**(3): p. 159-170.
121. Wasungu, L. and D. Hoekstra, *Cationic lipids, lipoplexes and intracellular delivery of genes.* Journal of Controlled Release, 2006. **116**(2): p. 255-264.
122. Pack, D.W., et al., *Design and development of polymers for gene delivery.* Nature Reviews Drug Discovery, 2005. **4**(7): p. 581-593.
123. Rejman, J., et al., *mRNA transfection of cervical carcinoma and mesenchymal stem cells mediated by cationic carriers.* Journal of Controlled Release, 2010. **147**(3): p. 385-391.
124. Plank, C., et al., *Enhancing and targeting nucleic acid delivery by magnetic force.* Expert opinion on biological therapy, 2003. **3**(5): p. 745-758.
125. Luo, D. and W.M. Saltzman, *Enhancement of transfection by physical concentration of DNA at the cell surface.* Nature biotechnology, 2000. **18**(8): p. 893-895.
126. Cerda, M.B., et al., *Enhancement of nucleic acid delivery to hard-to-transfect human colorectal cancer cells by magnetofection at laminin coated substrates and promotion of the endosomal/lysosomal escape.* RSC Advances, 2015. **5**(72): p. 58345-58354.
127. Grześkowiak, B.F., et al., *Nanomagnetic Activation as a Way to Control the Efficacy of Nucleic Acid Delivery.* Pharmaceutical research, 2015. **32**(1): p. 103-121.
128. Sanchez-Antequera, Y., et al., *Magselectofection: an integrated method of nanomagnetic separation and genetic modification of target cells.* Blood, 2011. **117**(16): p. e171-e181.
129. Mykhaylyk, O., et al., *Generation of magnetic nonviral gene transfer agents and magnetofection in vitro.* Nature protocols, 2007. **2**(10): p. 2391-2411.
130. Scherer, F., et al., *Magnetofection: enhancing and targeting gene delivery by magnetic force in vitro and in vivo.* Gene therapy, 2002. **9**(2): p. 102-109.
131. Xenariou, S., et al., *Using magnetic forces to enhance non-viral gene transfer to airway epithelium in vivo.* Gene therapy, 2006. **13**(21): p. 1545-1552.
132. Hughes, C., et al., *Streptavidin paramagnetic particles provide a choice of three affinity-based capture and magnetic concentration strategies for retroviral vectors.* Molecular Therapy, 2001. **3**(4): p. 623-630.
133. Pandori, M.W., D.A. Hobson, and T. Sano, *Adenovirus–Microbead Conjugates Possess Enhanced Infectivity: A New Strategy for Localized Gene Delivery.* Virology, 2002. **299**(2): p. 204-212.
134. Chan, L., et al., *Conjugation of lentivirus to paramagnetic particles via nonviral proteins allows efficient concentration and infection of primary acute myeloid leukemia cells.* Journal of virology, 2005. **79**(20): p. 13190-13194.
135. Wang, W., et al., *Non-viral gene delivery methods.* Current pharmaceutical biotechnology, 2013. **14**(1): p. 46-60.
136. Dewitte, H., et al., *Nanoparticle design to induce tumor immunity and challenge the suppressive tumor microenvironment.* Nano Today, 2014. **9**(6): p. 743-758.
137. Lonez, C., M. Vandenbranden, and J.-M. Ruysschaert, *Cationic lipids activate intracellular signaling pathways.* Advanced drug delivery reviews, 2012. **64**(15): p. 1749-1758.
138. Health, U.D.o. and H. Services, *Bone health and osteoporosis: a report of the Surgeon General.* 2004, Rockville, MD: US Department of Health and Human Services, Office of the Surgeon General.
139. Jørgensen, N.R. and P. Schwarz, *Effects of anti-osteoporosis medications on fracture healing.* Current osteoporosis reports, 2011. **9**(3): p. 149-155.
140. Cruess, R.L. and J. Dumont, *Healing of Bone, Tendon and Ligament. In: Fractures.* 1975.
141. Frost, H.M., *Tetracycline-based histological analysis of bone remodeling.* Calcified Tissue International, 1969. **3**(1): p. 211-237.

142. Matsuo, K. and N. Irie, *Osteoclast–osteoblast communication.* Archives of biochemistry and biophysics, 2008. **473**(2): p. 201-209.

143. Andersen, T.L., et al., *A physical mechanism for coupling bone resorption and formation in adult human bone.* The American journal of pathology, 2009. **174**(1): p. 239-247.

144. Salama, R. and S. Weissman, *The clinical use of combined xenografts of bone and autologous red marrow. A preliminary report.* Journal of Bone & Joint Surgery, British Volume, 1978. **60**(1): p. 111-115.

145. Gan, Y., et al., *The clinical use of enriched bone marrow stem cells combined with porous beta-tricalcium phosphate in posterior spinal fusion.* Biomaterials, 2008. **29**(29): p. 3973-3982.

146. Marcacci, M., et al., *Stem cells associated with macroporous bioceramics for long bone repair: 6-to 7-year outcome of a pilot clinical study.* Tissue engineering, 2007. **13**(5): p. 947-955.

147. Khan, S.N. and J.M. Lane, *The use of recombinant human bone morphogenetic protein-2 (rhBMP-2) in orthopaedic applications.* Expert opinion on biological therapy, 2004. **4**(5): p. 741-748.

148. Valentin-Opran, A., et al., *Clinical evaluation of recombinant human bone morphogenetic protein-2.* Clinical orthopaedics and related research, 2002. **395**: p. 110-120.

149. Dimitriou, R., E. Tsiridis, and P.V. Giannoudis, *Current concepts of molecular aspects of bone healing.* Injury, 2005. **36**(12): p. 1392-1404.

150. Fischer, G.W., et al., *Noninvasive cerebral oxygenation may predict outcome in patients undergoing aortic arch surgery.* The Journal of thoracic and cardiovascular surgery, 2011. **141**(3): p. 815-821.

151. Smeets, R., et al., *Impact of rhBMP-2 on regeneration of buccal alveolar defects during the osseointegration of transgingival inserted implants.* Oral Surgery, Oral Medicine, Oral Pathology, Oral Radiology, and Endodontology, 2009. **108**(4): p. e3-e12.

152. Ueblacker, P., et al., *In vivo analysis of retroviral gene transfer to chondrocytes within collagen scaffolds for the treatment of osteochondral defects.* Biomaterials, 2007. **28**(30): p. 4480-4487.

153. Raty, J., et al., *Gene therapy: the first approved gene-based medicines, molecular mechanisms and clinical indications.* Current molecular pharmacology, 2008. **1**(1): p. 13-23.

154. Baba, M., et al., *Treatment of neurological disorders by introducing mRNA in vivo using polyplex nanomicelles.* Journal of Controlled Release, 2015. **201**: p. 41-48.

155. Zangi, L., et al., *Modified mRNA directs the fate of heart progenitor cells and induces vascular regeneration after myocardial infarction.* Nature biotechnology, 2013. **31**(10): p. 898-907.

156. Elangovan, S., et al., *Chemically modified RNA activated matrices enhance bone regeneration.* Journal of Controlled Release, 2015. **218**: p. 22-28.

157. Ferizi, M., et al., *Stability analysis of chemically modified mRNA using micropattern-based single-cell arrays.* Lab Chip, 2015. **15**(17): p. 3561-71.

158. Waggoner, S.A. and S.A. Liebhaber, *Identification of mRNAs associated with αCP2-containing RNP complexes.* Molecular and cellular biology, 2003. **23**(19): p. 7055-7067.

159. Kozak, M., *Features in the $5'$ non-coding sequences of rabbit α and β-globin mRNAs that affect translational efficiency.* Journal of molecular biology, 1994. **235**(1): p. 95-110.

160. Bonehill, A., et al., *Efficient presentation of known HLA class II-restricted MAGE-A3 epitopes by dendritic cells electroporated with messenger RNA encoding an invariant chain with genetic exchange of class II-associated invariant chain peptide.* Cancer research, 2003. **63**(17): p. 5587-5594.

161. Teufel, R., et al., *Human peripheral blood monuclear cells transfected with messenger RNA stimulate antigen-specific cytotoxic T-lymphocytes in vitro.* Cellular and Molecular Life Sciences CMLS, 2005. **62**(15): p. 1755-1762.

162. Chen, J.-M., C. Férec, and D.N. Cooper, *A systematic analysis of disease-associated variants in the 3′ regulatory regions of human protein-coding genes I: general principles and overview.* Human genetics, 2006. **120**(1): p. 1-21.

163. Gaspar, P., et al., *mRNA secondary structure optimization using a correlated stem–loop prediction.* Nucleic acids research, 2013. **41**(6): p. e73-e73.

164. Baudouin-Legros, M., et al., *Cell-specific posttranscriptional regulation of CFTR gene expression via influence of MAPK cascades on 3′ UTR part of transcripts.* American Journal of Physiology-Cell Physiology, 2005. **289**(5): p. C1240-C1250.

165. Grishok, A., et al., *Genes and mechanisms related to RNA interference regulate expression of the small temporal RNAs that control C. elegans developmental timing.* Cell, 2001. **106**(1): p. 23-34.

166. Knight, S.W. and B.L. Bass, *A role for the RNase III enzyme DCR-1 in RNA interference and germ line development in Caenorhabditis elegans.* Science, 2001. **293**(5538): p. 2269-2271.

167. Vogel, C. and E.M. Marcotte, *Insights into the regulation of protein abundance from proteomic and transcriptomic analyses.* Nat Rev Genet, 2012. **13**(4): p. 227-32.

168. Kozak, M., *Regulation of translation via mRNA structure in prokaryotes and eukaryotes.* Gene, 2005. **361**: p. 13-37.

169. Hoover, D., et al., *Pim-1 protein expression is regulated by its 5'-untranslated region and translation initiation factor elF-4E.* Cell growth & differentiation: the molecular biology journal of the American Association for Cancer Research, 1997. **8**(12): p. 1371-1380.

10.   List of Publications

1. Ferizi, M., Leonhardt, C., Meggle, C., Aneja, M. K., Rudolph, C., Plank, C., & Rädler, J. O. (2015). Stability analysis of chemically modified mRNA using micropattern-based single-cell arrays. *Lab on a Chip*, *15*(17), 3561-3571.

11.   Appendix

11.1 Publication

Lab on a Chip

Stability analysis of chemically modified mRNA using micropattern-based single-cell arrays†

Mehrije Ferizi,‡[a] Carolin Leonhardt,‡[b] Christian Meggle,[b] Manish K. Aneja,[c] Carsten Rudolph,[c] Christian Plank[ac] and Joachim O. Rädler*[b]

The measurement of mRNA turnover in living cells plays an important role in the search for stable mRNA constructs for RNA-based therapies. Here we show that automated time-lapse microscopy combined with micropatterned arrays allows for efficient high-throughput monitoring of fluorescent reporter protein expression at the single-cell level. The fluorescence time courses after mRNA transfection yield the distribution of individual mRNA expression and degradation rates within a population. We compare mRNA constructs with combinations of 5′ and 3′ UTR sequences and find a systematic broadening and shift towards longer functional half-lives for UTR stabilized mRNA. At the same time the life time distribution of the destabilized EGFP reporter protein was found to be constant and narrowly distributed. Using mathematical modeling, we show that mRNA functional life-time predicts the time-integrated protein level, *i.e.* the area under the curve (AUC) of mRNA translation. Our approach paves the way for quantitative assessment of hitherto unexplored mRNA functional life time heterogeneity, possibly predicated on multiple mRNA secondary structures and its dependence on UTR sequences.

Introduction

In recent years, messenger RNA (mRNA) has become increasingly relevant as a new drug entity. As opposed to DNA-based gene therapeutics, mRNA does not need to be transported into the nucleus but is directly translated into protein in the cytoplasm.[1,2] This makes mRNA safer in avoiding potential insertional mutagenesis, an unlikely but existent risk of DNA gene medicines. As a consequence, mRNA therapeutics are emerging as promising alternatives for gene and protein replacement therapies in a broad variety of medical indications.[1–4] However, the strong immunogenicity as well as the limited stability of conventional mRNA has to be overcome to further establish its clinical applicability. In particular, mRNA stability is an essential parameter for envisaged medical applications because it determines, for example, dosing and the dosing intervals of mRNA drugs.

Several strategies have proven successful both at increasing the stability and reducing the immunogenic response

triggered by mRNA administered to cells or organisms. Amongst these is the inclusion of chemically modified nucleotides.[5] Kormann *et al.* have shown that the replacement of only 25% of uridine and cytidine residues by 2-thiouridine and 5-methyl-cytidine suffices to increase mRNA stability as well as to reduce the activation of innate immunity triggered by externally administered mRNA *in vitro*.[3]

Also, untranslated regions (UTRs) in mRNAs have been reported to play a pivotal role in regulating both mRNA stability and mRNA translation. UTRs are known to influence translational initiation, elongation, and termination, as well as mRNA stabilization and intracellular localization through their interaction with RNA binding proteins.[6,7] Depending on the specific motives within the UTR, it can either enhance or decrease mRNA turnover.[8–11] Recently, data on mRNA half-lives and the corresponding UTR sequences have been published.[12,13]

One mRNA with a particularly long half-life is the one transcribed from the human cytochrome b-245 alpha polypeptide (CYBA) gene. The CYBA gene comprises specific 5′ and 3′ UTRs. In general, 5′ UTR motives such as upstream open reading frames (uORFs) or internal ribosomal entry sites (IRES) are known to be involved in gene regulation, particularly in translational initiation.[14] The 3′ UTRs can comprise even more regulatory functions than the 5′ UTRs, some of them even hindering mRNA translation.[15] While no regulatory motives are known for the CYBA 5′ UTR unit, the CYBA 3′ UTR contains two of them. Firstly, the polyadenylation signal (PAS), which interacts with the cytoplasmic polyadenylation

[a] Institute of Molecular Immunology - Experimental Oncology, Technische Universität München, Munich, 81675 Germany
[b] Faculty of Physics and Center for NanoScience, Ludwig Maximilian University, Munich, 80539 Germany. E-mail: raedler@lmu.de; Fax: +49 89 2180 3182; Tel: +49 89 2180 2438
[c] Ethris GmbH, Planegg, 82152 Germany
† Electronic supplementary information (ESI) available: Table S1, S2; Figure S1–S5. See DOI: 10.1039/c5lc00749f
‡ Equal contribution.

element binding protein (CPEB), as well as with the cleavage and polyadenylation signaling factor (CPSF).[11] CPEB is responsible for the prolongation of the poly-A tail in the cytoplasm, whereas CPSF primes the pre-mRNA through cleavage at a specific site for the upcoming addition of poly-A.[11,15] As a second regulatory motif, the CYBA 3′ UTR contains the insulin 3′ UTR stability element (INS_SCE). The INS_SCE sequence has been shown to bind to the polypyrimidine tract binding protein (PTB) under reducing conditions, increasing the mRNA half-life of insulin.[16] UTRs of CYBA are shown in Table S2.† Another important feature influencing mRNA translation efficiency is the poly A-tail, which is located on the 3′ end. It has been shown that a prolongation of the poly A-tail to 120 nucleotides has beneficial effects on protein expression, assumingly because of the protective effect of longer poly A-tails against mRNA degradation.[17] In contrast to long poly A-tails, mRNAs with poly A-tails shorter than 50 nucleotides are claimed not to be translated at all.[11,18] Hence, in mRNA therapy, recombinant mRNA constructs are advantageously furnished with a poly A-tail of 120 nucleotides. Degradation of most mRNAs in eukaryotic cells begins with 3′ to 5′ exonucleolytic deadenylation, resulting in removal of most of the poly A-tail. Subsequently, two major pathways that are responsible for the degradation of the rest of the mRNA body are known to come into play. On the one hand, the 5′ end is decapped by the Dcp1/Dcp2 complex, followed by 5′–3′ exonucleolytic degradation that is catalyzed by Xrn1p. On the other hand, the exosome enables 3′–5′ exoribonucleolytic degradation with the 5′ cap being retained.[19] Moreover, it is known that the 5′ cap interaction with the 3′ poly A-tail results in circular forms of the mRNA. It is assumed that the circular shape of the mRNA increases the initiation rate of ribosomes and also protects mRNA against degradation.[20]

We were interested in whether the reported long half-life of natural CYBA mRNA can be conferred to a foreign mRNA by virtue of flanking its coding sequence with combinations of CYBA 5′- and 3′-UTRs. So far, mRNA stability and turnover have been measured by a variety of approaches including metabolic labelling, mass spectrometry, quantitative real-time reverse transcription polymerase chain reaction (qRT-PCR), microarrays, or fluorescence labelling techniques for imaging mRNA inside cells.[17,21–26] Most of these are ensemble measurements and data represent mean of all cells without taking into account the fluctuations in the expression amounts (high vs. low) or timing of expression (early or late). Hence, population measurements exhibit an averaged response and are of limited use for computational analysis of the underlying biochemical network. In contrast, single-cell distribution functions provide additional information about the heterogeneity in transfection experiments.

Recently, we have shown that single-cell analysis of mRNA transfection time-lapse movies is capable of assessing individual expression time-courses, yielding mRNA decay rates at the single-cell level.[27] Furthermore, we have reported on the use of regular micropatterns to position cells on a regular grid of adhesion sites.[28] Hence, we were interested in

applying this single-cell micro-array technology to screen and compare different mRNA constructs in a more rapid and standardized format than single-cell studies in diluted culture can do. To address this question, we have chosen the coding sequence of destabilized enhanced green fluorescence protein (d2EGFP) to artificially shorten the life cycle of the reporter protein inside the cell.[29] The combinations included insertion of the respective CYBA UTRs at 5′ or 3′ ends, respectively, at both 5′- and 3′ ends, at the 5′ end combined with two repeats of the 3′ UTR at the 3′ end, or two repeats of 3′ UTR without 5′ UTR. All of these compared to a control construct without UTRs. Protein and mRNA functional life times and the expression rates from each of the compared transcripts were assessed using both the single-cell approach and population based methods like flow cytometry, fluorescence microscopy and qRT-PCR. As expression of d2EGFP is a direct readout of the functionality of d2EGFP stable non-immunogenic mRNA (SNIM® RNA), expression kinetics were used to determine the "functional" half-life of d2EGFP SNIM® RNA.

Results

Fluorescence microscopy and analysis *via* flow cytometry (FC)

To evaluate the effect of different UTR combinations on transgene expression kinetics, two different cells lines were transfected using Lipofectamine™ 2000 with different d2EGFP mRNA constructs containing a 5′ UTR alone, a 3′ UTR, 5′ + 3′ UTR, two copies of 3′ UTR and 5′ + 2 × 3′ UTR. A schematic representation of the building blocks of all constructs can be seen in Fig. 1A.

At different time points through three days post-transfection, d2EGFP expression was quantified using FC. An exemplary dot plot for $t = 24$ h, illustrating d2EGFP expression levels of live A549 cells, is shown in Fig. 1C (see Fig. S4B† for corresponding Huh7 data). In addition, we imaged the cells using fluorescence microscopy (see Fig. 1B and D and Fig. S4A and C†). Comparable transfection efficiencies for all mRNA constructs were confirmed 24 hours post transfection (Fig. 1B and S5A†). Thereby, we can rule out differential transfer efficiencies to be a causal factor for the observed differences in expression kinetics. Based on fluorescence microscopy images, we detected a drastic reduction of d2EGFP expression for all constructs at 48 h post-transfection (see Fig. 1B and D, S4A and C†). However, higher d2EGFP expression levels with respect to the control were found for all UTR-stabilized mRNAs. More specifically, mRNA constructs containing 3′ UTRs seemed to enhance expression more than constructs without 3′ UTRs. We observed this for A549 and Huh7 cells (see Fig. 1 and S4,† respectively). At time points later than 48 h, this effect was even more pronounced (data not shown). In Fig. 2A and B, the time-courses of the mean fluorescence intensities (MFI) as determined by FC are shown for all constructs in both cell types.

Also here, all UTR-containing mRNA constructs showed higher MFI values than the control construct in both cell lines at all time points. Taken together, our fluorescence microscopy and FC data suggest that mRNA molecules
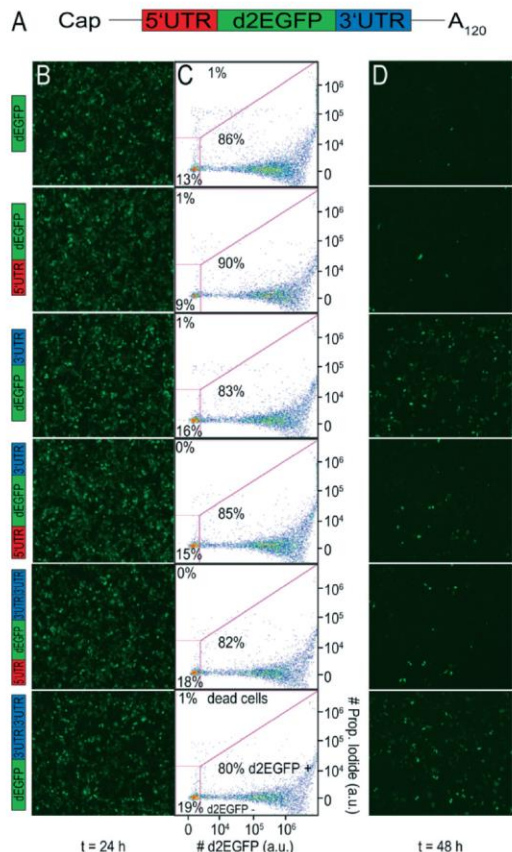
Lab on a Chip

Fig. 1 Fluorescence microscopy and flow cytometry data of A549 cells. (A) Schematic illustration of therapeutic mRNA, consisting of a 5′ cap, a 5′ UTR, an encoding region, a 3′ UTR and a poly-A tail. (B) Fluorescence microscopy pictures taken with 4× magnification (JULY™) at 24 h post-transfection. All constructs showed improved protein expression levels as compared to the control. (C) The percentage of d2EGFP positive cells as determined by FC is similar for all constructs. Propidium iodide was used to detect dead cells. The applied gates ensured exclusion of dead cells and untransfected cells. (D) At 48 h post transfection, sustained protein expression was higher for the stabilized constructs as compared to the control.

Fig. 2 Time-courses of protein expression as determined by FC for A549 cells (A) and Huh7 cells (B). Mean fluorescence intensities normalized to the control are plotted *versus* time in a log-linear plot. With increasing time post transfection, the elevated protein expression levels of the stabilized constructs become more and more evident. The green, red and blue bars correspond to the control/5′ UTR/3′ UTR constructs, respectively. The purple, orange and grey bars correspond to the constructs that are shown on the bottom of the figure.

furnished with CYBA UTRs show persistent d2EGFP expression for more than 24 hours.

Quantitative real-time PCR

We conducted qRT-PCR measurements as an additional approach to determine the physical mRNA half-life of the different constructs. Binding of our selected primers to d2EGFP occurred 600 nt downstream of the start codon. Hence, measurements of physical mRNA half-life comprise both intact mRNAs and those which have either been decapped but not yet degraded or both decapped and degraded up to base 599.

It also includes mRNA that has been removed from the translational pool and stored in P-bodies.[30-33] Only intact mRNAs yield d2EGFP protein, while decapped and/or partially degraded transcripts and those in P-bodies do not lead to any expression. Determination of physical mRNA half-lives did not reveal any significant life time prolongation by the UTRs compared to the control in the A549 and Huh7 cells (see ESI† S5A and B, respectively). Interestingly, we observed a decrease in mRNA physical half-lives for 5′, 3′, 5′ + 2 × 3′ and 2 × 3′ UTR constructs in both cell lines.

Single-cell expression arrays

We fabricated microstructured, cell-adhesive substrates as shown in Fig. 3A and B as a platform for single-cell time-lapse microscopy.
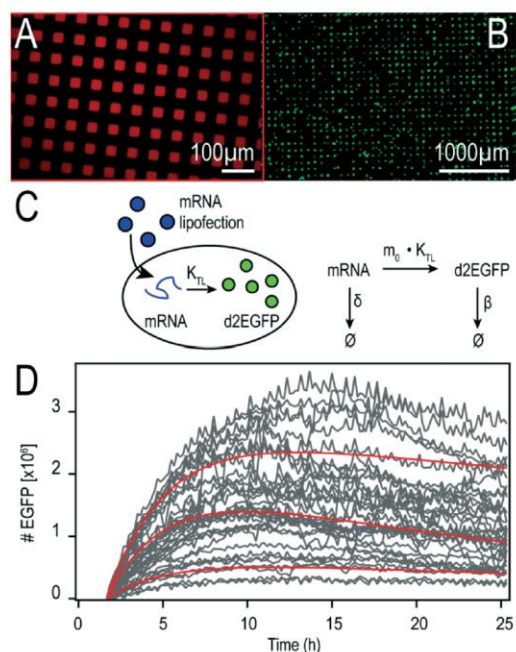
Fig. 3 Microstructured multi-channel slides for parallel single-cell assays to test differently stabilized mRNA constructs. (A) Cell-adhesive, microstructured protein patterns with cell-repellent PEG areas in between allow ordered cell arrangement. Fluorescently labeled fibronectin was used to visualize the micropattern. (B) Fluorescent A549 cells adhering to fibronectin patterns inside a microchannel (three hours after seeding). (C) Schematic drawing of mRNA lipofection (on the left) and reaction scheme underlying our analytical solution (on the right). (D) Exemplary time-courses of mRNA-mediated d2EGFP expression in A549 cells. Red lines are representative fits to the theoretical translation model.

The rectangular squares are functionalized with the extracellular matrix protein fibronectin, while the surrounding dark area is passivated with cell repellent PLL-*g*-PEG. Cells were seeded at an appropriately dilute cell density such that after about three hours cells adhered to the rectangular squares. This cellular self-organization process has been studied in detail before.[28] The size of the squares was 30 μm for optimal filling with single cells. The distance between the squares was just big enough (60 μm) to minimize bridging effects of cells adhering to more than one square at the same time. Time-lapse fluorescence microscopy and automated image analysis of the fluorescence signal per square yields hundreds of individual time-courses. A typical set of background corrected raw data is shown in Fig. 3D. The red lines represent exemplary fits to the mathematical expression for mRNA translation (see also Materials and Methods section). Data were analyzed as described recently[27] by fitting each time-course with the analytical solution for mRNA-induced protein expression,

$$G_{d2EGFP}(t) = \frac{K}{\delta - \beta} \times \left(1 - e^{-(\delta-\beta)(t-t_0)}\right) \times e^{-\beta(t-t_0)} \quad (1)$$

using IgorPro software. Here, G denotes the amount of protein, K is the expression rate, δ is the degradation rate of functional mRNA, and β is the degradation rate of the reporter protein d2EGFP. The expression rate $K = m_0 \times k_{TL}$ is the product of the initial amount of mRNA molecules inside the cell (m_0) and the translation rate k_{TL}. The time-course that is described by eqn (1) will be discussed in detail in below section "master curves of protein expression".

***In vitro* transfection on cell arrays**

In a typical experiment, cells were allowed to adhere to the micropatterns for three hours before transfection. Each of the six microchannels was filled with a different lipoplex solution, containing one of the constructs of interest. In initial experiments, we compared two different, commercially available transfection reagents (namely Lipofectamine™ 2000 and DOGTOR). We found higher transfection efficiencies for Lipofectamine™ 2000 than for DOGTOR (see Fig. S1†). Because we additionally obtained high cell viability rates of above 80% with Lipofectamine™ 2000 (data not shown), all further transfection experiments were conducted using Lipofectamine™ 2000. As mRNA-mediated protein expression starts shortly after transfection, incubation time was kept to a minimum. Accordingly, the ratio between mRNA dosage and incubation time was adjusted to achieve high transfection efficiencies (see also Fig. S1†) and negligible toxic effects caused by over-expression of the reporter protein. At an mRNA dose of 5 pg per cell, an incubation time of one hour was found to be optimal.

Expression rates

All results for the two cell types are based on four independent measurements under the same experimental conditions. Time-lapse data of about thousand A549 cells and thousand Huh7 cells have been analyzed. The distributions of the obtained expression rates K are shown in Fig. 4A and the corresponding mean values can be seen in Fig. 4D.

Both the mean expression rates and the shape of their distributions were found to be rather similar for the different constructs.

mRNA functional half-lives

We converted the fitted mRNA-degradation rates δ into mRNA functional half-lives according to

$$\tau = \frac{\ln 2}{\delta}. \quad (2)$$

Fig. 4B shows the functional half-life distributions of the examined mRNA constructs in A549 and Huh7 cells, respectively. Here, it becomes evident that for constructs with
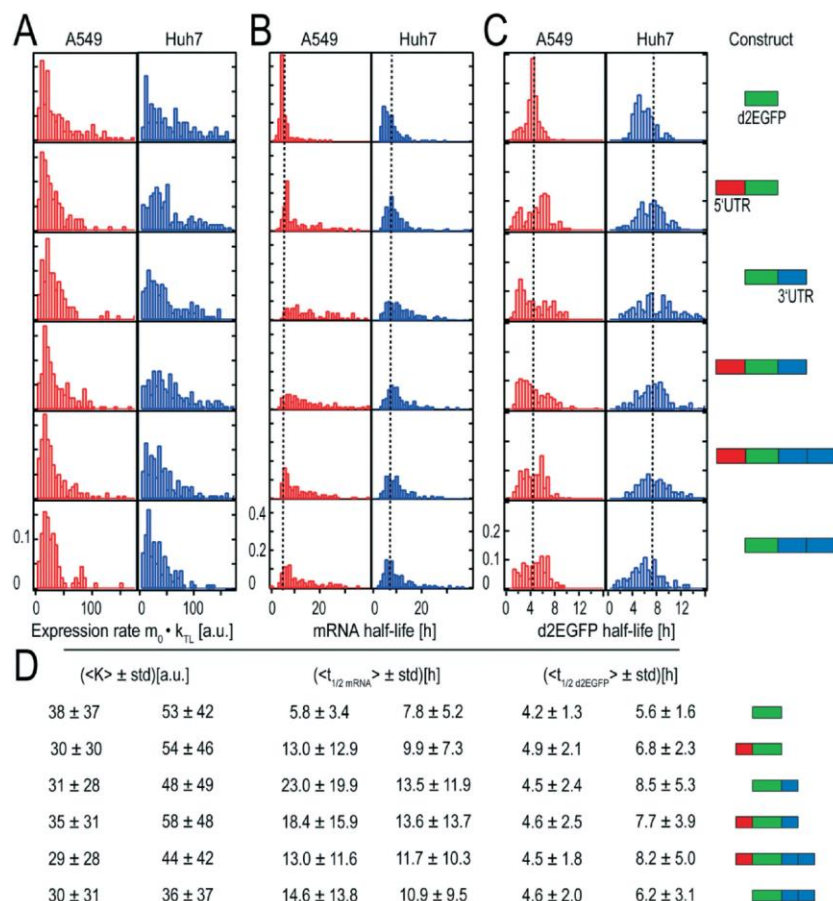
Lab on a Chip

Paper

(<K> ± std)[a.u.]		(<t_{1/2 mRNA}> ± std)[h]		(<t_{1/2 d2EGFP}> ± std)[h]	
38 ± 37	53 ± 42	5.8 ± 3.4	7.8 ± 5.2	4.2 ± 1.3	5.6 ± 1.6
30 ± 30	54 ± 46	13.0 ± 12.9	9.9 ± 7.3	4.9 ± 2.1	6.8 ± 2.3
31 ± 28	48 ± 49	23.0 ± 19.9	13.5 ± 11.9	4.5 ± 2.4	8.5 ± 5.3
35 ± 31	58 ± 48	18.4 ± 15.9	13.6 ± 13.7	4.6 ± 2.5	7.7 ± 3.9
29 ± 28	44 ± 42	13.0 ± 11.6	11.7 ± 10.3	4.5 ± 1.8	8.2 ± 5.0
30 ± 31	36 ± 37	14.6 ± 13.8	10.9 ± 9.5	4.6 ± 2.0	6.2 ± 3.1

Fig. 4 Distributions of expression rates K, mRNA functional life times, and d2EGFP life times and corresponding mean values with schematic representations of the constructs. (A) Distributions of expression rate K, which is the product of the initial number of mRNA molecules and the translation rates. The fact that the distributions are similarly shaped indicates that the transfection kinetics and the translation rates are very similar. (B) The distributions of the mRNA functional half-lives show great variations in their broadness. As a guide to the eye, dotted lines indicate the mean half-life of the control. (C) Distributions of d2EGFP half-lives. As expected, the distributions of the different constructs are similarly shaped and show comparable mean values. As a guide to the eye, the overall mean half-life of d2EGFP based on all measured half-lives is shown as a dotted line. (D) Mean values and the corresponding standard deviations (std) of the fitted rates. Although the control construct yields high mean K values in both cell types, the short mRNA functional half-life of this construct leads to small AUC values as compared to the stabilized constructs. This can be seen in Fig. 6. Schematic representations of the constructs can be seen on the right hand side. All constructs have the same 5′ cap and a poly A-tail. Data from 895 single A549 and 1355 Huh7 cells were analysed.

UTRs, both mean functional half-life and broadness of the underlying distribution increase as compared to the reference construct without UTRs.

An overview of all determined functional half-lives is given in Fig. 4D. Both for A549 and for Huh7 cells, we found longer functional half-lives for mRNAs stabilized by UTR elements compared to the control construct (5.8 hours for A549 cells and to 7.8 hours for Huh7 cells) that does not contain any stabilizing UTR. The functional life time prolonging effect was more pronounced in A549 cells.

Protein half-lives

The distributions of protein (d2EGFP) degradation life times are presented in Fig. 4C. As expected, the half-lives of the expressed protein do not vary for the different mRNA constructs. The determined mean life times range from 4.2 to 4.9 hours for A549 cells and from 5.6 to 8.5 hours for Huh7 cells as shown in Fig. 4D. The coefficients of variation are about 0.29 (A549) and 0.45 (Huh7) and hence are significantly smaller than the coefficient of variation of up to 0.6 that we

found for the distribution on mRNA functional life times. As a control, we also measured the half-lives in an alternative approach, where translation was inhibited by addition of cyclo-heximide at a given time point, t_0, after transfection (see Fig. S3†). In this case, protein expression is induced for a while and then stopped. The exponential decay in fluorescence after inhibition yields protein life times. These half-lives were found to be smaller by a factor of about two, compared to the above experiments without inhibition. In both experiments, however, the relative ratios of the protein life times in Huh7 cells as compared to those in A549 cells is the same.

Master curves of protein expression

The features of mRNA induced protein expression become evident in the so-called master curve of protein expression as depicted in Fig. 5A (A549) and B (Huh7).

The master curve is the population average of the onset-time corrected single-cell traces, i.e. all onset-times were shifted to time point zero. Fluorescence intensities were converted into actual numbers of d2EGFP as described before in reference.[27] The superior properties of the 3′ and the 5′ + 3′ UTR mRNA constructs are illustrated in the master curve plot. These constructs showed the shallowest decrease in protein expression with time and hence the longest functional half-lives in addition with higher protein expression values as compared to the other constructs.

Area under the curve (AUC)

In pharmacokinetics, the concentration-time curve of a drug in the blood circulation is known as the "area under the curve" (AUC) which is a measure of the bio-availability of a drug. Here, we use the term for the cumulative time-dose of

the protein that is encoded by the mRNA. In this respect, the AUC simultaneously quantifies the translational efficiency and the stability and hence the overall efficacy of a chosen mRNA construct. Given the biochemical rate model (see Fig. 3A), the AUC can be explicitly calculated (see also Fig. S2†):

$$AUC = 0.48 \times m_0 \times k_{TL} \times \tau_{mRNA} \times \tau_{d2EGFP} \qquad (3)$$

Hence an optimal therapeutic mRNA construct should desirably have both long mRNA function half-life, τ_{mRNA}, as well as a protein half-life, τ_{d2EGFP}, and high translational efficiency, k_{TL}. In addition, the transfer efficiency which determines the initial amount of therapeutic mRNA, m_0, is directly proportional to the AUC. An illustrative explanation for the theoretical time-course of protein expression and the calculated AUC can be seen in Fig. 6A.

If there was no protein degradation ($\beta = 0$), the amount of protein inside a cell would run into a steady state level as a consequence of a balanced flux of mRNA translation and mRNA degradation. In this case, the expression dynamics follows $\frac{K}{\delta}\left(1 - e^{-\delta t}\right)$. The same would be true in an analogous manner for the case where δ was equal to zero. The superposition of this with the permanent, exponential decay of the d2EGFP protein (following $e^{-\beta t}$) results in the characteristic shape of the AUC as shown in Fig. 6A. Fig. 6B and C show the overall mean relative AUCs as well as the "per-experiment" relative AUCs normalized to the mean AUC of the control, the latter being the AUC of protein expression after transfection with the control construct. In both cell types, we find the highest relative AUCs for the 3′ UTR- and the 5′ + 3′ UTR-stabilized construct. This is consistent with the observed long functional half-lives for these constructs, because they contribute to the AUC as seen in eqn (3). The detailed, single-cell AUC distributions can be found in Fig. S2 of the ESI.†

Functional life time prolongation factor

The functional life time prolongation factors for A549 and Huh7 cells are shown in Fig. 6D and E, respectively. As expected, all UTR-flanked constructs yield functional life time prolongation factors higher than one, meaning that the insertion of UTRs at either end causes mRNA stabilization. However, the 3′ UTR mRNA construct shows longer mRNA functional life times than the 2 × 3′ UTR construct. Similarly, the 5′ + 3′ UTR construct is more persistent than the 5′ + 2 × 3′ construct. These results hold true for both cell types. Interestingly, the stabilizing effects are significantly more pronounced in A549 cells than in Huh7 cells in all cases.

Discussion

Determination of mRNA functional stability and its expression are two major factors to be considered when it comes to developing new mRNA therapeutics. Here, we used different combinations of UTRs, a 5′ UTR, 3′ UTR, a 5′ + 3′ UTR, 5′ + 2 ×
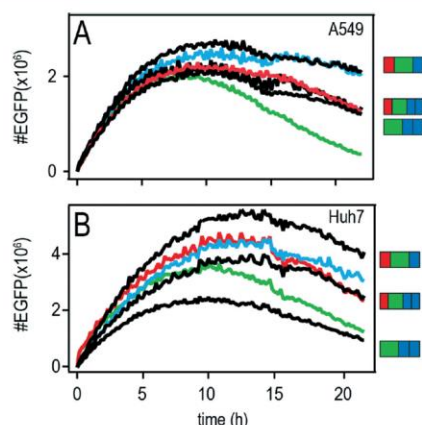
Fig. 5 Master curves of the different constructs. Population averages of A549 (A) and Huh7 (B) cells with the onset-time shifted to zero. The green, red, and blue curves correspond to the control/5′ UTR/3′ UTR constructs, respectively. The black curves correspond to the constructs on the right hand side.
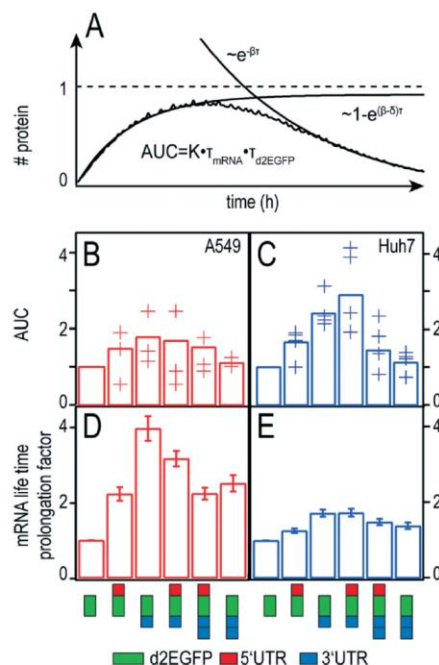
Lab on a Chip

Fig. 6 AUC and mRNA functional life time prolongation factors of the different constructs. (A) Schematic representation of the AUC to illustrate the interplay between mRNA translation and degradation of mRNA and protein. (B) and (C) AUC of the different constructs as analysed for $t \rightarrow \infty$. Crosses show relative AUCs of different experiments, the bars correspond to the mean of all single-cell AUCs. (D) and (E) mRNA functional life time prolongation factors. All modifications result in prolonged mRNA functional life times as compared to the control. Similar trends are observed in A549 (D) and Huh7 (E) cells. Error bars in (D) and (E) indicate standard deviation.

3′ UTR, and two copies 3′ UTR to improve mRNA in terms of functional stability and its expression. The AUC of the d2EGFP time-course is also evaluated, because the total protein expression is relevant for a sustained therapeutic effect. In order to get detailed time-resolved data and monitor protein expression dynamics at the single-cell level, we used microstructured single-cell arrays for parallel, quantitative measurements of mRNA stability and translational efficiency. The regular arrangement of cells guaranteed reproducible microenvironments and enabled fast and automated image-analysis, which are prerequisites for comparative, high-throughput single-cell studies. The approach allows the determination of distribution functions for (i) protein half-life, (ii) expression rates, and (iii) functional mRNA half-life.

In both A549 and Huh7 cells, mean protein half-lives of d2EGFP were narrowly distributed and independent of the UTR sequence. The calculated half-life values of 4.5 hours for A549 cells and 7.4 hours for Huh7 cells could be attributed to cell type specific differences between the compared cell lines. Such cell specific differences in d2EGFP half-life have been

published previously. A study in NIH3T3 cells using a similar imaging cytometry approach recorded a half-life of 2.8 h within a measurement window of 12 hours.[34] An even shorter half-life of less than two hours has been reported for CHO cells by Li *et al.*[35] Here, protein degradation was measured by Western blotting and flow cytometry for three hours only.

To validate our findings from single-cell data analysis, we additionally determined d2EGFP life times in direct measurements using cycloheximide (see Fig. S3†). We found shorter life times as compared to the values observed from single-cell data analysis. This might be due to the fact that in single-cell data analysis, a constant initial number of mRNA molecules was assumed as part of the combined expression rate $K = m_0 \times k_{TL}$ (see eqn (1)). However, regardless of the fact that cells have been washed after one hour incubation time, it is still likely that the number of mRNA molecules is not constant from the start of observation. As a consequence, mRNA molecules that are available for translation later on, leading to protein expression, might result in longer half-life values obtained from single-cell expression time-course fitting. When we compare the mean half-life determined for A549 cells with the mean half-life determined for Huh7 cells, we find the same ratio of roughly 1.64 for both measurement methods. Also, even a possible systematic over-estimation of mRNA and protein half-lives does not change the qualitative order of the mRNA performance as determined by us.

The expression rate depends on the initial number of mRNA molecules, m_0, as well as on the translation rate K_{TL}. Note that the number of successfully delivered mRNA molecules varies due to the intrinsic stochasticity of the delivery process. The mean number of mRNA molecules, however, is expected to be the same, since the transfection protocol has scrupulously been kept up in all experiments. In contrast, the translational activity (K_{TL}) of the various UTR constructs might vary. Still, the fact that the distributions as well as the mean values of the expression rate K are rather similar for all constructs (see Fig. 4A and D) indicates that the translation rate is merely influenced by the inserted UTRs.

The parameter of highest interest is the mRNA functional half-life. Here, we compared functional mRNA half-life to physical mRNA half-life. Our results with single-cell transfection studies suggest that any insertion of 5′ or 3′ UTRs into the mRNA sequence increases its functional half-life which was observed for all modifications tested in this study (see Fig. 4 and 6) as measured by fluorescence microscopic imaging and FC (see Fig. 1 and 2). In contrast to the functional mRNA half-life, the physical mRNA half-life determined by qRT-PCR showed a decrease in mRNA stability for 5′, 3′, 5′ + 2 × 3′ and 2 × 3′ UTR in both cell lines (see Fig. S5A and B†).

One major difference is that the physical half-life as measured by qPCR does not reflect the translational ("functional") productivity of a given mRNA construct. qPCR as used here merely quantifies the physical presence of an mRNA fragment and is inappropriate to predict the utility of an mRNA construct in a therapeutic application. Similar findings have been reported by Gallie *et al.*[36] In contrast, the

Appendix

functional half-life as measured here is a function of the translational capacity of an mRNA, determines the amount of total protein produced (Area Under the Curve) and predicts the utility of an mRNA construct for a therapeutic application. For a therapeutic mRNA, it can be imperative that the molecule is functional for as long or as short as possible and yields a maximum or a minimum of protein. Furthermore, the heterogenic distribution of the functional half-lives points out the importance of single-cell measurement techniques, because these effects are obscured in ensemble measurements (see Fig. 2, 4 and S5A† and B). An interesting conclusion from the observed discrepancy of physical and functional half-lives is that obviously cells make more productive use of moderate amounts of mRNA than of the initial high amounts present at the early time points after transfection. In fact, the impact of the UTRs examined here on mRNA productivity become increasingly evident at the later time points after transfection.

Interestingly, a positive effect on protein expression was observed for 5′ UTR alone, although so far, no known motif in the CYBA 5′ UTR has been discovered. For the first time, we could show that CYBA UTRs at either end suffice to increase both peak and persistence of protein expression in both cell lines. These findings are consistent with publications claiming individual or synergistic behaviour of 5′ UTRs and 3′ UTRs.[15] In contrast to Holtkamp et al.,[17] no additional increase in protein expression or mRNA functional stability could be observed with two sequential copies of the 3′ UTR as compared to one single 3′ UTR (see Fig. 4). Conversely, it even resulted in shorter functional life times both for 5′ + 3′ versus 5′ + 2 × 3′ UTR insertion and for 3′ versus 2 × 3′ UTR insertion. This might be due to the fact that a different type of cells (namely dendritic cells) was used in the study by Holtkamp et al.[17] Similar cell type-specific effects have been reported for hepatocytes, too.[37] Another contributing factor affecting mRNA functional stability might be the secondary structure of the different mRNAs. Such effects of mRNA secondary structure in regulating gene expression have been reported before.[38,39]

Important structural characteristics together with their minimum free energy for the mRNA constructs used in the current study are summarized in Table S1.† The persistent protein expression of the 5′ + 3′ UTR stabilized construct could be due to binding of the 5′ to the 3′ end, which facilitates circularization of the mRNA.[20] Because we could not find any stable secondary structures within the 5′ UTR, we assume that this feature enables an early expression onset.[40] In contrast, we identified secondary structures within the 3′ UTRs. These might protect the mRNA from the 3′–5′ degradation pathway. Two 3′ UTRs showed even more secondary structures (two hairpins) with the best minimum free energy, indicating more persistent expression. Taken together, these findings could be the explanation for the inferior onset expression of the 2 × 3′ UTR compared to the 5′ UTR and the persistent expression at later time points of mRNA constructs containing 3′ UTRs.

In accordance with protein half-lives, longer functional half-life values were obtained for mRNAs stabilized with UTRs. This was observed in both cell lines with cell-specific differences most likely affecting the absolute values. In A549 cells, mRNA functional half-lives for the constructs with UTRs ranged from 13.0 h to 23.0 h as compared to 5.8 h for the control. In Huh7 cells, functional half-lives from 9.9 h to 13.6 h were measured for UTR-containing constructs, as opposed to a functional half-life of 7.8 h for the control mRNA. The functional half-life of the 3′ UTR-flanked mRNA in A549 cells is in good agreement with mRNA life times of similarly stabilized mRNAs that were reported previously.[17,27] The fact that functional stability and decay kinetics of mRNA and protein differ in different cell types is most likely due to differences in the complex networks of interactions between mRNA and proteins which are very likely to be cell-type dependent.

Taken together, our results in both A549 and Huh7 cells, independent of the analysis method (FC or single-cell analysis), suggest that sustained, high levels of protein expression can be induced by CYBA UTR flanked mRNA. The choice of UTR combination depends on the need of the experiment of application. Where persistent protein expression with reduced mRNA decay is desired, mRNA flanked with a 3′ UTR alone might serve the purpose. However, the combination of 5′ + 3′ UTR results in additional desirable features of early onset, high peak and cumulative protein expression.

Our study demonstrates that micro-array based single-cell analysis of mRNA-induced protein expression is a means to characterize and improve kinetic properties of mRNA constructs. Using automated time-lapse microscopy and automated image analysis, we were able to assess the intracellular bioavailability of different mRNA constructs at the single-cell level in a highly parallel format. The micro-arrays provide a standardized platform to transfect arrayed cells at high number density on a chip and with defined boundary conditions such as the cell area. This allows to acquire single-cell time traces from equally treated cells and hence a more reliable basis to identify sequences yielding sustained protein expression. We found prolonged persistence of protein expression for constructs stabilized by UTR insertions using a single-cell model and FC analysis in two cell types. This finding is desired in case of developing mRNA therapeutics. Messenger RNA constructs with persistent protein expression over a period of time (AUC) is desirable and allows proper reduced dosing into a patient with a final therapeutic outcome. We hope that our study helps to further refine strategies for the manipulation of mRNA stability for future pharmaceutical applications.

Experimental

Plasmid vectors

Destabilized Enhanced Green Fluorescent Protein (d2EGFP) was excised from pd2EGFP-N1 (Clontech) and cloned in pVAXA120 (ref. 3) to generate pVAXA120-d2EGFP. Based on

112

previously published data with respect to mRNA stability, preselected 5′ and 3′ UTR sequences of CYBA gene were synthesized by Eurofins MWG (Germany) and cloned upstream (5′ UTR) and/or downstream (3′ UTR or 2 × 3′ UTR) of d2EGFP in pVAXA120-d2EGFP, thereby generating the constructs with respective UTR combinations.

mRNA production

To generate *in vitro* transcribed mRNA (IVT mRNA), plasmids were linearized downstream of the poly-A tail by NotI digestion and purified by chloroform extraction and ethanol precipitation. Purified linear plasmids were used as template for *in vitro* transcription using RiboMax Large Scale RNA production System-T7 (Promega, Germany). Anti-Reverse Cap Analog (ARCA) was added to the reaction mix to generate 5′ capped mRNA. Additionally for the production of SNIM® RNAs, chemically modified nucleotides namely methyl-CTP and thio-UTP (Jena Bioscience, Germany) were added to a final concentration of ATP : CTP : UTP : methyl-CTP : thio-UTP : GTP of 7.57 mM : 5.68 mM : 5.68 mM : 1.89 mM : 1.89 mM : 1.21 mM. The complete IVT mix was incubated at 37 °C for 2 hours followed by a DNA disgestion with DNaseI for 20 minutes at 37 °C. RNA was precipitated with ammonium acetate (final concentration 2.5 M) and washed with 70% EtOH. The washing step was performed twice. Finally, the RNA pellet was re-suspended in RNAse-free water. All mRNAs were verified on 1% agarose gels. A schematic representation of an exemplary mRNA construct can be seen in Fig. 1A. The exact sequences of the UTRs are given in the ESI† (Table S1).

Flow cytometry (FC)

The experimental set-up looks as follows: 20 000 cells in 150 μl medium were seeded per well in 96-well plates and transfected 24 hours post-seeding. Cells were transfected at a dose of 5 pg mRNA per cell using the commercial transfection reagent Lipofectamine™ 2000. Complexes were prepared at a ratio of 2.5 μl Lipofectamine™ 2000 per 1 μg mRNA. For the formation of lipoplexes, Lipofectamine™ 2000 and mRNA were diluted separately in OptiMEM transfection medium in a total volume of 50 μl, each. These mixtures were incubated at room temperature for 5 minutes. The mRNA solution was then mixed with the Lipofectamine™ 2000 solution, followed by another 20 minutes of incubation at room temperature. After incubation, 900 μl of OptiMEM were added to the lipoplex solution. Finally, 50 μl of the complex solution were added to the cells and incubated for 1 hour. For every mRNA construct, biological triplicates were prepared. After incubation, the lipoplex-solution was discarded and fresh 150 μl medium was added to each well. d2EGFP expression was measured after 8, 24, 36, 48, 60 and 72 hours using FC. Fluorescence microscopy images were taken at each of these time points. For FC measurements, the cell culture medium was discarded and the cells were washed with 1× DPBS (Gibco Life Technology). Subsequently, 20 μl of TrypLE Express (Gibco

Life Technology) were added per well and incubated for 5 min at 37 °C. The reaction was neutralized by adding 80 μl 1 × PBS, supplemented with 2% FBS. Cells were mixed by pipetting and were transferred into a 96 well plate appropriate for flow cytometric measurements. Finally, 5 μl of Propidium iodide (final concentration 1 μg ml⁻¹) were added per well and measured with Attune Auto Sampler (Applied Biosystems). Please note that fluorescence images were taken prior to FC analysis with a JULY™ microscope.

Quantitative real-time PCR

A qRT-PCR analysis was used to determine the d2EGFP mRNA amount at time intervals of 4, 8, 24, 36, 48, 60 and 72 hours in A549 and Huh7 cells. Additionally, the mRNA expression kinetic itself was used to calculate the mRNA half-life of each UTR. Here, the cells were transfected similarly to the protocol described above (see FC). A cell density of 200 000 cells per well was found to be sufficient for RNA isolation. RNA isolation was performed according to the manufacturer's protocol using NucleoSpin RNA (Macherey Nagel). The isolated total RNA was examined in RNA concentration and quality by spectrophotometric measurements and gel analysis. Further, 0.5 μg of the total RNA of each UTR constructs and the control were used for cDNA synthesis using Oligo(dT)s from First Strand cDNA Synthesis Kit (Thermo Scientific). Equivalent amounts of cDNA (diluted 1 : 50) were tested with 125 nM of each d2EGFP-Primer (forward Primer: 5′-CAA CCA CTA CCT GAG CAC CC-3′; reverse Primer:5′-GTC CAT GCC GAG AGT GAT CC-3′) using SsoAdvanced™ Universal SYBR® Green Supermix (BioRad). As a standard for the absolute quantification, pure d2EGFP mRNA produced by IVT was used for synthesis of cDNA. Absolute mRNA quantification was performed on a Lightcycler 96 device (Roche).

Surface patterning and sample preparation

Microstructured surfaces were produced by selective oxygen plasma treatment (Femto Diener, 40 W for 3 min) on a top as substrate (ibidi GmbH) with subsequent passivation. Selectivity was achieved using a polydimethylsiloxane (PDMS) stamp (cast from a master produced by photolithography) as a mask. The parts exposed to plasma were passivated by incubation for 30 min with PLL(20k)-*g*(3.5)-PEG(2k) at a concentration of 1 mg ml⁻¹ in aqueous buffer (10 mM HEPES pH 7.4 and 150 mM NaCl). Thereafter, the samples were rinsed with PBS and the PDMS stamps were removed. The foils were then fixed to adhesive six-channel slides (sticky μ-slide VI). Each channel was filled with a solution of 50 μg ml⁻¹ fibronectin in PBS for one hour to render the remaining sectors cell-adhesive. Probes were thoroughly rinsed with PBS three times. The samples were stored in cell medium at room temperature before cell seeding. For this study, square adhesion sites of 30 μm × 30 μm were used because this size turned out to be reasonable for single-cell adhesion of A549 as well as Huh7 cells. Cells were seeded at a density of 10 000 cells per channel so that roughly one cell could

Paper

adhere on each cell-adhesive island. To obtain fluorescent micropatterns as shown in Fig. 3A, a mixture of 20 µg ml^{-1} fibronectin and 30 µg ml^{-1} fibrinogen conjugated with Alexa Fluor 488 was used.

Materials

FBS, Leibovitz's L-15 Medium (Gibco), Lipofectamine™ 2000, and OptiMEM (Gibco) were purchased from Invitrogen, Germany. Sterile PBS was prepared in-house. Ham's F-12K, DMEM, and Trypsin-EDTA were purchased from c.c.pro GmbH, Germany. Channel slides were purchased from ibidi, Germany. Fibronectin was purchased from Yo Proteins, Sweden. PLL-g-PEG was purchased from SuSoS AG, Switzerland. Alexa Fluor 488 was purchased from Life Technologies, Germany. The plasmid pd2EGFP-N1 was purchased from BD Biosciences Clontech, Germany.

Cell culture

A human alveolar adenocarcinoma cell line (A549, ATCC CCL-185) was grown in Ham's F12K medium supplemented with 10% FBS. A human hepatoma epithelial cell line (Huh7, JCRB0403, JCRB Cell Bank, Japan) was cultured in DMEM medium, supplemented with 10% fetal bovine serum. All cell lines were grown in a humidified atmosphere at 5% CO_2 level.

In vitro transfection

Three hours prior to transfection, 10 000 cells per channel were seeded in a 6-channel slide. Cells were transfected at a dose of 5 pg mRNA per cell using the commercial transfection reagent Lipofectamine™ 2000 at a ratio of 2.5 µl Lipofectamine™ 2000 per 1 µg mRNA. The complex formation was prepared as follows: Lipofectamine™ 2000 and mRNA were separately diluted in OptiMEM transfection medium to add up to a total volume of 45 µl, each. These mixtures were incubated at room temperature for 5 minutes. The Lipofectamine™ 2000 solution was then mixed with the mRNA solution, followed by another 20 minutes of incubation at room temperature. Please note that the microchannels were never empty during all subsequent rinsing steps: immediately before transfection, the cells were washed with PBS. Finally, the lipoplex solutions containing different mRNAs constructs were filled into the six channels. All five different mRNA constructs plus the reference construct could thus be measured under the same experimental conditions. The cells were incubated in a total transfection volume of 90 µl at 37 °C (5% CO_2 level) for one hour. The transfection medium was thereafter removed and the cells were washed with PBS. Subsequently, the cells were re-incubated with Leibovitz's L-15 Medium containing 10% FBS. A drop of anti-evaporation oil (ibidi GmbH, Germany) was added on top of each medium reservoir before microscopic monitoring of d2EGFP expression.

Data acquisition and quantitative image analysis

Live-cell imaging was performed on a motorized inverted microscope (Nikon, Eclipse Ti-E) equipped with an objective lens (CFI PlanFluor DL-10×, Phase1, N.A. 0.30; Nikon) and with a temperature-controlled mounting frame for the microscope stage. We used an ibidi heating system (Ibidi GmbH, Germany) with a temperature controller to stabilize the temperature of the samples at 37 °C (±2 °C) throughout the measurements. To acquire cell images, we used a cooled CCD camera (CLARA-E, Andor). A mercury light source (C-HGFIE Intensilight, Nikon) was used for illumination and a filter cube with the filter set 41 024 (Chroma Technology Corp., BP450-490, FT510, LP510-565) was used for d2EGFP detection. An illumination shutter control was used to prevent bleaching. Images were taken at 10 fold magnification with a constant exposure time of 600 ms at 10 minute-intervals for at least 25 hours post-transfection. Fluorescence images were consolidated into single-image sequence files. Quantitative analysis of characteristic parameters of single-cell expression kinetics allows the comparison of various vector performances in terms of expression efficiency and stability. Image analysis consisted of several steps and was done using in-house-developed software based on ImageJ. First, a rectangular grid was overlaid with the original time-lapse movie and adjusted to the size and orientation of the underlying cell-pattern. Next, the software automatically detected d2EGFP-expressing cells by reading out the fluorescence intensities of all squares. Unoccupied squares were used for background correction. The software calculates the cells' fluorescence over the entire sequence and connects corresponding intensities to time courses of the fluorescence per cell. Finally, single-cell fluorescence intensities per square were extracted.

Data were then analyzed as described recently by fitting each time-course with the analytical solution for mRNA-induced protein expression (see eqn (1)) using IgorPro software, which is the solution to the differential equations for mRNA and d2EGFP,

$$\frac{d}{dt}mRNA = -\delta \times m \quad (4)$$

$$\frac{d}{dt}d2EGFP = k_{TL} \times m - \beta \times d2EGFP \quad (5)$$

A schematic representation of the underlying simplistic model assumed for mRNA-induced protein expression is depicted in Fig. 3C.

Conclusions

Single-cell micro-arrays present themselves as a highly parallel and standardized tool for rapid transfection and quantitation of mRNA expression kinetics in a much shorter time frame compared to the conventional, population-based molecular biological measurements. The resulting data at the single-cell level are in good correlation with those measured

114

with quantitative real-time and FC analysis. As such, this work represents an advance in automated assessment and predictive modeling of mRNA structures with respect to their expression kinetics and functional stability at the single-cell level.

Conflict of interest statement

CP and CR are founders and shareholders of Ethris GmbH, a company which develops mRNA therapeutics. MKA is an employee of Ethris GmbH.

Notes and references

1   G. Tavernier, O. Andries, J. Demeester, N. N. Sanders, S. C. De Smedt and J. Rejman, *J. Controlled Release*, 2011, **150**, 238–247.
2   A. Yamamoto, M. Kormann, J. Rosenecker and C. Rudolph, *Eur. J. Pharm. Biopharm.*, 2009, **71**, 484–489.
3   M. S. D. Kormann, G. Hasenpusch, M. K. Aneja, G. Nica, A. W. Flemmer, S. Herber-Jonat, M. Huppmann, L. E. Mays, M. Illenyi, A. Schams, M. Griese, I. Bittmann, R. Handgretinger, D. Hartl, J. Rosenecker and C. Rudolph, *Nat. Biotechnol.*, 2011, **29**, 154–157.
4   M. Esteller, *Nat. Rev. Genet.*, 2011, **12**, 861–874.
5   K. Kariko and D. Weissman, *Curr. Opin. Drug Discovery Dev.*, 2007, **10**, 523.
6   G. Pesole, G. Grillo, A. Larizza and S. Liuni, *Briefings Bioinf.*, 2000, **1**, 236–249.
7   T. V. Pestova, J. R. Lorsch and C. U. Hellen, *Translational Control in Biology and Medicine*, 3rd edition of Cold Spring Harbor Monograph Archive, 2007, vol. 48, pp. 87–128.
8   L. Barrett, S. Fletcher and S. Wilton, *Cell. Mol. Life Sci.*, 2012, **69**, 3613–3634.
9   F. Mignone, G. Grillo, F. Licciulli, M. Iacono, S. Liuni, P. J. Kersey, J. Duarte, C. Saccone and G. Pesole, *Nucleic Acids Res.*, 2005, **33**, D141–D146.
10 M. J. Moore, *Science*, 2005, **309**, 1514–1518.
11 X. Pichon, L. A. Wilson, M. Stoneley, A. Bastide, H. A. King, J. Somers and A. E. Willis, *Curr. Protein Pept. Sci.*, 2012, **13**, 294–304.
12 P. A. C. 't Hoen, M. Hirsch, E. J. D. Meijer, R. X. D. Menezes, G. J. van Ommen and J. T. D. Dunnen, *Nucleic Acids Res.*, 2011, **39**, 556–566.
13 L. V. Sharova, A. A. Sharov, T. Nedorezov, Y. Piao, N. Shaik and M. S. Ko, *DNA Res.*, 2009, **16**, 45–58.
14 G. Pesole, F. Mignone, C. Gissi, G. Grillo, F. Licciulli and S. Liuni, *Gene*, 2001, **276**, 73–81.
15 F. Gebauer and M. W. Hentze, *Nat. Rev. Mol. Cell Biol.*, 2004, **5**, 827–835.
16 L. Tillmar, C. Carlsson and N. Welsh, *J. Biol. Chem.*, 2002, **277**, 1099–1106.
17 S. Holtkamp, S. Kreiter, A. Selmi, P. Simon, M. Koslowski, C. Huber, O. Tureci and U. Sahin, *Blood*, 2006, **108**, 4009–4017.
18 C. H. D. Moor, H. Meijer and S. Lissenden, *Semin. Cell Dev. Biol.*, 2005, **16**, 49–58.
19 N. L. Garneau, J. Wilusz and C. J. Wilusz, *Nat. Rev. Mol. Cell Biol.*, 2007, **8**, 113–126.
20 E. Szostak and F. Gebauer, *Briefings Funct. Genomics*, 2013, **12(1)**, 58–65.
21 S. Tyagi, *Nat. Methods*, 2009, **6**, 331–338.
22 H. Y. Park, H. Lim, Y. J. Yoon, A. Follenzi, C. Nwokafor, M. Lopez-Jones, X. Meng and R. H. Singer, *Science*, 2014, **343**, 422–424.
23 C. Miller, B. Schwalb, K. Maier, D. Schulz, S. Dümcke, B. Zacher, A. Mayer, J. Sydow, L. Marcinowski, L. Dölken, D. E. Martin, A. Tresch and P. Cramer, *Mol. Syst. Biol.*, 2011, 7.
24 T. Nolan, R. E. Hands and S. A. Bustin, *Nat. Protoc.*, 2006, **1**, 1559–1582.
25 M. Rabani, J. Z. Levin, L. Fan, X. Adiconis, R. Raychowdhury, M. Garber, A. Gnirke, C. Nusbaum, N. Hacohen, N. Friedman, I. Amit and A. Regev, *Nat. Biotechnol.*, 2011, **29**, 436–442.
26 B. Schwanhausser, D. Busse, N. Li, G. Dittmar, J. Schuchhardt, J. Wolf, W. Chen and M. Selbach, *Nature*, 2011, **473**, 337–342.
27 C. Leonhardt, G. Schwake, T. R. Stögbauer, S. Rappl, J.-T. Kuhr, T. S. Ligon and J. O. Rädler, *Nanomed.: Nanotechnol., Biol. Med.*, 2014, **10**, 679–688.
28 P. J. F. Rottgermann, A. P. Alberola and J. O. Radler, *Soft Matter*, 2014, **10**, 2397–2404.
29 P. Corish and C. Tyler-Smith, *Protein Eng.*, 1999, **12**, 1035–1040.
30 J. J. Rossi, *Nat. Cell Biol.*, 2005, **7**, 643–644.
31 U. Sheth and R. Parker, *Cell*, 2006, **125**, 1095–1109.
32 A. Jakymiw, K. M. Pauley, S. Li, K. Ikeda, S. Lian, T. Eystathioy, M. Satoh, M. J. Fritzler and E. K. L. Chan, *J. Cell Sci.*, 2007, **120**, 1317–1323.
33 R. Parker and U. Sheth, *Mol. Cell*, 2007, **25**, 635–646.
34 M. Halter, A. Tona, K. Bhadriraju, A. L. Plant and J. T. Elliott, *Cytometry, Part A*, 2007, **71A**, 827–834.
35 X. Li, X. Zhao, Y. Fang, X. Jiang, T. Duong, C. Fan, C.-C. Huang and S. R. Kain, *J. Biol. Chem.*, 1998, **273**, 34970–34975.
36 D. R. Gallie, *Genes Dev.*, 1991, **5**, 2108–2116.
37 B. Kren and C. Steer, *FASEB J.*, 1996, **10**, 559–573.
38 J.-M. Chen, C. Férec and D. Cooper, *Hum. Genet.*, 2006, **120**, 301–333.
39 P. Gaspar, G. Moura, M. A. Santos and J. L. Oliveira, *Nucleic Acids Res.*, 2013, **41**, e73–e73.
40 J. R. Babendure, J. L. Babendure, J.-H. Ding and R. Y. Tsien, *RNA*, 2006, **12**, 851–861.

Supplementary Information

Stability Analysis of Chemically Modified mRNA Using Micropattern-Based Single-Cell Arrays

M. Ferizi[1], C. Leonhardt[2], C. Meggle[2], M.K. Aneja[3], C. Rudolph[3], C. Plank[1,3] and J. O. Rädler[2,*]

[1] Institute of Experimental Oncology and Therapy Research, Technical University of Munich, Munich, 81675 Germany
[2] Faculty of Physics and Center for NanoScience, Ludwig Maximilian University, Munich, 80539 Germany
[3] Ethris GmbH, Martinsried, 82152 Germany
* To whom correspondence should be addressed. Tel: +49 89 2180 2438; Fax: +49 89 2180 3182; Email: raedler@lmu.de

The authors wish it to be known that, in their opinion, the first two authors should be regarded as Joint First Authors.

Table S1: Secondary structures (mfold)

d2EGFP	ΔG	5'end	3' end	5' UTR	3'UTR
control	-358,9	partial binding with cds (8/8)	loose (8/8)	none	none
5' CYBA	-375	partial binding with 5' CYBA UTR (7/8)	loose (8/8)	binds with cds (6/8)	none
3' CYBA	-411,6	partial binding with 3' CYBA UTR (8/8)	binds with 5'end (4/4)	none	forms one hairpin (7/8)
5'+3' CYBA	-405,7	binds with 3' CYBA UTR (3/8)	binds with 5'end (4/4)	binds with 3' CYBA UTR (4/8)	forms one hairpin (7/8)
5'+2x3' CYBA	-437,7	binds with 3'UTR (8/8)	loose (8/8)	binds with 3'UTR and gene (6/8)	1st 3'UTR: hairpin; 2nd 3'UTR: hairpin (7/8)
2x3' CYBA	-444,1	binds with itself and forms hairpin (8/8)	loose (7/8)	none	1st 3'UTR: hairpin; 2nd 3'UTR: two hairpins (3/8)

In Table S1, features of the mRNA constructs such as free minimum energy (ΔG) and secondary structures found at both ends and within the UTRs are listed. The folding platform mfold was used to predict mRNA secondary structures (1). For each construct, we compared the eight secondary structures that have the highest free energy. The highest free energy values are predicted for the 2x3' UTR and the 3' UTR constructs. The 5' end of each mRNA

construct partially binds with the 3'UTR or the 5'UTR, except for the control construct, which binds to the coding sequence (cds). Interestingly, the 5' end of the 2x3' mRNA construct forms a stabilizing hairpin with itself. However, hairpin loops near the 5' end can also hinder protein translation (2). Another feature was found in the 3' end of the 3' UTR and 5'+3' UTR mRNA constructs: There, the 3' end binds with the 5' end, minimizing the distance from each other and thus can enable faster initiation of translation. Unlike the 5'UTRs, the 3' UTR of each mRNA construct forms at least one hairpin with itself.

Table S2: Human CYBA and its UTRs

Untranslated region	DNA sequence (from 5' to 3')
5'	CGCGCCTAGCAGTGTCCCAGCCGGGTTCGTGTCGCC
3'	<u>CCTCGCCCCGGACCTGCCCTCCCGCCAGGTGCACCC ACCTGC**AATAAA**TGCAGCGAAGCCGGGA</u>

Table S2 shows the sequence of the human CYBA gene UTRs from the 5' to the 3' end. The polyadenylation signal (PAS) of the 3' UTR is shown in bold letters and the insulin 3'UTR stability element (INS_SCE) is underlined. The 5' UTR consists of 36 base pairs, whereas the 3' UTR contains 64 base pairs. Noteworthy, both UTRs are shorter than average human UTRs, for instance 5' UTRs consist of around 200 nucleotides and in case of 3'UTRs the average length is approximately 1000 nucleotides.

Transfection efficiencies on microstructured substrates

The percentage of successfully transfected cells was assessed to compare two different transfection agents and to ensure that transfection efficiencies were not hampered by microstructured cell growth (see Figure S1). Here, all cells grew on microstructured protein arrays. We obtained higher transfection efficiencies for Lipofectamine™2000 as compared to DOGTOR. Using a commercial Live/Dead cell viability assay (Molecular Probes, Germany), we found high cell viability rates above 80% (data not shown).
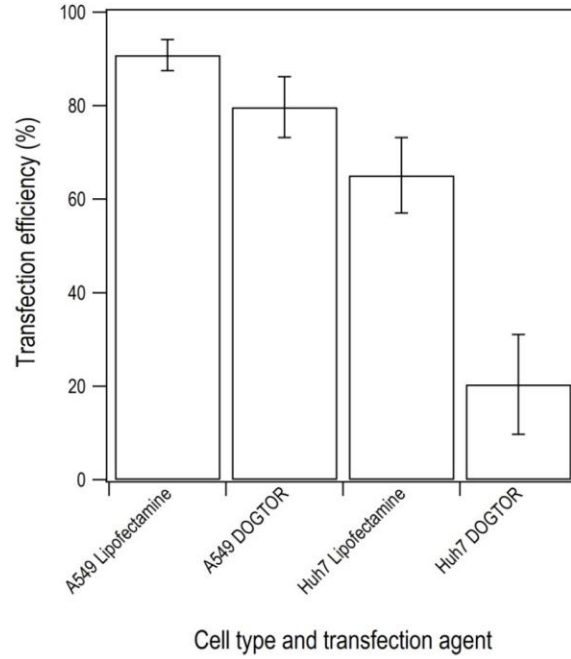
Figure S1. Transfection efficiencies on microstructured substrates. Percentage of transfected cells and corresponding standard deviations for A549 cells and Huh7 cells transfected with SNIM RNA with help of Lipofectamine™2000 or DOGTOR. We find higher transfection efficiencies for cells transfected with Lipofectamine™2000.

Area under the curve (AUC)

Assuming biochemical rate equations (4) and (5) for translation and degradation according to Fig. 3C, the amount of expressed protein after mRNA transfection is given by

$$G_{d2EGFP}(t) = \frac{K}{\delta - \beta} \cdot \left(1 - e^{-(\delta - \beta)(t - t_0)}\right) e^{-\beta(t - t_0)} \qquad \text{(Equation 1 of the main text).}$$

The area under the curve (AUC) is calculated by integrating the expression level $G_{d2EGFP}(t)$ from t_0, when expression sets in to long times ($t \to \infty$):

$$AUC = \int_{t = t_0}^{t = \infty} G(t) = \frac{K}{\delta - \beta} \int_0^\infty [e^{-\beta \tau} - e^{-\delta \tau}] d\tau = \frac{K}{\delta - \beta} \cdot \left[\frac{1}{\beta} - \frac{1}{\delta}\right] = \frac{K}{\delta \cdot \beta}$$

with $\tau = t - t_0$.

Using $\tau_{mRNA} = ln2/\delta$, $\tau_{d2EGFP} = ln2/\beta$, and $K = m_0 \cdot k_{TL}$ we obtain equation 3 of the main text:

$$AUC = 0.48 \cdot m_0 \cdot k_{TL} \cdot \tau_{mRNA} \cdot \tau_{d2EGFP}$$

The time course of $G_{d2EGFP}(t)$ and the AUC is schematically depicted in Figure 6A.

The experimental single-cell AUC distributions can be seen in Figure S2. Because the AUC depends linearly from the mRNA and protein life times, the single-cell AUC distributions are closely related to the mRNA and protein half-life distributions that are shown in Figure 4B and 4C of the main text.
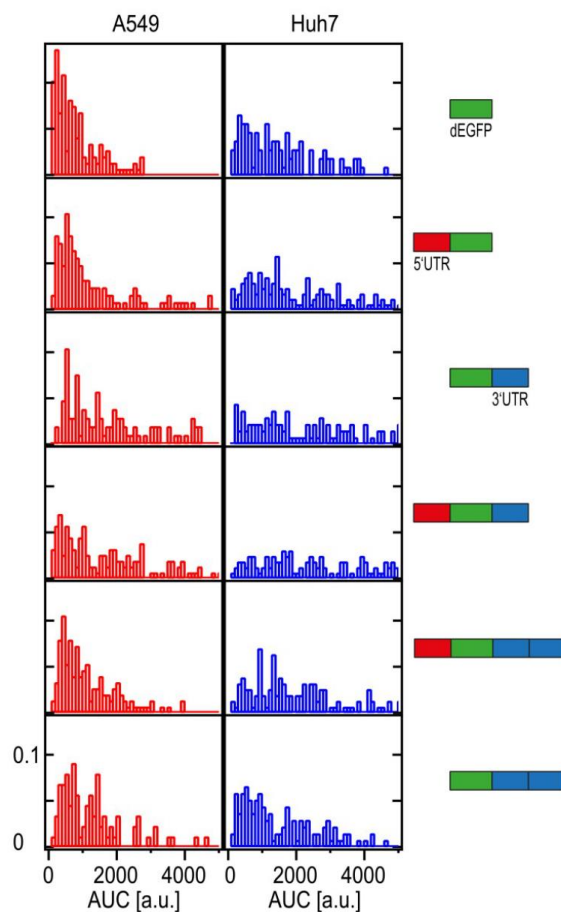
Figure S2. Distribution of the single-cell AUCs. AUCs were calculated according to equation 3 of the main text. A549 data are shown in red, Huh7 data are shown in blue.

Degradation rate of the reporter protein

To check the fitted d2EGFP degradation rates, we independently measured the degradation rate of d2EGFP inside A549 and Huh7 cells in microstructured six-channel slides. Protein synthesis was blocked by the antibiotic cycloheximide, which interferes with peptidyl transferase activity (3). Single-cell fluorescence intensity time courses were monitored for approximately 20h (see Figure S3). Control experiments ensured that the decrease in fluorescence intensity was not due to photobleaching of the chromophore. Single-cell time courses were fitted by a single exponential fit, yielding distributions of protein degradation rates. The mean degradation rates were found to be 0.28/h (std 0.08/h) in A549 cells and 0.17/h (std 0.08/h) in Huh 7 cells, corresponding to protein life times of 2.46 h and 4.04 h, respectively. Although these life times are significantly shorter than the life times as determined by single-cell time course analysis of mRNA mediated protein expression, the ratio between the mean life times of d2EGFP inside Huh7 and A549 cells is the same (4.04 h/2.46 h=1.64 as measured by translational blocking compared to 7.4 h/4.5 h=1.64 as determined by fitting the analytical solution for mRNA expression).
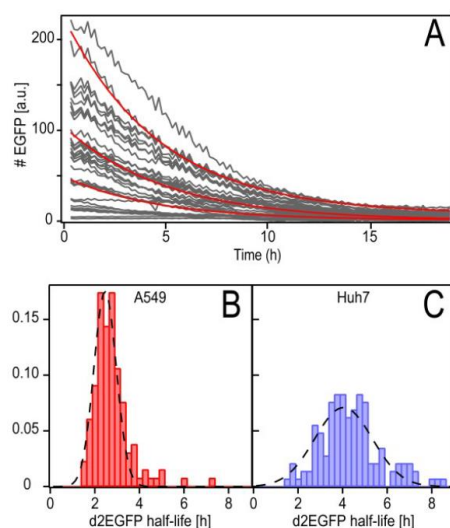
Figure S3. Distributions of directly measured d2EGFP half-lives. **(A)** Exemplary time courses of cycloheximide-induced d2EGFP degradation in Huh7 cells. Red lines are simple exponential fits for protein degradation. **(B)** Distribution of d2EGFP half-lives measured in A549 cells, yielding a mean half-life of 2.46 h (std 0.71 h). **(C)** Distribution of d2EGFP half-lives measured in Huh7 cells, yielding a mean half-life of 4.04 h (std 1.82 h).
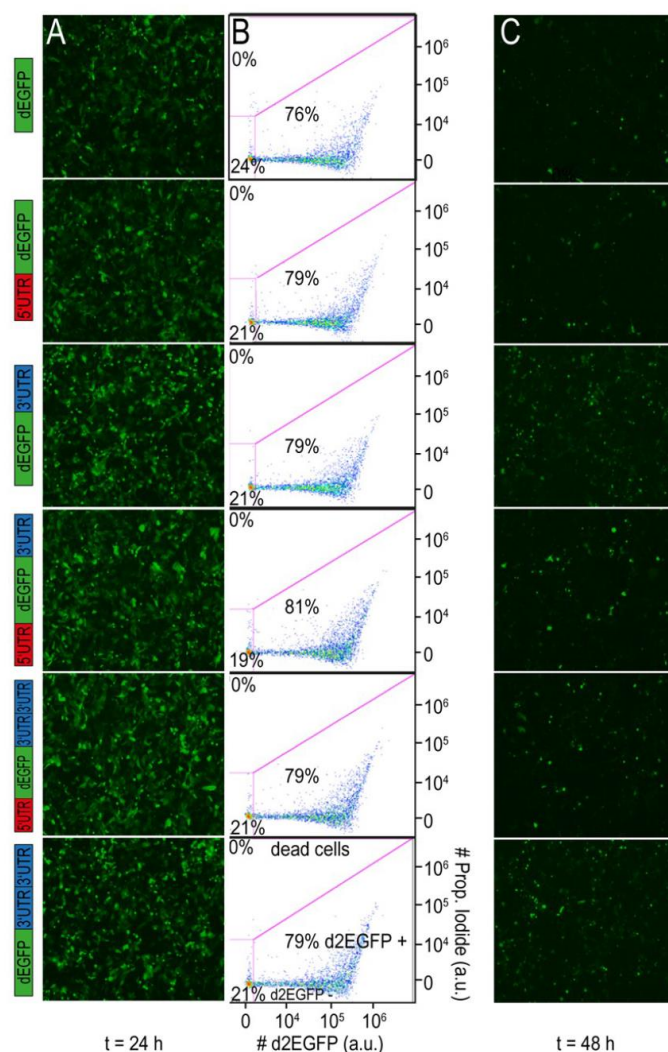
Figure S4. Fluorescence microscopy and flow cytometry data of Huh7 cells. **(A)** Fluorescence microscopy pictures taken with 4x magnification (JULY™) at 24 h post-transfection. All constructs showed improved protein expression levels as compared to the control. **(B)** The percentage of d2EGFP positive cells as determined by FC is similar for all constructs. Propidium iodide was used to detect dead cells. The applied gates ensured exclusion of dead cells and untransfected cells. **(C)** At 48 h post transfection, sustained protein expression was higher for the stabilized constructs as compared to the control.

Determination of physical mRNA half-life by qRT-PCR in A549 and Huh7 cells

In an additional experiment, we investigated the physical mRNA half-life of the different mRNA constructs with qRT-PCR, which is a conventional approach (see Figure S5). Therefore, the mRNA constructs were transfected as described in Materials & Methods. At the end, we obtained the absolute mRNA amount at each specific time point and calculated the physical mRNA half-life for each mRNA furnished with UTRs. We could detect an

increase of mRNA stability for mRNA furnished with 5'+3' UTR. However, no significant physical mRNA stabilization effects for any of the selected mRNA constructs as compared to the control were observed.
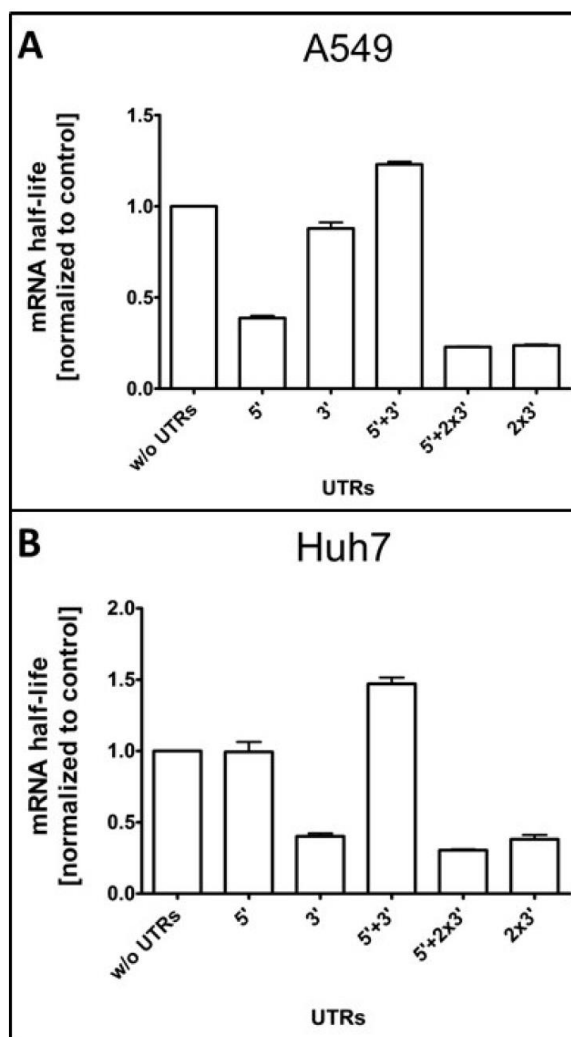
Figure S5 **Determination of physical mRNA half-life by qRT-PCR in A549 and Huh7 cells**

The cells were transfected according to the protocol in Materials & Methods part. Absolute mRNA quantification at 4, 8, 24, 36, 48, 60, 72 hours for all mRNA constructs was determined in A549 (see Figure S5 A) and in Huh7 (see Figure S5 B). Out of this data the physical mRNA half-life was calculated. The physical half-lives were normalized to the control.

Supplementary References

1. Zuker, M. (2003) Mfold web server for nucleic acid folding and hybridization prediction. *Nucleic acids research*, **31**, 3406-3415.
2. Babendure, J.R., Babendure, J.L., Ding, J.-H. and Tsien, R.Y. (2006) Control of mammalian translation by mRNA structure near caps. *RNA (New York, N.Y*, **12**, 851-861.
3. Siegel, M.R. and Sisler, H.D. (1963) Inhibition of Protein Synthesis in vitro by Cycloheximide. *Nature*, **200**, 675-676.

11.2   Abbreviations

A	Adenosine
APCs	Antigen-presenting cells
ARCA	Anti-reverse cap analog
β-S-ARCA	Diastereomers ARCA
ATP	Adenosine triphosphate
AUC	Area Under the Curve
AUE	Adenosine/Uridine-rich elements
BMP	Bone Morphogenetic Protein
bp	base pairs
C	Cytosine
cds	coding sequence
CPEB	Cytoplasmic poly-adenylation element binding protein
CPS	Counts per seconds
CPSF	Cleavage and polyadenylation signaling factor
CTP	Cytosine triphosphate
CYBA	Cytochrome b-245 alpha plypeptide
D2EGFP	destabilized EGFP
Da	Dalton
DCs	Dendritic cells
DECR1	2-4-dienoyl-CoA reductase
DFG	Dreamfect Gold™
DMEM	Dulbecco's Modified Eagle Medium
DNA	Deoxyribonucleic acid

dNTPs	deoxy-Nucleotide-Tri-Phosphate
ds	Double-stranded
E.coli	*Escherichia coli*
eGFP	Enhanced Green Fluorescent Protein
eIF4E	Eukaryotic initiation factor 4E
ELISA	Enzyme Linked Immuno Sorbent Assay
E-PAP	*Escherichia coli* poly(A) polymerase
EST	Expressed Sequence Tag
EtOH	Ethanol
FBS	Fetal bovine serum
Fe	*Ferrum*
FGF	Fibroblast growth factor
FL-*Met*Luc	full-length *Met*Luc
FRW	forward
G	Guanosine
GM-CSF	Granulocyte/macrophage colony-stimulating factor
GMFG	Glia maturation factor gamma
GTP	Guanosin tripoosphate
h	hours
HPLC	High-performance liquid chromatography
IFN	Interferon
IGF	Insulin-like growth factors
IL	Interleukin
INS_SCE	Insulin 3'UTR stability element
IP	Interferon gamma-induced protein

IRE	Iron-responsive elements
IRES	Internal ribosome entry sites
IRF	Interferon regulatory factor
IRP	Iron-regulatory protein
IVT	*In vitro* transcribed
k	*Kilo*
LB medium	Luria-Bertani medium
LGP2	Laboratory of genetics and physiology 2
M	Molar
m	Milli (10^{-3})
m^7G	7-methylguanosine
MAPBPIP	Mitogen-activated protein-binding protein-interacting protein
MDA5	Melanoma differentiation-associated protein 5
MEM	Minimum Essential Medium
mEpo	Murine Erythropoietin
*Met*Luc	*Metridia* Luciferase
MFE	Minimum Free Energy
min	minutes
MPC-1	mitochondrial pyruvate carrier 1
mRNA	Messenger Ribonucleic Acid
mRNP	Messenger Ribonucleoprotein
MSCs	Mesenchymal stem cells
MTT	3-(4,4-dimethylthiazol-2-yl)-2,5-diphenyl-tetrazolium bromide
MyD88	Myeloid differentiation primary response gene

	88
MYL6B	Myosin, light chain 6B
n	nano (10^{-9})
nm	nanometers
nt	nucleotide
ng	nano gramm
NFκB	Nuclear Factor-κB
NLRs	NOD-like receptors
p	Pico (10^{-12})
PABP	poly(A)-binding protein
PARN	poly(A) ribonuclease nucleases
PAS	Polyadenylation Signal
PBS	Phosphate Buffered Saline
PCR	Polymerase Chain Reaction
PDGF	Platelet-derived growth factors
pDNA	Plasmid deoxyribonucleic acid
poly(A)	poly Adenosine
PRRs	Pattern recognition receptors
PTB	Polypyrimidine tract binding protein
PTH	Parathyroid hormone
ppp	5' to 5' triphosphate bridge
qRT-PCR	Quantitative Real time PCR
REV	reverse
RIG-I	Retionoid-inducible gene I
RLU	Relative light units

RNA	Ribonucleic Acid
rRNA	Ribosomal RNA
rpm	rounds per minute
RT	Room temperature
SAGE	Serial analysis of gene expression
SEM	Standard error of the mean
SNP	small nucleotide polymorphism
SP-B	Surfactant protein B
ss	Single-stranded
TAE buffer	Tris Acetate EDTA buffer
TfR	Transfection Reagent
TGF	Transforming growth factors
TLR	Toll-like receptor
TNF	Tumor necrosis factor
TRIF	TIR-domain-containing adaptor-inducing IFN-β
tRNA	Transfer RNA
TTP	Tristetraprolin
U	Units (enzyme activity)
U	Uracil
uORF	Upstream Open reading frame
UTP	uridine triphosphate
UTRs	Untranslated regions

11.3 Tables

11.4   Figures

Acknowledgements

This thesis would not have been possible without the help of many people who have accompanied me with their energetic support.

This work was carried out during the years 2011-2015 at the company Ethris GmbH. I am deeply grateful to P.D. Carsten Rudolph and Prof. Dr. Christian Plank, owners of the company Ethris GmbH in Planegg, who provided me with this great opportunity to pursue my scientific carrier in the field of RNA therapeutics.

I would like to express the deepest appreciation to my first supervisor Professor Dr. Christian Plank for his optimism concerning this work, enthusiasm, encouragement and support. I also express my warmest gratitude to my two mentors P.D. Carsten Rudolph and Univ.- Prof. Dr. Dr. Martijn van Griensven, group leader of the Experimental Trauma Surgery at the Klinikum rechts der Isar, for giving me constructive comments and warm encouragement. Their help regarding manuscript's proof-reading is also well-appreciated.

I would also like to thank Prof. Dr. Percy Knolle, director of the Institute of Molecular Immunology – Experimental Oncology (IMI-Experimental Oncology), and former director Prof. Dr. Bernd Gänsbacher of the former Institute of Experimental Oncology and Therapy Research (IEOT) for giving me the opportunity to carry out my work at the faculty.

I owe my deepest heartfelt gratitude to Dr. Manish K. Aneja, who has been extraordinarily tolerant and supportive. Without his encouragement and wise comments, my both dissertation and publication would not have materialized. Dear Manish, thank you for your constructive and intellectual comments, invaluable suggestions, guidance and persistent help during my thesis. It was a big pleasure to work with you together, despite the Döner I owe you.

I would like to offer my special thanks to the group of Prof. Christian Plank and my colleagues of Ethris, for their support and insightful comments and suggestions during work. I really felt welcome and enjoyed taking part in the social events, in particular "Kicker- sessions". I would particularly like to thank Dr. Olga Mykhailyk for providing me with magnetic nanoparticles.

Acknowledgements

I special thanks to the "Spaß-Box", who delighted my day any time ☺. Not only them, but also the members of the "Crazy scientist" for helping me keeping track with the regulatory requirements of the PhD program.

I owe a very important debt to my closest friends. Thank you so much for your time and support during my thesis. I know that it was not always easy to find or stick to an appointment. I am deeply grateful to call you my best friends.

Last but not the least, my heartfelt gratitude to my parents and my siblings, and also the family of Zykolli, especially Hasime Zykolli, who always been there for me.

Curriculum Vitae

Personal information

Surname(s) / First name(s)	**Ferizi Mehrije**
Address(es)	Forggenseestraße 26, 81539 Munich
Telephone(s)	Mobile: 0176/32642911
E-mail	Mehrije.Ferizi@lrz.tu-muenchen.de
Nationality	Austrian
Date of birth	11. 01. 1986

Acquired Qualification

Dipl.-Ing. (FH) for technical and scientific work

Education and training

PhD Studies

Duration	March 2011 – present
PhD Thesis/Topic	Modified messenger RNA and its application in bone tissue engineering
Supervisor	Prof. Dr. Christian Plank
Organisation	Klinikum r.d. Isar, Technische Universität München
	Institute for Molecular Immunology and Experimental Oncology
	Ismaninger Straße 22
	81675 Munich

Master Studies

Duration	September 2004 - February 2009
Topic	Expression of tetraspanin CD63 correlates with the expression of Hif-1α
Supervisor	Prof. Achim Krüger
	Univ. Prof. Ernst Müllner
Organisation	University of Applied Life Sciences
	FH Campus Vienna Biotechnology
	Helmut-Qualtinger-Gasse 2
	1030 Vienna

Highschool Diploma

Duration
September 2000 - June 2004

Organisation
Bundesoberstufenrealgymnasium
Brennerweg 8
A- 2130 Mistelbach

Work experience

Dates
March 2009 – March 2011

Occupation or position held
Technical Assistant

Activities
Participation in the development and evaluation of a clinical trial

Employer
Klinikum r.d. Isar, Technische Universität München
Institute of Experimental Oncology and Therapy Research
Ismaninger Straße 22
81675 Munich

Awards and Honors

Scholarships
October 2011- November 2012
Scholarship of the Faculty of Medicine, TUM (KKF)
October 2011:

Travel award of the IDK-NBT (Elite Network of Bavaria)
April 2015:

Oral presentation in Ulm (8th Student Symposium on
Molecular Medicine) April 2015

Membership
October 2011-present
CeNS (Center for Nanoscience)
Faculty Graduate Center of Medicine (FGC MED) at TUM
Elitenetzwerk Bayern

Activities
March 2012-April 2012
International PhD Exchange Program
University of California, Santa Barbara

Declaration

I solemnly declare that I have written the dissertation entitled

Modified messenger RNA and its application in bone tissue engineering _____

_____

and submitted it to the Department of Medicine of the Technical University Munich for doctoral examination at the

_____

under the guidance and supervision of

Prof. Dr. Christian Plank _____

without other help and, while writing it, only used aids in accordance with the academic and examination regulations of the PhD program in Medical Life Science and Technology.

[   ]   I have not involved any organization that offers doctoral advisors for a fee or partially or entirely fulfills examination obligations required of me on my behalf.

[   ]   I have not submitted the dissertation in this or a similar form in another examination procedure as an examination achievement.

[   ]   The complete dissertation was published in

_____.
The Department of Medicine has approved the advance publication.

[   ]   I have not yet acquired the Doctor of Philosophy and I have not definitively failed in a previous doctoral procedure for the Doctor of Philosophy.

[   ]   I have already submitted a dissertation with the subject

_____
at the Department of _____
of the university _____
on _____ to apply for admission to the doctoral examination with the result:
_____

I am familiar with the academic and examination regulations of the PhD program in Medical Life Science and Technology of the Technical University Munich.

Munich, _____

_____
Signature